Journal of Statistical Physics, Vol. 124, No. 1, July 2006 (© 2006)
DOI: 10.1007/s10955-006-9103-1

On the Dynamics of the Glass Transition on Bethe Lattices

Andrea Montanari[1,*] and Guilhem Semerjian[2]

Received September 15, 2005; accepted March 22, 2006
Published Online: July 12, 2006

The Glauber dynamics of disordered spin models with multi-spin interactions on sparse random graphs (Bethe lattices) is investigated. Such models undergo a dynamical glass transition upon decreasing the temperature or increasing the degree of constrainedness. Our analysis is based upon a detailed study of large scale rearrangements which control the slow dynamics of the system close to the dynamical transition. Particular attention is devoted to the neighborhood of a zero temperature tricritical point.

Both the approach and several key results are conjectured to be valid in a considerably more general context.

KEY WORDS: Glass transition, Bethe lattice, energy barriers, p-spin model

PACS Numbers:75.50.Lk (Spin glasses), 64.70.Pf (Glass transitions), 89.20.Ff (Computer science

1. INTRODUCTION

1.1. Motivation

Bethe lattices[3] can be used to define a large variety of analytically tractable statistical mechanics models. A sophisticated (and still improving) theory has been developed for computing the thermodynamic properties of such systems in great generality (cf. for instance [1] and references therein). Among the recurring predictions of this theory is the occurrence (in models with frustration or self-induced frustration) of a *dynamical phase transition* (DPT).[2] While the system free energy

[1] Laboratoire de Physique Théorique de l'Ecole Normale Supérieure, UMR 8549, Unité Mixte de Recherche du Centre National de la Recherche Scientifique et de l' Ecole Normale Supérieure.
[2] Dipartimento di Fisica, INFM (UdR and SMC centre), Università di Roma "La Sapienza"
[3] We denote by this term random graphs with arbitrary degree distribution (but bounded average degree). A more precise definition is given in Section 2 for the particular case studied here.

remains analytic at the DPT, this is revealed by more refined thermodynamic potentials[3] (such as the configurational entropy) which indicate the appearance of a broken-ergodicity phase.

Despite its eminently dynamical character, the dynamics itself at the DPT is poorly understood. For fully-connected (FC) mean field models, in which each degree of freedom (spin, particle, etc.) interacts with all the others, one can usually solve the dynamics in terms of a closed set of equations for the two points correlation and response functions. This is no longer true for models on Bethe lattices, which have finite connectivity (each degree of freedom interacts with a finite number of neighbors). Correlation and response functions involving an arbitrary number of times are relevant in this case.[4] This is somehow healthy: there is no hope to obtain a finite set of closed equations describing the dynamics of realistic (finite-dimensional) systems. Alternative approaches developed for Bethe lattice models may, on the other hand, prove more general.

Consider the relaxation of a particular degree of freedom, for instance a spin. As the DPT is approached, dynamics slows down because, in order for the spin to decorrelate, a larger and larger number of degrees of freedom have to be rearranged coherently. Our approach consists in computing some detailed properties (e.g. their minimal size or the minimal energy barrier to be overcome in order to realize them) of such rearrangements and then using these properties to estimate relaxation times. While we shall develop these ideas on a specific Bethe-lattice model, they are susceptible of generalization to a variety of other examples. The cases of k-core percolation and kinetically constrained models[5] are, for instance, quite straightforward, and will be treated in a related publication[6] (the model treated in the present paper is in fact strictly related to 2-core percolation on random hypergraphs).

Due to the lack of a simple order parameter and the extensive configurational entropy, the broken ergodicity phase is often referred to as a "glassy" phase. In the 80s, Kirkpatrick, Wolynes and Thirumalai[7,8] stressed the analogy between the DPT (in the context of fully-connected models) and the mode coupling transition,[9–11] thus motivating a considerable effort aimed at a theoretical understanding of structural glasses. One recent advance has been the definition a "dynamical length scale" associated to the dynamical slowing down.[12,13] Within mean-field models and mode coupling theory (MCT) this length scale diverges at the DPT.[14–16] However, the relation between this phenomenon and the diverging relaxation time is poorly understood. Also, the basic physical mechanism underlying this divergence in glasses is presumably different from the one occurring in simpler system, and is still mysterious.[17] Finally, it would be useful to establish a quantitative relation between the dynamical slowing down and some purely static observable.

In order to clarify these points, let us contrast our understanding of the DPT with the one we have of the paramagnetic-to-ferromagnetic transition in the Ising

model. In this case a typical configuration close to the transition looks like a patchwork of positively and negatively magnetized regions. The typical linear size of each region is the correlation length ξ, and total magnetization is $\sqrt{\chi}$ (χ being the susceptibility). Assuming that the magnetization performs a random walk, we can estimate the relaxation time as $\tau \gtrsim \chi$. Since standard scaling theory predicts $\chi \sim \xi^{\gamma/\nu}$, we get $\tau \gtrsim \xi^{\gamma/\nu}$. In fact the dynamical scaling hypothesis states that $\tau \sim \xi^z$ with exponent $\geq \gamma/\nu$.[18]

A further source of motivation is to understand the role of activation at the DPT. Much of our understanding of this phase transition comes from the study of a particular model: the p-spin spherical spin glass.[19–21] MCT has been shown to be exact for this model.[10] Moreover, the energy landscape and its relation to dynamics are relatively simple.[22] Above the transition temperature, the system never visits minima and moves among saddles. As temperature is lowered the number of energy-decreasing directions decreases, slowing down the dynamics.[23] Below the critical point, the system is typically found near a local minimum and is separated by diverging (in the thermodynamic limit) energy barriers from other minima. Activation is therefore irrelevant both above and below the DPT. It is not necessary in the first case, and it cannot take place within physical time-scales in the second. This has lead to question whether activated processes could spoil the predictions of MCT for more realistic (finite-dimensional) models. In this case a standard nucleation argument suggests that ergodicity is restored within a finite (in the thermodynamic limit) time.[24]

Like other mean-field systems, models on Bethe lattices are characterized by diverging energy barriers within the broken ergodicity phase. Therefore, they cannot help understanding the role of activation in this regime. On the other hand, finite energy barriers are present in the ergodic phase and one may ask whether they modify the MCT critical behavior upon approaching the DPT. Notice that such a question is in general not well-defined because the distinction between activated and non-activated processes becomes sharp only in the zero-temperature limit. In the following we shall study in detail a zero-temperature multi-critical point where the distinction makes sense.

1.2. Overview of the Paper

The model and some basic notations are introduced in Sec. 2. The phase diagram is described in terms of two basic parameters: the temperature T, and α which quantify the degree of constrainedness of the system. We then discuss the critical properties of the DPT in Secs. 3 and 4. Let $T_{\rm d}$ be the phase transition temperature. We will show that n-points susceptibilities stay finite at $T_{\rm d}$ for any given n. On the other hand, we introduce a correlation length ℓ using point-to-set correlations and show that $\ell \sim (T - T_{\rm d})^{-1/2}$. This correlation length is connected

to relaxation times using a disagreement percolation argument which implies a bound of the form $\tau \gtrsim (T - T_{\rm d})^{-1/2}$.

We then consider the $T \to 0$, finite α limit (still within the ergodic phase). In this regime, the dynamics is dominated by activated processes and the relaxation time can be derived from a standard Arrhenius argument. The relevant large scale rearrangements minimize the energy barrier to be overcome in order to realize them, cf. Sec. 6. The barriers height diverges as α increases and approach the DPT point $\alpha_{\rm d}$ (at which $T_{\rm d} = 0$). In Sec. 7, we compute several properties of these rearrangements, such as their size, depth and cooperativity. We also consider minimal size rearrangements (cf. Sec. 5), which share several properties with minimal barrier ones, and are somewhat easier to analyze. We compare the critical behavior as $\alpha \to \alpha_{\rm d}$ with standard MCT predictions. We find that several of these predictions are violated. More surprisingly some universal properties of MCT (such as the divergence of the four point susceptibility) hold even in this extremely activated regime.

The point ($\alpha = \alpha_{\rm d}$, $T = 0$) is a tricritical point, analogous to the percolation point in diluted ferromagnets. In Sec. 8, we use standard scaling theory in order to connect the $T \to 0$, $\alpha < \alpha_{\rm d}$ and $T \to T_{\rm d}(\alpha) > 0$, $\alpha > \alpha_{\rm d}$ regimes. The scaling hypothesis is verified through numerical simulations. Under this hypothesis, temperature is a relevant variable and a crossover from an activation-dominated to a thermal regime takes place. We argue that the thermal regime is controlled by usual MCT critical behavior at any finite temperature.

Some conclusive remarks are put forward in Sec. 9, while most of technical calculations are collected in the Appendices.

A synthetic account of our results was published in Ref. 25.

2. DEFINITIONS AND NOTATIONS

2.1. Model

In this paper we focus on Ising models with p-spin ($p \geq 3$) interactions:

$$H(\sigma) = \sum_{(i_1 \dots i_p) \in \mathcal{G}} (1 - J_{i_1 \dots i_p} \sigma_{i_1} \dots \sigma_{i_p}) \,, \tag{1}$$

Here $\sigma_i = \pm 1$ are N Ising spins, $\mathcal{G}$ is a set of $M = N\alpha$ p-uples of indices, and $J_{i_1 \dots i_p}$ are quenched couplings taking values ± 1 with equal probability. The above Hamiltonian is twice the number of violated constraints $\sigma_{i_1} \dots \sigma_{i_p} = J_{i_1 \dots i_p}$. Since this condition can be written as the exclusive OR of p boolean variables, the problem is known in computer science as XORSAT.[26] Any configuration satisfying all these constraints has zero energy (is unfrustrated).

In order to complete our definition, we need to specify the (hyper) graph of interactions $\mathcal{G}$. In this paper we consider $\mathcal{G}$ to be a random graph constructed

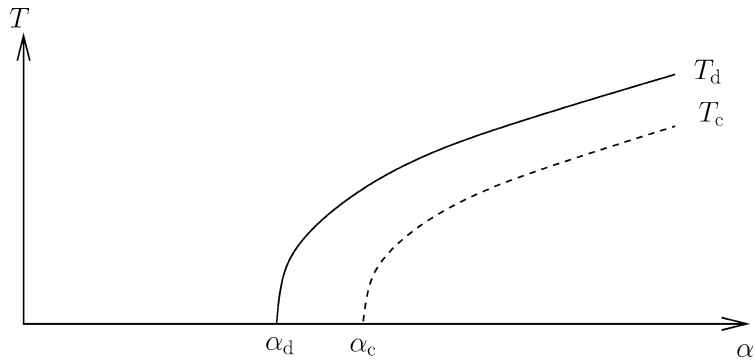

Fig. 1. Schematic view of the phase diagram of the diluted p-spin model.

by taking the M interacting p-uples of sites $\{(i_1 \dots i_p)\}$ to be quenched random variables uniformly distributed in the set of $\binom{N}{p}$ possible p-uples.[27] In the thermodynamiclimit $N \to \infty$, the number of interactions a given spin belongs to (its degree) is a Poisson random variable with parameter $p\alpha$. Moreover, the shortest loop through such a spin is (typically) of order $\log_c N$ with $c = p(p-1)\alpha$.[28]

This property allows (at least in principle) for an exact treatment of the thermodynamics. The phase diagram is sketched in Fig. 1. For $\alpha < \alpha_d$ and above the critical line $T_d(\alpha)$ the system is ergodic and the free energy density is given by the usual paramagnetic expression $-\beta f = \log 2 + \alpha((\log\cosh\beta) - 1)$. The free energy density remains analytic across the line $T_d(\alpha)$, but ergodicity is broken in the whole region $T < T_d(\alpha)$. Finally, a true thermodynamic transition of the random-first order type[7,8] takes place at $T_c(\alpha)$.

Two regimes have attracted particular attention. In the "fully-connected" limit $\alpha \to \infty$, $T \propto \sqrt{\alpha}$, both statics and dynamics can be treated analytically, showing a typical MCT transition.[7,29] The relaxation time diverges as $|T - T_d|^{-\gamma_{mct}}$.

In the zero-temperature, finite α limit, probabilistic methods can be used to show that zero-energy ground states with finite entropy density exist for $\alpha < \alpha_c$. However, the set of ground states gets splitted in an exponential number of clusters with extensive Hamming distance (number of spins with different value) separating them for $\alpha_d < \alpha < \alpha_c$.[30,31] A finite fraction of the spins does not vary among the ground states of a particular cluster, while they change when passing from a cluster to the other. At α_d the fraction of frozen spins jumps from 0 to a finite value ϕ_d. For instance $\alpha_d \approx 0.818469$, $\alpha_c \approx 0.917935$, and $\phi_d \approx 0.715332$ when $p = 3$. This phase transition can be characterized in a purely geometrical way. It corresponds to the appearance of a 2-core, i.e. a subgraph of $\mathcal{G}$ such that any of its vertices has degree at least 2 in the subgraph. The largest 2-core in $\mathcal{G}$, denoted as $\mathcal{G}_{core}$, includes $|\mathcal{G}_{core}| = O(N)$ vertices above α_d. The subgraph of frozen spins will be referred to as "backbone," $\mathcal{G}_{bone}$ and can be constructed recursively as

follows. Start from $\mathcal{G}_{\rm bone} = \mathcal{G}_{\rm core}$, add to it any hyperedge of $\mathcal{G}$ having at most one vertex not yet in $\mathcal{G}_{\rm bone}$, and repeat until such an hyperedge exist. In view of these remarks, it is not surprising that several results of this paper can be generalized to kinetically constrained models (in this case the relevant geometrical transition is the k-core percolation.[5,32])

No exact result exists for the dynamics at any finite value of α. Standard generating function methods allow to formally derive a hierarchy of dynamical equations for multi-time correlation and response functions.[4] Several approximation schemes have been proposed[33,34] for this hierarchy. Such approximations have been developed mostly within models with a continuous transition (typically, the model (1) with $p = 2$). However, their generalization to models undergoing a discontinuous transition is straightforward. Unfortunately such approximations break down in the critical regime $T \downarrow T_{\rm d}(\alpha)$.

In the following we shall use repeatedly two useful properties of this model. First: as long as there exist at least one zero-energy ground-state, all such ground-states are equivalent. Suppose that $\sigma^{(*)}$ is such a ground state, and that σ is an equilibrium configuration for the Hamiltonian (1) at temperature T. Define $\sigma'_i = \sigma_i^{(*)}\sigma_i$ (this is often called a "gauge" transformation). Then σ' is distributed according to the Boltzmann measure with an Hamiltonian of the form (1), with the same graph $\mathcal{G}$ and temperature T as the original model, but with $J_{i_1\dots i_p} = +1$ for all the interactions (ferromagnetic model). Therefore any property of $\sigma^{(*)}$ which is invariant under this change of variable can be computed for the $\sigma^{(+)} = (+1,\dots,+1)$ ground state of the ferromagnetic model. In particular, for $T = 0$ this implies that the ground states of the $J = \pm 1$ model as observed from $\sigma^{(*)}$, "look like" the ground states of the ferromagnetic model as observed from $\sigma^{(+)}$.

The second property will be used uniquely in numerical simulations and can be stated in two parts: (i) As long as $\mathcal{G}$ does not contain hyperloops (i.e. subgraphs such that each site has even degree) the partition function of the model is *exactly* given by the annealed computation, i.e. $Z_{N,\beta}(J) = 2^N(e^{-\beta}\cosh\beta)^M$. (ii) Under the same hypothesis, sampling the sign of the couplings $J \equiv \{J_{i_1\dots i_p}\}$ (for a given graph $\mathcal{G}$) and then the configuration σ according to the Boltzmann distribution is equivalent to sampling σ from the uniform distribution and then the couplings as independent random variables with distribution

$$\mathbb{P}\left(J_{i_1\dots i_p}|\sigma\right) = \frac{1}{2\cosh\beta}\ \exp\{\beta J_{i_1\dots i_p}\sigma_{i_1}\dots\sigma_{i_p}\}\,. \tag{2}$$

The proof of this statement is deferred to Appendix A. It is a consequence of the results of Refs. 30, 31 that, for $\alpha < \alpha_{\rm c}$ a random graph $\mathcal{G}$ constructed as above does not contain any hyperloop with high probability.

Sampling first σ and then J is much simpler than the opposite. We shall adopt this procedure in order to generate thermalized configurations for simulating the equilibrium dynamics. It is an open (and interesting) problem whether the same

procedure can be useful in the region $\alpha > \alpha_c$, $T > T_c(\alpha)$ (at least for large enough systems).

2.2. Averages, Factor Graphs and Messages

In this paper we shall denote by $\langle \cdot \rangle$ expectation with respect to the Boltzmann measure at inverse temperature β, and by $\mathbb{E}(\cdot)$ expectation with respect to the quenched disorder (i.e. the graph $\mathcal{G}$ and the couplings $J_{i_1 \dots i_p} \in \{+1, -1\}$). Connected correlation functions (see, for instance,[35] for a definition) are denoted by $\langle \cdot \rangle_c$.

Factor graphs[36] provide an useful representation of models like the one studied in this paper. These graphs have two types of nodes, one for interactions ("function nodes," squares of Fig. 2) and one for spins ("variable nodes," circles). Edges connect each interaction with the spins involved in it. The graph is obviously bipartite.

We shall use indices $\alpha, \beta, \dots$ to denote function nodes, and $i, j, k, \dots$ for variables. Directed edges in the graph will support *messages* of two types, $u_{\alpha \to i}$, and $v_{i \to \alpha}$, with various meanings depending on the context. We denote by $\partial\alpha$ the set of variables in the interaction α, and by ∂i the set of interactions the variable i belongs to. In this context\will denote the subtraction of an element from a set.

Let $\mathcal{F}$ be the factor graph associated to the model (1). The degree of function nodes in $\mathcal{F}$ is fixed to p, whereas the one of a generic variable node converges to Poisson random variable of parameter $p\alpha$. A path in $\mathcal{F}$ is a sequence of nodes, such that any two successive nodes are joined by an edge. The distance between two variable nodes i and j is the length (number of function nodes in it) of the shortest path graph joining them. Two variables are said to be "adjacent" if their distance is equal to one, and connected if there is a path joining them. A set of variables is connected if its elements are pairwise connected. An important property of

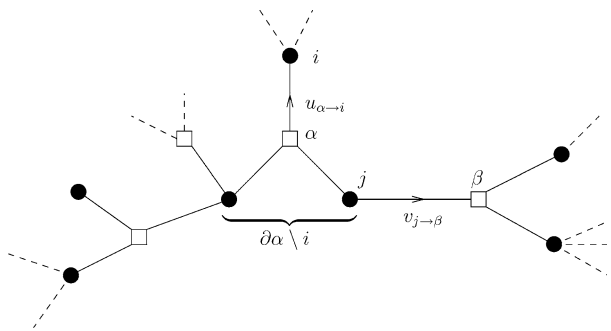

Fig. 2. Example of factor graphs.

random graphs, on which we shall come back later, is that, in the $N \to \infty$ limit, any finite neighborhood of a generic site is, with high probability, a tree.

Finally, for asymptotic behaviors (here as $n \to \infty$) we write: $a_n \sim b_n$ if (a_n/b_n) is bounded away from 0 and ∞ for n large enough; $a_n \simeq b_n$ if $(a_n/b_n) \to 1$. Further $a \approx b$ if a is numerically close to b.

2.3. Glauber Dynamics

Most of our results can be applied to general single-spin flip Markov dynamics satisfying the detailed balance condition. Furthermore, the generalization to block (multi-spin flip) dynamics is in several cases straightforward as far as the block size is kept finite as $N \to \infty$.

For the sake of definiteness, the reader may refer to Glauber dynamics in continuous time. At each spin σ_i, a flip is proposed in a time interval dt with probability dt (i.e. according to a Poisson process of rate 1). Whenever a spin flip is proposed at site i, the new value of σ_i is drawn from the conditional distribution, given the neighboring spins

$$P_\beta(\sigma_i|\sigma_{[N]\setminus i}) \propto \exp\left\{\beta\sigma_i \sum_{\alpha\in\partial i} J_a \sum_{j\in\partial\alpha\setminus i} \sigma_j\right\}, \tag{3}$$

(the constant hidden in the $\propto$ symbol is here independent of σ_i). Whenever precise non-asymptotic estimates on correlation times will be given, they will refer to these transition rates.

The basic observables we shall use in order to probe this stochastic dynamics are single spin correlation functions

$$C_i(t) = \langle\sigma_i(0)\sigma_i(t)\rangle\,. \tag{4}$$

Here expectation is taken with respect to the equilibrium dynamics, i.e. $\sigma(0)$ is an equilibrated configuration, and $\sigma(t)$ is the configuration obtained by applying the above dynamics for a time interval t. One can also consider the global correlation function $C(t)$, defined by averaging $C_i(t)$ uniformly over the spin position.

3. ORIGIN OF THE DYNAMICAL TRANSITION

Since purportedly, the dynamics gets slower and slower upon approaching $T_{\rm d}(\alpha)$, it is quite natural to think that spatial correlations in the equilibrium measure must become stronger in the same regime. In this Section we first show that n-point correlations remain short ranged at the dynamical transition. On the contrary, point-to-set correlations diverge at $T_{\rm d}(\alpha)$. We show that this indeed implies a divergence in properly defined relaxation times.

3.1. n-Points Correlation Functions

A simple way for characterizing correlations in the system consists in considering n-points spin-glass susceptibilities

$$\chi^{\mathrm{SG}}_{n,N} \equiv \frac{1}{N} \sum_{i_1 \dots i_n} \langle \sigma_{i_1} \dots \sigma_{i_n} \rangle_{\mathrm{c}}^2 \,. \tag{5}$$

We are eventually interested in the thermodynamic limit. The rationale for considering the spin-glass susceptibility is that $\mathbb{E}\,\langle \sigma_{i_1} \dots \sigma_{i_n} \rangle_{\mathrm{c}} = 0$ unless $i_1 = \dots = i_n$ and n is even.[4] We claim that for any fixed n, the susceptibilities (5) remain finite across the dynamic transition $T_{\mathrm{d}}(\alpha)$. More precisely, for all $T > T_{\mathrm{c}}(\alpha)$, with high probability

$$\chi^{\mathrm{SG}}_{n,N} \le C_n(\beta, \alpha) \,, \tag{6}$$

for some bounded functions $C_n(\beta, \alpha)$. In other words, n-points correlation functions give no hint[5] about the dynamic transition *as far as n is finite*. Here we will sketch a proof of this claim in the zero-temperature limit (the approach is essentially rigorous in this case) for $n \le 2$. Technical calculations, together with a cavity argument for $n > 2$ or $T > 0$ are presented in Appendix B.

Consider $\alpha < \alpha_{\mathrm{c}}$: the system will typically contain an unfrustrated ground state $\sigma^{(*)}$, so we apply a gauge transformation and reduce ourselves to the ferromagnetic model $J_{i_1 \dots i_p} = +1$. Since $(\sigma_i^{(*)})^2 = 1$, the definition (5) remains unchanged in the new variables (which we still denote as σ). In the ferromagnetic system $\langle \sigma_{i_1} \dots \sigma_{i_n} \rangle_{\mathrm{c}} = 0$ or $+1$ for any $i_1, \dots, i_n$ and $n \le 3$. In fact $\langle \sigma_{i_1} \dots \sigma_{i_n} \rangle = 0$ or 1 (for the not-connected correlation function). If $\sigma_{i_1} \dots \sigma_{i_n} = +1$ in all the ground states then $\langle \sigma_{i_1} \dots \sigma_{i_n} \rangle = +1$ trivially. If on the other hand there exist a ground state $\sigma^{(-)}$ such that $\sigma^{(-)}_{i_1} \dots \sigma^{(-)}_{i_n} = -1$, this is the case for exactly one half of the ground states (for each ground state with $\sigma_{i_1} \dots \sigma_{i_n} = +1$ we can construct one of the other type multiplying it by $\sigma_i^{(-)}$) and therefore $\langle \sigma_{i_1} \dots \sigma_{i_n} \rangle = 0$. As for the connected correlation $\langle \sigma_{i_1} \dots \sigma_{i_n} \rangle_{\mathrm{c}}$, being sum of products of ordinary correlations, it is an integer. Furthermore, it is non-negative because of Griffiths inequality for $n = 1, 2$, and by simple enumeration of the possible values of $\langle \sigma_{i_1} \sigma_{i_2} \sigma_{i_3} \rangle$, $\langle \sigma_{i_1} \sigma_{i_2} \rangle$, and so on, for $n = 3$. Using the definition of $\langle \cdots \rangle_{\mathrm{c}}$ it is finally easy to show that it cannot be larger than one. We therefore proved the simplified expression

$$\chi^{\mathrm{SG}}_{n,N} \equiv \frac{1}{N} \sum_{i_1 \dots i_n} \langle \sigma_{i_1} \dots \sigma_{i_n} \rangle_{\mathrm{c}}, \quad \text{for} \quad T = 0, \quad n \le 3, \quad \text{and} \quad \alpha < \alpha_{\mathrm{c}}. \tag{7}$$

[4] Whenever $\{i_1, \dots, i_n\}$ contain an index i repeated an odd number of times, a simple gauge transformation implies that $\mathbb{E}\,\langle \sigma_{i_1} \dots \sigma_{i_n} \rangle_{\mathrm{c}} = -\mathbb{E}\,\langle \sigma_{i_1} \dots \sigma_{i_n} \rangle_{\mathrm{c}}$.

[5] One may wonder whether derivatives of $\chi^{\mathrm{SG}}_{n,N}$ with respect to T (or α) may give some useful information. It is not hard to generalize our arguments to show that this is not the case.

Let $L = \{j_1, \dots, j_l\}$ with $j_k \in \{1, \dots, N\}$ a list of (not necessarily distinct) spin positions denote by $Z_{\mathcal{G}}(L)$ the number of unfrustrated ground states such that $\sigma_i = +1$ for any $i \in L$. We take l to have Poisson distribution with mean $N\lambda$ (with $\lambda \geq 0$) and $\{j_1, \dots, j_l\}$ i.i.d. uniformly distributed in $\{1, \dots, N\}$. Let

$$\psi_{\mathcal{G}}(\lambda) \equiv \frac{1}{N}\mathbb{E}_L \log_2 Z_{\mathcal{G}}(L), \tag{8}$$

denote the ground state entropy of the system in which we forced $\sigma_i = +1$ for any $i \in L$. Simple calculus reveals that

$$\left.\frac{d\psi_{\mathcal{G}}}{d\lambda}\right|_0 = -\frac{1}{N}\sum_{i=1}^{N}(1 - \langle\sigma_i\rangle)\,, \qquad \left.\frac{d^2\psi_{\mathcal{G}}}{d\lambda^2}\right|_0 = \frac{1}{N}\sum_{i,j}\langle\sigma_i\sigma_j\rangle_{\rm c}\,. \tag{9}$$

Therefore, proving the thesis for $n \leq 2$ is equivalent to proving that the first two derivatives of $\psi_{\mathcal{G}}(\lambda)$ are bounded.

By computing derivatives at $\lambda > 0$, one can sho1w that $\psi_{\mathcal{G}}(\lambda)$ is non-increasing and convex in λ. Furthermore, since each constraint (either $\sigma_{i_1} \dots \sigma_{i_p} = +1$ for $(i_1 \dots i_p)$ edge of $\mathcal{G}$ or $\sigma_j = +1$ for $j \in L$) at most halves the number of zero-energy ground states, we have the bound $\psi_{\mathcal{G}}(\lambda) \geq (1 - \alpha - \lambda)$. Moreover, it is simple to derive an upper bound through an annealed computation (we refer to Appendix B for the details). Define

$$\psi_{\rm ann}(\lambda) \equiv \sup_{\omega\in[0,1]}\left\{\mathcal{H}(\omega) + \alpha\log_2\left[\frac{1 + (1-2\omega)^p}{2}\right] + \lambda\log_2(1-\omega)\right\}\,, \tag{10}$$

where $\mathcal{H}(\omega) = -\omega\log_2\omega - (1-\omega)\log_2(1-\omega)$ is the binary entropy function. Then one can prove that, given $\varepsilon > 0$, $\psi_{\mathcal{G}}(\lambda) \leq \psi_{\rm ann}(\lambda) + \varepsilon\lambda^2$ for any $\lambda \geq 0$ with high probability. It turns out that there exist $\alpha_{\rm ann}$, with $\alpha_{\rm d} \leq \alpha_{\rm ann} \leq \alpha_{\rm c}$, such that, if $\alpha < \alpha_{\rm ann}$,

$$\psi_{\rm ann}(\lambda) = 1 - \alpha - \lambda + \frac{1}{2\log 2}\lambda^2 + O(\lambda^3)\,. \tag{11}$$

For instance we obtain $\alpha_{\rm ann} \approx 0.889493,\ 0.967147,\ 0.989163$ for, respectively, $p = 3, 4, 5$. These bounds imply in turn

$$\left.\frac{d\psi_{\mathcal{G}}}{d\lambda}\right|_0 = -1, \qquad 0 \leq \left.\frac{d^2\psi_{\mathcal{G}}}{d\lambda^2}\right|_0 \leq \frac{1}{\log 2}. \tag{12}$$

Thus proving that $\chi^{\rm SG}_{n,N}$, $n = 1, 2$, remains bounded for $T = 0$ and $\alpha < \alpha_{\rm ann}$. In Appendix B, we argue that in fact the result remains true up to $\alpha_{\rm c}$.

3.2. Point-to-Set Correlations

A much stronger criterion for correlations decay is obtained by considering observables depending on arbitrary number of spins (i.e. not necessarily bounded

by a constant independent of N and α as in the previous Section). Here we describe a concrete way for verifying such a criterion and show that it allows to define a correlation length diverging at $T_{\rm d}(\alpha)$.

Fix a configuration $\sigma^{(0)}$ drawn from the equilibrium Boltzmann distribution at temperature T. Let $i \in \{1, \ldots, N\}$ be a site in the system and ℓ a positive integer. Consider a configuration σ distributed according to the Boltzmann measure, conditioned to $\sigma_j = \sigma_j^{(0)}$ for all sites j whose distance from i is at least ℓ. In other words, if $\mathcal{G}_\ell(i)$ denotes the subgraph including all the sites at distance smaller than ℓ from i the distribution of σ is

$$P_{\beta,\ell}(\sigma) = \begin{cases} \exp\{-\beta H(\sigma)\}/Z_{\beta,\ell} & \text{if } \sigma_j = \sigma_j^{(0)} \ \forall j \notin \mathcal{G}_\ell(i) \\ 0 & \text{otherwise.} \end{cases} \tag{13}$$

If ℓ is small, σ_i will be highly correlated with $\sigma_i^{(0)}$. However, we expect this correlation to decay as $\ell \to \infty$ if the temperature is high enough. We are therefore led to define a correlation length as follows (a similar length scale has been discussed in ref. 37)

$$\ell_{i,*}(\varepsilon) \equiv \min\left\{ \ell : \mathbb{E}_{\sigma^{(0)}} \sigma_i^{(0)} \langle \sigma_i \rangle_\ell \le \varepsilon \, , \right\}. \tag{14}$$

Here $\mathbb{E}_{\sigma^{(0)}}[\,\cdot\,]$ denotes expectation with respect to the reference configuration $\sigma^{(0)}$ and $\langle\,\cdot\,\rangle$ is the expectation with respect to the measure $P_{\beta,\ell}(\sigma)$. Our definition depends upon the parameter $\varepsilon \in (0, 1)$. However this dependency is irrelevant[6] and we can think of it as a fixed small number e.g. $\varepsilon = 0.1$.

The main result of this Section is that $\ell_{i,*}(\varepsilon)$ diverges as the dynamical transition line $T_{\rm d}(\alpha)$ is approached. More precisely, with non-vanishing probability–with respect to the choice of the site i–, we have (the thermodynamic limit being taken at the outset)

$$\ell_{i,*}(\varepsilon) \sim (T - T_{\rm d}(\alpha))^{-1/2}. \tag{15}$$

Equivalently, if the dynamical transition is approached by increasing the number of constraints in the system: $\ell_{i,*}(\varepsilon) \sim (\alpha_{\rm d}(T) - \alpha)^{-1/2}$.

Let us consider, for the sake of simplicity the case $T = 0$ and $\alpha \uparrow \alpha_{\rm d}$. The finite temperature case will be discussed in Appendix B (we also refer to Ref. 41, for a more detailed discussion of this issue). The reference configuration $\sigma^{(0)}$ is, for $T = 0$, chosen uniformly at random among the exponentially numerous unfrustrated ground states. Without loss of generality we can assume that the model is ferromagnetic and $\sigma^{(0)} = \sigma^{(+)}$ is the 'all-plus' configuration. Repeating the type of arguments already used in the previous Section, one can show that, at zero temperature, $\langle \sigma_i \rangle_\ell$ is either $+1$ (if σ_i is completely determined by the boundary

[6] The single-site Edwards Anderson order parameter[38–40] must however be larger than ε to get a non-trivial result.

condition together with the requirement of satisfying all the interactions) or 0 (in the opposite case). As a consequence $\ell_{i,*}(\varepsilon)$ does not depend upon ε: we have $\langle\sigma_i\rangle_\ell = 1$ for $\ell < \ell_{i,*}$ and $\langle\sigma_i\rangle_\ell = 0$ for $\ell \geq \ell_{i,*}$.

Let ϕ_ℓ be the probability that $\langle\sigma_i\rangle_\ell = 1$. Obviously $\phi_0 = 1$. Furthermore, for any $\ell \geq 0$, the following recursion relation holds

$$\phi_{\ell+1} = \sum_{l=0}^{\infty} e^{-p\alpha}\frac{(p\alpha)^l}{l!}\left[1-\left(1-\phi_\ell^{p-1}\right)^l\right] = 1-\exp\left\{-p\alpha\phi_\ell^{p-1}\right\}. \quad (16)$$

This formula is proved by summing over the degree of site i the probability that the degree is l (factor $e^{-p\alpha}(p\alpha)^l/l!$) times the probability that at least one of the interactions has all the remaining spins determined by their ℓ-th neighbors.

The dynamical transition point is given by

$$\alpha_{\rm d} = \sup\{\alpha \,:\, \phi > 1-\exp\{-p\alpha\phi^{p-1}\} \text{ for } \phi \in (0,1]\}. \quad (17)$$

Numerical values of $\alpha_{\rm d}$ are given in Table I. A simple asymptotic study of the recursion (16) shows that $\phi_\ell \to 0$ for $\alpha < \alpha_{\rm d}$, while $\phi_\ell \to \phi_*(\alpha)$ for $\alpha \geq \alpha_{\rm d}$, $\phi_*(\alpha)$ being the largest solution of $\phi = 1-\exp\{-p\alpha\phi^{p-1}\}$. Hereafter we shall use the notation $\phi_{\rm d} = \phi_*(\alpha_{\rm d})$. For any $p \geq 3$, $\phi_{\rm d} > 0$ and $\phi_*(\alpha) = \phi_{\rm d} + {\rm cst}\sqrt{\alpha-\alpha_{\rm d}} + O(\alpha-\alpha_{\rm d})$ for $\alpha \gtrsim \alpha_{\rm d}$. As already mentioned, $\alpha_{\rm d}$ is the critical value for the appearance of a backbone (and a 2-core) in the graph $\mathcal{G}$ and is easy to realize that its typical size is about $N\phi_*(\alpha)$ for $\alpha \geq \alpha_{\rm d}$. In the present picture, the spins in the backbone are frozen because they are determined by spins arbitrarily far away.

As $\alpha_{\rm d}$ is approached from below, the convergence of ϕ_ℓ to 0 becomes slower and slower. As can be seen in Fig. 3, ϕ_ℓ first develops a plateau near $\phi_{\rm d}$, whose length scales as $(\alpha_{\rm d}-\alpha)^{-1/2}$ and then decreases to 0 right after this plateau (i.e. it decreases below any given constant in a fixed number of iterations). The behavior around the plateau is described by the scaling form

$$\phi_\ell \simeq \phi_{\rm d} + (\alpha_{\rm d}-\alpha)^{1/2}\mathcal{K}[(\alpha_{\rm d}-\alpha)^{1/2}(\ell-\ell_0(\alpha))], \quad (18)$$

Table I. Values of the critical parameters and exponents for the minimal size rearrangements

p	$\alpha_{\rm d}$	$\phi_{\rm d}$	λ	a	b	ν
3	0.818469	0.715332	0.397953	0.422096	1.221834	1.593787
4	0.772280	0.851001	0.350174	0.433412	1.341647	1.526313
5	0.701780	0.903350	0.320971	0.439997	1.421808	1.488035
6	0.637081	0.930080	0.300707	0.444431	1.481191	1.462601
7	0.581775	0.945975	0.285554	0.447677	1.527913	1.444121
8	0.534997	0.956381	0.273649	0.450187	1.566174	1.429899
9	0.495255	0.963661	0.263961	0.452205	1.598411	1.418505
10	0.461197	0.969008	0.255868	0.453873	1.626162	1.409102

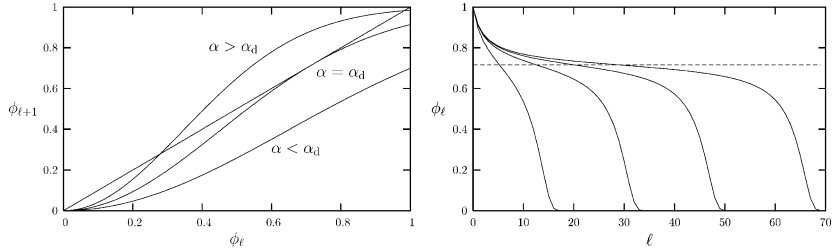

Fig. 3. Point-to-set correlation function for $p = 3$. Left: graphical representation of the recursion $\phi_{\ell+1} = 1 - \exp\left\{ - p\alpha\phi_\ell^{p-1}\right\}$. Right: function ϕ_ℓ for $\alpha = 0.75, 0.8, 0.81\ 0.814$.

where

$$\ell_0(\alpha) = \frac{\pi}{2\sqrt{A_0 A_2}}\,(\alpha_{\rm d} - \alpha)^{-1/2}\,, \qquad \mathcal{K}(x) = -\sqrt{\frac{A_0}{A_2}}\,\tan\left\{\sqrt{A_0 A_2}\,x\right\}, \tag{19}$$

and

$$\begin{aligned} A_0 &= p\phi_{\rm d}^{p-1}\, e^{-p\alpha_{\rm d}\phi_{\rm d}^{p-1}}\,, \\ A_2 &= \frac{1}{2}p(p-1)\,\alpha_{\rm d}\phi_{\rm d}^{p-3} e^{-p\alpha\phi^{p-1}}\left\{p(p-1)\alpha_{\rm d}\phi_{\rm d}^{p-1} - (p-2)\right\}. \end{aligned} \tag{20}$$

Therefore, for any given sample, a fraction $\phi_{\rm d}$ of the sites i is such that

$$\ell_{i,*}(\varepsilon) = \frac{\pi}{\sqrt{A_0 A_2}}\,(\alpha_{\rm d} - \alpha)^{-1/2} + O(1), \tag{21}$$

independently of $\varepsilon \in (0, 1)$.

To conclude this Section, in Fig. 4 we show the results of a recursive finite-T calculation of $\mathbb{E}_{\sigma^{(0)}}[\sigma_i^{(0)}\langle\sigma_i\rangle_\ell]$ as a function of ℓ, averaged over the graph realization. This allows to extract the typical point-to-set correlation length defined as

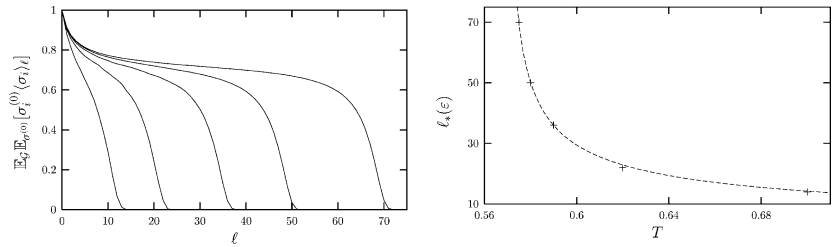

Fig. 4. *Left*: expected point to set correlation at $\alpha = 1$ and, from left to right, $T = 0.7, 0.62, 0.59, 0.58$ and 0.575, as computed using the recursive approach of Appendix B.3. Right: point-to-set correlation length $\ell_*(\varepsilon)$, as extracted from this data with $\varepsilon = 0.1$. The dashed line is a fit to this data according to the asymptotic expression $\ell_*(\varepsilon) = C\,(T - T_{\rm d})^{-1/2}$, with $T_{\rm d} = 0.51695$.

(here $\mathbb{E}_{\mathcal{G}}$ denotes expectation over the graph realization)

$$\ell_*(\varepsilon) \equiv \min\left\{ \ell : \mathbb{E}_{\mathcal{G}}\mathbb{E}_{\sigma^{(0)}}\left[\sigma_i^{(0)}\langle\sigma_i\rangle_\ell\right] \le \varepsilon \right\}. \tag{22}$$

Since $\mathbb{E}_{\mathcal{G}}\mathbb{E}_{\sigma^{(0)}}[\sigma_i^{(0)}\langle\sigma_i\rangle_\ell]$ decreases rapidly to 0 above $\ell_*(\varepsilon)$, it is not hard to argue that $\ell_{i,*}(\varepsilon) \le C_1\ell_*(\varepsilon)$ with high probability and $\ell_{i,*}(\varepsilon) > C_0\ell_*(\varepsilon)$ for a finite fraction of sites/graphs (C_0, C_1 being two positive constants). We also plot $\ell_*(\varepsilon)$ as a function of the temperature for $\varepsilon = 0.1$. As anticipated, the scaling $\ell_*(\varepsilon) \sim (T - T_{\rm d}(\alpha))^{-1/2}$ is remarkably well verified allowing for a precise determination of $T_{\rm d}(\alpha)$. The approach followed for this computation is described in Appendix B.3.

3.3. Implications for Dynamics

As we have seen, at the dynamic transition line $T_{\rm d}(\alpha)$, the point-to-set correlation length $\ell_*(\varepsilon)$ diverges. It is intuitively clear that this should induce a diverging relaxation time, associated to the (dynamical) glass transition. Imagine for instance to perturb the spin σ_i. In order for a new equilibrated configuration (under the perturbed Hamiltonian) to be produced, the effect of the perturbation must propagate over a distance at least of the order of $\ell_{i,*}$, taking a time at least of order $\ell_{i,*}$. Therefore $\ell_{i,*}$ yields (up to a finite proportionality constant) a lower bound on the relaxation time for σ_i.

Remarkably, this handwaving argument can be turned into a mathematical derivation. For doing this, we need a precise definition for the relaxation time of σ_i. We consider the spin autocorrelation function $C_i(t)$, and define

$$\tau_i(\delta) = \min\{t > 0 \,:\, C_i(t) \le \delta\}. \tag{23}$$

Notice that $C_i(t)$ is a continuous and non increasing function of t (the last property follows from the spectral representation of the Markov dynamics[42]). Therefore $C_i(t) \le \delta$ for any $t \ge \tau_i(\delta)$. The precise value of δ is irrelevant, and it should be thought as a small fixed number. Close to $T_{\rm d}(\alpha)$, we expect $C_i(t)$ to develop a plateau. The definition (23) correctly gives the slow time scale for the relaxation of σ_i as soon as δ is smaller than the plateau height, which is in turn equal to the local Edwards Anderson order parameter.[38,39]

We also need to introduce a cutoff radius $\bar{\ell}_i$: this is the largest integer ℓ such that the subgraph $\mathcal{G}_\ell(i)$ is a tree.

Proposition 1. *Assume that* $\bar{\ell}_i$, $\ell_{i,*}(2\delta) > \log_2(4/\delta)$, $\tau_i(\delta) < (\bar{\ell}_i - 1)/(2\kappa_i e)$ *and that the number of sites at distance* ℓ *from* i *is at most* κ_i^ℓ *for any* $\ell > 0$ *and some* $\kappa_i > 0$. *Then*

$$\tau_i(\delta) \ge \frac{1}{2\kappa_i e}\,\ell_{i,*}(2\delta). \tag{24}$$

Proof: The proof is an application of some probabilistic arguments developed in Refs. 43–45. For greater convenience of the reader, we shall provide a self contained presentation of most of these ideas.

Let $\sigma^{(0)}$ be an equilibrium configuration for the system under consideration, $\ell \geq 0$ an integer and recall the definition of $\mathcal{G}_\ell(i)$. Consider two Markov trajectories $\{\sigma^{(1)}(t),\ t \geq 0\}$ and $\{\sigma^{(2)}(t),\ t \geq 0\}$ defined as follows. The initial condition is the same for both processes and is given by the reference configuration $\sigma^{(0)}$: $\sigma^{(1)}(t = 0) = \sigma^{(2)}(t = 0) = \sigma^{(0)}$. At times $t > 0$, spin flips are proposed simultaneously in both systems according to the usual Glauber dynamics rule (each spin attempts a flip according to a Poisson process of rate 1). If the spin whose flip is proposed lies outside $\mathcal{G}_\ell(i)$, the flip is never accepted for $\sigma^{(1)}$, and is accepted according to the usual transition probability for $\sigma^{(2)}$. If, on the other hand, the spin which attempts a flip, let us say j, is within $\mathcal{G}_\ell(i)$, the update is done in the two systems as follows. Let $\{p_+^{(1)}, p_-^{(1)}\}$ be the probabilities for $\sigma_j^{(1)}$ to take values, respectively, $+1$ or -1 after the flip. In the case of Glauber dynamics, these are computed according to Eq. (3). Denote by $\{p_+^{(2)}, p_-^{(2)}\}$ the same transition probabilities for system (2), and assume, for instance, that $p_+^{(1)} \geq p_+^{(2)}$. Then, with probability $p_+^{(2)}$, we set $\sigma_j^{(1)} = \sigma_j^{(2)} = +1$; with probability $p_+^{(1)} - p_+^{(2)}$, we set $\sigma_j^{(1)} = +1$ and $\sigma_j^{(2)} = -1$; finally, with probability $1 - p_+^{(1)}$, $\sigma_j^{(1)} = \sigma_j^{(2)} = -1$.

Recall that the transition probabilities $p_{+/-}^{(\cdot)}$ only depend on the values of the spins on the neighbors of j. Therefore, the new values of $\sigma_j^{(1)}$, $\sigma_j^{(2)}$ will coincide whenever $\sigma_{j'}^{(1)} = \sigma_{j'}^{(2)}$ for all the sites j' at distance one from j. Furthermore, it is easy to see that when considered separately, the Markov processes $\{\sigma^{(1)}(t),\ t \geq 0\}$, $\{\sigma^{(2)}(t),\ t \geq 0\}$ have a very simple description. The latter is the usual Glauber dynamics with equilibrated initial condition $\sigma^{(0)}$. The former is Glauber dynamics for the subsystem formed by spins in $\mathcal{G}_\ell(i)$, with initial condition $\sigma^{(0)}$, and boundary condition (outside $\mathcal{G}_\ell(i)$) also given by $\sigma^{(0)}$. The joint process is in fact a "Markovian coupling" of these two dynamics.

At $t = 0, \sigma^{(1)}(t) = \sigma^{(2)}(t)$ by definition. Since the two dynamics are different outside $\mathcal{G}_\ell(i)$ $\sigma^{(1)}(t)$ and $\sigma^{(2)}(t)$ will rapidly disagree there. However, inside $\mathcal{G}_\ell(i)$, disagreement can only propagate at a finite velocity, starting from sites at distance $\ell - 1$ from i and moving inward. It is intuitively clear that, in order for the disagreement to reach σ_i, a time of order ℓ is needed. This intuition can be precised mathematically. Assume $\ell < \bar{\ell}_i$ and denote by $N(\ell)$ the number of sites at distance ℓ from i. Then

$$\mathbb{P}\left\{\sigma_i^{(1)}(s) = \sigma_i^{(2)}(s)\ \forall\, s \leq t\right\} \geq 1 - \left(\frac{et}{\ell}\right)^{\ell} N(\ell). \tag{25}$$

This inequality is essentially adapted from, Ref. 43 and we refer to this paper for a proof.

We now turn to the main steps of the proof. Using the definition of $\{\sigma^{(1)}(t)\}$ and the fact that $\langle\sigma_i^{(1)}(0)\sigma_i^{(1)}(t)\rangle$ is a non increasing function of t, we have

$$\mathbb{E}_{\sigma^{(0)}}\left[\sigma_i^{(0)}\langle\sigma_i\rangle_\ell\right] = \lim_{t\to\infty}\left\langle\sigma_i^{(1)}(0)\sigma_i^{(1)}(t)\right\rangle \le \left\langle\sigma_i^{(1)}(0)\sigma_i^{(1)}(t)\right\rangle. \tag{26}$$

Denote $\mathbb{I}(t)$ the indicator function for the event that disagreement did not percolate0 to i up to time t. More explicitly

$$\mathbb{I}(t) = \begin{cases} 1 & \text{if } \sigma_i^{(1)}(s) = \sigma_i^{(2)}(s)\ \forall\, s \le t, \\ 0 & \text{otherwise.} \end{cases} \tag{27}$$

Continuing from the above inequality we get, for $\ell < \bar{\ell}_i$,

$$\begin{aligned}
\mathbb{E}_{\sigma^{(0)}}\left[\sigma_i^{(0)}\langle\sigma_i\rangle_\ell\right] &\le \left\langle\sigma_i^{(1)}(0)\sigma_i^{(1)}(t)\right\rangle = \left\langle\sigma_i^{(2)}(0\sigma_i^{(2)}(t)\,0.\mathbb{I}(t)\right\rangle \\
&+ \left\langle\sigma_i^{(1)}(0)\sigma_i^{(1)}(t)\,[1-\mathbb{I}(t)]\right\rangle = \left\langle\sigma_i^{(2)}(0)\sigma_i^{(2)}(t)\right\rangle - \left\langle\sigma_i^{(2)}(0)\sigma_i^{(2)}(t)\right. \\
&\times [1-\mathbb{I}(t)]\rangle + \left\langle\sigma_i^{(1)}(0)\sigma_i^{(1)}(t)\,[1-\mathbb{I}(t)]\right\rangle \\
&\le \left\langle\sigma_i^{(2)}(0)\sigma_i^{(2)}(t)\right\rangle + 2\langle 1-\mathbb{I}(t)\rangle \le C_i(t) + 2\left(\frac{et}{\ell}\right)^\ell N(\ell).
\end{aligned} \tag{28}$$

Taking $t = \tau_i(\delta)$, we obtain

$$\mathbb{E}_{\sigma^{(0)}}\left[\sigma_i^{(0)}\langle\sigma_i\rangle_\ell\right] \le \delta + 2\left(\frac{e\tau_i(\delta)}{\ell}\right)^\ell N(\ell). \tag{29}$$

Now set $\ell = \max[\lceil 2\kappa_i e\tau_i(\delta)\rceil, \lceil\log_2(2/\delta)\rceil]$.[7] Under the hypothesis of the proposition, $\ell < \bar{\ell}_i$ and $N(\ell) \le \kappa_i^\ell$. Therefore

$$\mathbb{E}_{\sigma^{(0)}}\left[\sigma_i^{(0)}\langle\sigma_i\rangle_\ell\right] \le \delta + 2\,2^{-\ell} \le 2\delta. \tag{30}$$

By the definition of $\ell_{i,*}(\varepsilon)$, the above equation implies $\ell \ge \ell_{i,*}(2\delta)$ thus proving our claim (using the hypothesis $\ell_{i,*}(2\delta) > \log_2(4/\delta)$).

□

Let us comment on the hypotheses of this Proposition. For a random graph $\mathcal{G}$, $\bar{\ell}_i$ is, with high probability, close to $\log_{p(p-1)\alpha} N$.[28] The hypothesis $\bar{\ell}_i > \log_2(4/\delta)$ is therefore satisfied with high probability (although in any given sample there is a vanishing fraction of sites i for which this is not the case).

Furthermore, within any fixed distance ℓ from i, $\mathcal{F}$ converges to a (Galton-Watson) tree. The number of offspring is a Poisson variable of mean $p\alpha$ for variable nodes, while it is deterministic and equal to $(p-1)$ for function nodes.

[7] Here and in the following, $\lceil x\rceil$ denotes the smallest integer greater than or equal to x, and $\lfloor x\rfloor$ the greatest integer smaller than or equal to x.

Let $N_{\rm tree}(\ell)$ the number of ℓ-th generation descendants in such a tree. It is easy to show that, for any $\kappa > p(p-1)\alpha$, $N_{\rm tree}(\ell) < \kappa^{\ell}$ with probability approaching one as $\ell \to \infty$. On the random graph $\mathcal{G}$, the number of neighbors $N(\ell)$ is in fact smaller than on the tree. As a consequence, κ_i is finite for most of the sites in the graph and, roughly speaking, of order $p\,(p-1)\alpha$ for a finite fraction of them. On the other hand, κ_i can be much larger (diverging as $N \to \infty$) for a vanishing fraction of sites. In particular, κ_i must be at least as large as the degree of i, and the maximal degree in such a random graph scales as $\log N/\log\log N$.

Finally, the inequality (24) is only interesting in strong correlation regimes, such that $\ell_{i,*}(\varepsilon) \gg 1$. Therefore, the hypothesis $\ell_{i,*}(2\delta) > \log_2(4/\delta)$ does not imply any loss of generality.

In the previous Section we argued that the typical point to set correlation length $\ell_*(\varepsilon)$ diverges as $(T - T_{\rm d}(\alpha))^{-1/2}$ upon approaching the glass transition temperature. Therefore we obtained the following lower bound on the typical relaxation time:

$$\tau(\delta) \gtrsim (T - T_{\rm d}(\alpha))^{-1/2}. \tag{31}$$

As explained below, the usual MCT predictions agree with such a bound.

4. FROM DYNAMICS TO REARRANGEMENTS

4.1. On the Relaxation Time Divergence

The inequality (31)—along with its derivation–explicitly shows how a divergent length scale induces a divergent time scale at the (dynamical) glass transition. However, several reasons suggest that this lower bound is not tight. A first indication is provided by the usual predictions of MCT. These imply

$$\tau(\delta) \sim (T - T_{\rm d})^{-\gamma_{\rm mct}}, \qquad \gamma_{\rm mct} = \frac{1}{2a_{\rm mct}} + \frac{1}{2b_{\rm mct}}, \tag{32}$$

with $a_{\rm mct}, b_{\rm mct} > 0$ determined by the equations

$$\frac{\Gamma(1-a_{\rm mct})^2}{\Gamma(1-2a_{\rm mct})} = \frac{\Gamma(1+b_{\rm mct})^2}{\Gamma(1+2b_{\rm mct})} = \lambda_{\rm mct}, \tag{33}$$

and $\lambda_{\rm mct}$ a positive, model-dependent constant between 0 and 1. It is easy to show, using these equations (see also Sec. 5), that $a_{\rm mct} \le 1/2$, and therefore $\gamma_{\rm mct} \ge 1$. Although MCT is not exact for the model studied here, we will argue below that several of its predictions are correct (in particular, this can be shown in the fully connected limit $\alpha \to \infty$[7]). If this is accepted, it follows that Eq. (31) does not predict the correct critical exponent.

A more fundamental reason for (31) not to be tight is the following. This estimate was derived by showing that a region of linear size $\ell_{i,*}(\varepsilon)$ requires a time

at least of order $\ell_{i,*}(\varepsilon)$ to relax. This is true because a perturbation propagates at finite speed under Glauber dynamics. However, the time required for equilibration on such a length scale can easily be much larger. Information can for instance propagate by diffusion (leading to $\tau \sim \ell^2$) or equilibration time may be related to the volume rather than to the linear size of highly correlated regions.

In order to understand this point, we shall hereafter focus on the low temperature limit at $\alpha < \alpha_{\rm d}$. In this regime, the system spends most of its time in quasi-ground states, and the leading relaxation mechanisms will be "jumps" from one such low-energy configuration to a different one. Since the properties of these jumps are likely to be continuous with respect to the energy of the starting and arrival points, we shall hereafter assume them to be exact ground states.

The time scale for relaxation of spin σ_i can be estimated in this limit through a standard Arrhenius argument. We have $\tau_i \sim \exp\{\beta \Delta_i\}$, where Δ_i is the smallest energy to be overcome during a rearrangement of the system which flips σ_i (a jump). Due to the definition of our Hamiltonian (1), Δ_i is an even number. For future convenience we shall write $\Delta_i = 2b_i$, and refer to the Arrhenius law in the form

$$\tau_i \sim \exp\{2\beta b_i\}. \tag{34}$$

We will sometimes call b_i the "barrier" for spin σ_i (although, strictly speaking, the energy barrier is $2b_i$).

A formal definition of rearrangements is given below. While it is clear that energy barriers are the relevant quantities determining time scales in the Arrhenius regime, it is rather involved to evaluate them. For pedagogical reasons we shall at first neglect barriers and look for minimal size rearrangements.

4.2. Rearrangements

A rearrangement R_i for the site i is a set of sites such that i belongs to R_i, and for every interaction α, an even number of the variables in $\partial\alpha$ belongs to R_i. If one starts from a ground state and flips all the spins in R_i, a new ground state is obtained with σ_i flipped (viceversa, any two ground states which differ at site i, differ in a whole rearrangement R_i). A rearrangement R_i is "simple" if it is connected and each interaction contains either zero or two sites of R_i. In the following we shall only consider simple rearrangements, and let this restriction understood. It will be clear that, for our purposes (and in particular within the $\alpha < \alpha_{\rm d}$ regime) there is no loss of generality in this restriction. $\mathcal{R}_i$ denotes the set of all simple rearrangements R_i.

We shall consider observables defined on the set $\mathcal{R}_i$, the simplest one $n(R_i)$ being the number of sites in the rearrangement. Let us discuss the general strategy on this example. The optimal value of the observable n, and the set of optimal

rearrangements with respect to their size are, respectively,

$$n_i = \min_{R_i \in \mathcal{R}_i} n(R_i) , \qquad \mathcal{R}_i^{(n)} = \{ R_i \in \mathcal{R}_i \,|\, n(R_i) = n_i \} . \tag{35}$$

Unless it diverges with the system size (which can be checked *a posteriori*), n_i, as well as the rearrangements in $\mathcal{R}_i^{(n)}$ can be constructed "as if" the graph $\mathcal{G}$ were a tree. A formal justification for this procedure is obtained as follows. Consider the neighborhood $\mathcal{G}_\ell(i)$ of radius ℓ around i. Let $\mathcal{R}_{i,\ell}$ be the set of rearrangements for the model whose factor graph is $\mathcal{G}_\ell(i)$. Denote by $n_{i,\ell}$ ($\mathcal{R}_{i,\ell}^{(n)}$) the corresponding minimum rearrangement size (set of optimal rearrangements). It is clear that, if $n_{i,\ell} < \ell$, the rearrangements in $\mathcal{R}_{i,\ell}^{(n)}$ are also rearrangements for the whole graph $\mathcal{G}$ and therefore $n_i \leq n_{i,\ell}$. Furthermore, any rearrangement belonging to $\mathcal{R}_i$ but not to $\mathcal{R}_{i,\ell}$ has size at least ℓ. Therefore $n_i = n_{i,\ell}$ and $\mathcal{R}_i^{(n)} = \mathcal{R}_{i,\ell}^{(n)}$. Consider now a sequence of random graphs $\mathcal{G}$ of increasing size: if n_i remains finite in the thermodynamic limit, ℓ can be chosen large enough that $n_i < \ell$ and $\mathcal{G}_\ell(i)$ is a tree with high probability.

A minimum-size rearrangement on a tree (and, by the argument above, on a random graph as long as the its size is finite) can be constructed through the following recursive procedure. The root i is by definition included in R_i. In each of the interactions $\alpha \in \partial i$ of its neighborhood, exactly one variable, call it j, among the $p-1$ distinct from i, has to be included in R_i. Let $R_{j\to\alpha}$ be an optimal rearrangement for site j in the subtree containing j but not α. Then R_i is obtained by chosing, for each α, the j which minimizes $n(R_{j\to\alpha})$. For instance, each time the interaction α contains a node j of degree 1, an optimal choice is $R_{j\to\alpha} = \{j\}$: this branch of the rearrangement R_i contains just one node.

If $\mathcal{G}$ is a random graph, any finite neighborhood of site i converges to a Galton–Watson random tree[8] rooted at i, call it $\mathcal{T}(i)$. The distribution of n_i is therefore asymptotically the same as the one of minimal rearrangements for the root of such a tree. Although, for $p(p-1)\alpha > 1$, $\mathcal{T}(i)$ is infinite with non vanishing probability (corresponding to the percolation of $\mathcal{G}$), the optimal rearrangement size turns out to be finite with probability one up to $\alpha_{\rm d}$ ($>1/p(p-1)$), confirming the validity of the procedure described above.

5. REARRANGEMENTS OF MINIMAL SIZE

We consider here rearrangements of minimal size, already defined in the previous Section. In computer science language, given a solution σ of the XORSAT

[8] More precisely, a *bipartite* tree with two offspring distributions for the two types of nodes: for variable nodes, this is Poisson of mean $p\alpha$, while function nodes have a fixed number $p-1$ of offsprings.

problem, we look for the solution σ' which minimizes the Hamming distance from σ, under the condition $\sigma'_i = -\sigma_i$.

The minimal rearrangement for any given site i is necessarily connected. The recursive construction of optimal rearrangements described above implies that, as long as n_i is finite, optimal rearrangements are simple.

5.1. Recursion Relations

As shown in the previous Section, we can describe the computation of n_i assuming that the underlying factor graph is a tree (we can picture it as a large tree-like neighborhood of i). We introduce two type of messages ('cavity fields') $\{v_{j\to\alpha}\}$ and $\{u_{\alpha\to j}\}$ associated to directed edges in the factor graph $\mathcal{F}$. We define $v_{j\to\alpha}$ to be the minimum rearrangement size for site j, relative to the subtree rooted at j but *not including* α (in other words $v_{j\to\alpha} = \min n(R_{j\to\alpha})$. Analogously, $u_{\alpha\to i} + 1$ is the size of the optimal rearrangement for site i, relative to the subtree rooted at i and *including only* α among its neighbors (the $+1$ is introduced to simplify the equations below). The recursive construction described above implies the following relations

$$v_{i\to\alpha} = 1 + \sum_{\beta\in\partial i\setminus\alpha} u_{\beta\to i}, \qquad u_{\alpha\to i} = \min_{j\in\partial\alpha\setminus i}[v_{j\to\alpha}]. \tag{36}$$

Finally, the optimal rearrangement for i in the original graph is obtained by combining optimal rearrangements for the subtrees rooted at i:

$$n_i = 1 + \sum_{\alpha\in\partial i} u_{\alpha\to i}. \tag{37}$$

Given the factor graph $\mathcal{F}$, the recursions (36), (37) can be solved by iteration (message-passing) starting from the initial condition $v_{i\to\alpha} = u_{\alpha\to i} = 0$. We found that this iteration converges rapidly for typical random graphs at $\alpha < \alpha_{\rm d}$, leading to an algorithm of linear time complexity.

5.2. Probabilistic Analysis

As already explained, the (asymptotic) probability distribution of n_i can be computed by considering the random tree $\mathcal{T}(i)$ rooted at i. In this case, the messages $\{v_{j\to\alpha}\}$ and $\{u_{\alpha\to j}\}$ become random variables. Because of the construction of $\mathcal{T}(i)$, they are identically distributed. We shall denote by q_n the common distribution of the $v_{j\to\alpha}$'s and by $\hat{q}_n$ the distribution of the $u_{\alpha\to j}$'s. The distribution of n_i is also q_n because of the memoryless property of Poisson random variables. Finally, as long as the corresponding subtrees are disjoint, these random variables are independent.

The relations (36) can be interpreted as recursive distributional equations. Explicit expressions are easily written by using the cumulative distributions

$$Q_n = \sum_{n' \geq n} q_{n'}, \qquad \widehat{Q}_n = \sum_{n' \geq n} \hat{q}_{n'}. \tag{38}$$

The recursive relations (36) imply:

$$q_n = \sum_{l=0}^{\infty} p_l \sum_{n_1,\ldots,n_l} \hat{q}_{n_1} \ldots \hat{q}_{n_l}\, \delta_{n,1+n_1+\cdots+n_l}, \tag{39}$$

$$\widehat{Q}_n = Q_n^{p-1}. \tag{40}$$

Here $p_l = e^{-\alpha p}(\alpha p)^l / l!$, is the (Poisson) offsprings distribution at variable nodes.

Equations (39) and (40) uniquely determine q_n, $\hat{q}_n$ and can be easily solved numerically: knowing the q_n and $\hat{q}_n$ for $n \leq m$ one can determine $q_{m+1}, \hat{q}_{m+1}$. The starting point is given by $q_1 = p_0, \hat{q}_1 = 1 - (1 - p_0)^{p-1}$.

We present in Fig. 5 the results of this computation. When the average degree α is raised towards its critical value $\alpha_{\rm d}$, a plateau appears in the integrated probability law Q_n (for $p \geq 3$), at $Q_n \approx \phi_{\rm d}$. This means that a fraction $\phi_{\rm d}$ of the spins σ_i have diverging minimum rearrangement size, consistently with the picture of freezing of some spins at the clustering transition $\alpha_{\rm d}$. These are of course the same spins for which ℓ_i diverges upon approaching the transition, cf. Sec. 3.2. They will belong to the backbone after the addition of a small fraction of constraints.

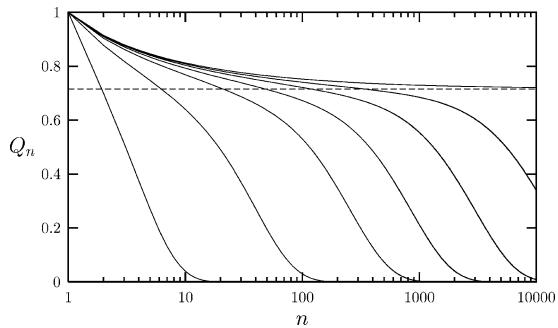

Fig. 5. The integrated distribution law of the minimal size of rearrangements. $p = 3$, from left to right $\alpha = 0.4, 0.7, 0.78, 0.8, 0.81, 0.815, \alpha_{\rm d}$. The dashed horizontal line is the order parameter at the transition, $\phi_{\rm d} \approx 0.715332$.

5.3. Asymptotic Behavior of the Distribution

The curves of Fig. 5 are strongly reminiscent of the time correlation functions obtained in the mode coupling theory of supercooled liquids. Indeed, the Eqs. (39) and (40) have a structure similar to the one of schematic MCT equations, cf. also Appendix C.1. The analogy becomes even stronger if we consider the asymptotic behavior as $\alpha \to \alpha_{\rm d}$: we present here a summary of results, while calculations are deferred to Appendix C.1.

For $\alpha = \alpha_{\rm d}$, the decay of Q_n towards its plateau value is algebraic, $Q_n \simeq \phi_{\rm d} + {\rm cst}\, n^{-a}$ as $n \to \infty$ (here and below cst denotes a generic positive constant). The exponent a is the positive solution of the transcendental equation

$$\frac{\Gamma^2(1-a)}{\Gamma(1-2a)} = \lambda, \tag{41}$$

where $\lambda = (p-2)/[\alpha_{\rm d} p(p-1)\phi_{\rm d}^{p-1}] \in [0,1]$ is a non-universal parameter. A graphical representation of this equation is provided in Fig. 6.

In the critical region $\alpha \lesssim \alpha_{\rm d}$, one can identify two distinct scaling regimes. The first one is $n \sim (\alpha_{\rm d} - \alpha)^{-1/2a}$, and corresponds to the behavior of Q_n around its plateau. We get

$$Q_n \simeq \phi_{\rm d} + (\alpha_{\rm d} - \alpha)^{1/2}\, \epsilon\big((\alpha_{\rm d} - \alpha)^{1/2a} n\big)\,, \tag{42}$$

where $\epsilon(\,\cdot\,)$ is a scaling function. One can show that $\epsilon(t) \simeq {\rm cst}\, t^{-a}$ as $t \to 0$ (thus matching the behavior at $\alpha = \alpha_{\rm d}$ and n fixed) and $\epsilon(t) \sim -{\rm cst}\, t^b$ as $t \to \infty$. The positive exponent b is fixed through

$$\frac{\Gamma^2(1+b)}{\Gamma(1+2b)} = \lambda\,, \tag{43}$$

see Fig. 6.

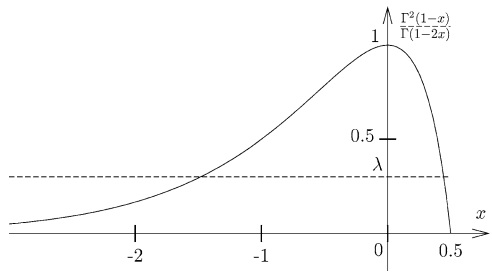

Fig. 6. The exponent a (respectively $-b$) is the positive (respectively negative) root of the equation represented here, see Eqs. (41), (43).

The second regime corresponds to the decay of Q_n from the plateau at ϕ_d to 0 and is defined by $n \sim (\alpha_d - \alpha)^{-\nu}$, where

$$a\nu = \frac{1}{2a} + \frac{1}{2b} \,. \tag{44}$$

We get the scaling form

$$Q_n \simeq Q_{\text{slow}}((\alpha_d - \alpha)^{\nu} n) \,, \tag{45}$$

with $Q_{\text{slow}}(t)$ a second scaling function. One finds that $Q_{\text{slow}}(t) \simeq \phi_d - \text{cst}\ t^b$ as $t \to 0$, while $Q_{\text{slow}}(t)$ vanishes faster than exponentially as $t \to \infty$. Numerical values of the various exponents for some values of p are collected in Table I.

Notice that the scale $(\alpha_d - \alpha)^{-\nu}$ has a very concrete interpretation. For any $\varepsilon > 0$, one may ask what is the smallest size n_ε, such that all but a fraction ε of the sites have a minimal rearrangement whose size is at most n_ε. If $\varepsilon < \phi_d$, one has $n_\varepsilon \sim (\alpha_d - \alpha)^{-\nu}$.

6. REARRANGEMENTS OF MINIMAL BARRIER

In the low temperature limit, the time scale for the occurrence (flip) of a rearrangement R_i, is given in terms of the corresponding energy barrier $b(R_i)$ by the Arrhenius law, cf. Eq. (34). In the previous Section we explained how to optimize R_i with respect to a simple observable: its size $n(R_i)$. We want now to apply the same strategy to a more involved quantity, the barrier $b(R_i)$, and use the result to estimate the relaxation time τ_i.

Before dwelling into the actual computation, it is worth stressing that energy barriers (and their distribution) are directly related to auto-correlation functions. Consider a spin i of barrier b_i. If b is a real number, fixed in the $\beta \to \infty$ limit, then

$$\lim_{\beta\to\infty} C_i(t = e^{2\beta b}) = \begin{cases} 1 & \text{if } b < b_i \,, \\ 0 & \text{if } b > b_i \,, \end{cases} \tag{46}$$

Let $Q^{\text{site}}_{[b]}$ (cf. also Sec. 6.4) be the fraction of sites i such that $b_i > b$. By averaging the above equation over the site, we obtain

$$\lim_{\beta\to\infty} C(t = e^{2\beta b}) = Q^{\text{site}}_{[b]} \,. \tag{47}$$

6.1. General Considerations

Let us first expose the basic idea in an informal way. Given a rearrangement R_i, consider the paths in configuration space[9] which lead from a ground state σ

[9] These are sequences of configurations such that any two successive configurations differ by one spin flip.

to the one obtained by flipping all the spins in R_i. The barrier $b(R_i)$ associated to this rearrangement will be the minimum among all paths of the maximal energy along the path. If we let $b_i = \min_{R_i} b(R_i)$, the asymptotic relaxation time for spin σ_i can be determined through Eq. (34).

Paths in configuration space are definitely complex objects. Let us make the simplifying assumption that on the optimal ones, each variable of the system is flipped at most once. In the worst case, under this assumption we will get an upper bound on b_i. We think that this upper bound is in fact tight: in Sec. 6.7 we shall provide a lower bound supporting this claim. Numerical experiments, cf. Sec. 8 also confirm this hypothesis.

Paths are thus defined by (i) the set of variables which are flipped, R_i; (ii) the order in which they are flipped, i.e. a permutation of the site indices in R_i. Arguing as in Sec. 4.2, one can show that, as long as optimal rearrangements remain finite in the thermodynamic limit, we can assume that R_i is simple. Their typical size will be computed in Sec. 7.1 validating this assumption for any $\alpha < \alpha_{\rm d}$.

Let us first consider the task of optimizing over (ii), i.e. the ordering of spins, for a given choice of the rearrangement R_i. Take the spins of the rearrangement to be the vertices of a graph, and put an edge between any two vertices corresponding to interacting spins. The resulting graph will be a tree with high probability as long as R_i is finite.

Imagine to put a ferromagnetic Ising model on this tree, with all spins initially up, and to flip them in the order defining our paths in configuration space. The energy of the original system along the path which flips R_i is equal to the one of this fictitious ferromagnetic Ising model. Therefore, $b(R_i)$ is just the energy barrier to be crossed for reversing the spins of a ferromagnetic Ising model defined on a tree associated to R_i (by flipping each spin exactly once). In the following Section we shall study this problem and define one way to solve it. Then we turn back to the optimal choice of the rearrangement R_i, cf. point (i).

6.2. The Minimal Cut-Width Problem and the Disjoint Strategy

As a first step, we must compute the energy barrier for reversing the spins of a ferromagnetic Ising model defined on a tree. For the sake of simplicity, we shall define the energy of this fictitious model as the number of links between spins with different values (plus and minus). The energy in the original model can be recovered by multiplying by a factor 2.

This problem was considered in Ref. 46, which gave an heuristic prediction of the behavior of b_i for large trees, and in Ref. 47, which considered the case of regular tree.

It is instructive to study two very simple instances of the problem. The first one is the case of an unidimensional graph of n sites. The optimal flipping order

consists obviously in starting from one end of the chain and then proceed along it by flipping successively neighboring variables. The minimal energy barrier in this example is then 1. Consider as a second simple case a star-like graph with one central site connected to l neighbors. After an instant of thought, one realizes that the minimal barrier is obtained by flipping first half of the external spins, then the central one, and finally the remaining half of the external sites. The energy barrier, achieved just before or just after the flip of the central site, is $\lceil \frac{l}{2} \rceil$.

An useful graphical representation of the problem is the following. If one draws the graph with its vertices aligned on an horizontal axis, ordered according to the temporal sequences in which the spins are flipped, the energy at a given instant of time is simply the number of edges which are drawn above this point of the temporal axis. The energy barrier is crossed at the point where this number of edges is maximal. In fact the problem of finding the ordering which minimizes the energy barrier is known in graph theory as the minimal cut-width problem, (see Ref. 59 for a review. On general graphs minimal cut-width is NP-complete. However, it becomes polynomial when restricted to particular families of graphs, such as trees.[60,61] We shall present now a simple strategy, known as *disjoint combination*,[60] which allows to construct "quasi optimal" orderings. The errors induced by this simple approach, together with the optimal strategy, are discussed in Sec. 6.6.

As often, a tree-structured problem is efficiently tackled by a recursive approach: if one knows a solution on a sub-tree, it is enough to combine the solution of the different branches to obtain a solution on the original tree. More precisely, let us consider a rooted tree T composed of the root 0 and l sub-trees $T_1, \ldots, T_l$, rooted at vertices $1, \ldots, l$. We shall denote by ϑ (respectively $\vartheta_1, \ldots, \vartheta_l$) a permutation of the vertices of T (resp. $T_1, \ldots, T_l$). Our aim is to find the optimal ϑ, as defined above. Within the disjoint strategy, one restricts to trajectories ϑ which forbid having two partially flipped sub-trees at the same time. In other words, one chooses a permutation π of $[1, l]$, an integer $j \in [0, l]$, and flips first all variables of the sub-tree $T_{\pi(1)}$, then those of $T_{\pi(2)}$, and so on until $T_{\pi(j)}$, then one flips the root 0, and proceed with the sub-trees $T_{\pi(j+1)}, \ldots, T_{\pi(l)}$. The permutation ϑ thus takes the form $(\vartheta_{\pi(1)}, \ldots, \vartheta_{\pi(j)}, 0, \vartheta_{\pi(j+1)}, \ldots, \vartheta_{\pi(l)})$. An example is provided in Fig. 7, where the rooted sub-trees are represented as bubbles. The optimization with respects to ϑ is now an optimization with respects to π, j and the sub-trajectories $\vartheta_1, \ldots, \vartheta_l$. The crucial simplification of the disjoint strategy is that the trajectories of the different sub-trees are non-overlapping in time (this is clear on Fig. 7), and can thus be performed independently of each other. Indeed, let us define $b(T, \vartheta)$ as the maximal energy encountered during the flips of a rooted tree T following the ordering ϑ, and $b_>(T, \vartheta)$ (resp. $b_>(T, \vartheta)$) the maximal energy encountered before (resp. after) the root of T has been flipped. From the graphical representation of Fig. 7, and considering the maximal energy reached in each period of time

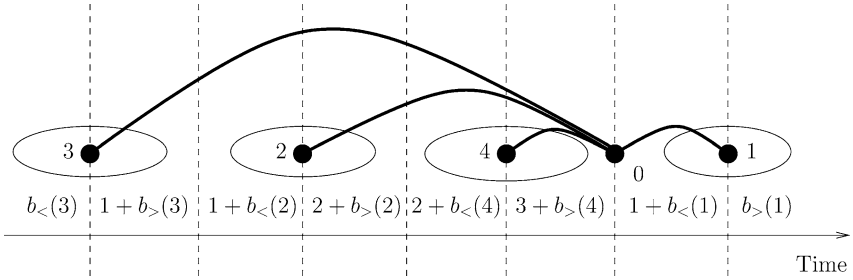

Fig. 7. The disjoint strategy. $l = 4$, $j = 3$, $\pi = (3, 2, 4, 1)$, we used the shorthand notations $b_>(i) = b_>(T_i, \vartheta_i)$, $b_>(i) = b_>(T_i, \vartheta_i)$. The numbers indicate the maximal energy inside each time epoch, delimitated by dashed lines.

corresponding to a different sub-tree, it is easy to convince oneself that

$$\begin{aligned} b(T, \vartheta) = \max \big\{ & b_>(T_{\pi(1)}, \vartheta_{\pi(1)}), 1 + b_>(T_{\pi(1)}, \vartheta_{\pi(1)}), \dots, j-1 \\ & + b_>(T_{\pi(j)}, \vartheta_{\pi(j)}), j + b_>(T_{\pi(j)}, \vartheta_{\pi(j)}), l - j \\ & + b_>(T_{\pi(j+1)}, \vartheta_{\pi(j+1)}), l - j - 1 + b_>(T_{\pi(j+1)}, \vartheta_{\pi(j+1)}), \dots, l \\ & + b_>(T_{\pi(l)}, \vartheta_{\pi(l)}), b_>(T_{\pi(l)}, \vartheta_{\pi(l)}) \big\}. \end{aligned} \tag{48}$$

The minimal barrier $b(T)$ within the disjoint strategy is then obtained by minimizing over π, j and the ϑ_i's. From the above expression it follows that the last optimization can be done independently, leading to an expression of the form $b(T) = f_l(\hat{b}(T_1), \dots, \hat{b}(T_l))$, where

$$\begin{aligned} f_l(\{\hat{b}_i\}) \equiv \min_{\pi, j} \max \big\{ & \hat{b}_{\pi(1)}, 1 + \hat{b}_{\pi(2)}, \dots, j - 1 + \hat{b}_{\pi(j)}, l - j - 1 \\ & + \hat{b}_{\pi(j+1)}, \dots, 1 + \hat{b}_{\pi(l-1)}, \hat{b}_{\pi(l)} \big\}, \end{aligned} \tag{49}$$

and $\hat{b}(T)$ is defined for an arbitrary rooted tree T by

$$\hat{b}(T) = \min_{\vartheta} \max[b_>(T, \vartheta), 1 + b_>(T, \vartheta)]. \tag{50}$$

The last quantity is the minimal energy barrier for the tree T supplemented by a link (*'anchor'*) between its root and a fictitious spin which is never flipped, hence the shift $+1$ on the energy after the flip of the root. Note that $\hat{b}(T)$ does not change if we inter-vert the role of $b_<$ and $b_>$ in the definition, a property which has been used in deriving Eq. (49). In other words, the relevant information on the sub-trees needed to choose the ordering ϑ is not their optimal barrier b but the anchored barrier $\hat{b}$. This happens because one has to take into account the energy of the links between the root 0 and the roots of the sub-trees.

The expression (49) for f_l can be simplified by noticing that for an optimal permutation π, the minimum with respect to j is reached for $j = \lceil \frac{l}{2} \rceil$. We get therefore

$$f_l(\{\hat{b}_i\}) = \min_{\pi} \max_{i \in [1,l]} \left[\hat{b}_{\pi(i)} + \left\lfloor \frac{i-1}{2} \right\rfloor \right]. \tag{51}$$

A slightly different recursive equation holds (within the disjoint strategy) for the anchored barriers. We have in fact $\hat{b}(T) = \hat{f}_l(\{\hat{b}(T_1), \ldots, \hat{b}(T_l)\})$, where

$$\begin{aligned} \hat{f}_l(\{\hat{b}_i\}) \equiv \min_{\pi, j} \max[&\hat{b}_{\pi(1)}, 1 + \hat{b}_{\pi(2)}, \ldots, j-1 \\ &+ \hat{b}_{\pi(j)}, l - j + \hat{b}_{\pi(j+1)}, \ldots, 2 + \hat{b}_{\pi(l-1)}, 1 + \hat{b}_{\pi(l)}]. \end{aligned} \tag{52}$$

Again the optimal choice of j is $\lceil \frac{l}{2} \rceil$, and the above expression simplifies to

$$\hat{f}_l(\hat{b}_1, \ldots, \hat{b}_l) = \min_{\pi} \max_{i \in [1,l]} \left[\hat{b}_{\pi(i)} + \left\lfloor \frac{i}{2} \right\rfloor \right]. \tag{53}$$

For a tree T containing only the root and no edge, one defines $b(T) = 0$, $\hat{b}(T) = 1$. Using this initial condition the above recursions can be efficiently applied to any tree. In particular one can reproduce the results of the two simple examples quoted before (linear and star-like trees).

6.3. Application to the p-Spin Model

Let us now come back to the original problem of determining the minimal energy barrier to flip one variable, say σ_i, in the p-spin model (1), ending up in a ground state. With respect to the computation presented in the previous Section, we have one more degree of freedom to optimize on: the choice of the rearrangement R_i. This step can also be performed recursively. For each of the function nodes α adjacent to i, we must choose a variable node $j \neq i$ in $\partial\alpha$, which belongs to R_i. The choice is of course dictated by the minimization of the anchored energy barrier in the corresponding cavity graph. Using again the message notation, we have

$$u_{\alpha \to i} = \min_{j \in \partial\alpha \setminus i} [v_{j \to \alpha}], \qquad v_{i \to \alpha} = \hat{f}_{|\partial i|-1}(\{u_{\beta \to i}\}_{\beta \in \partial i \setminus \alpha}), \tag{54}$$

where by convention $\hat{f}_0 = 1$. Given the graph $\mathcal{G}$, these equations can be efficiently solved through an iterative (message-passing) procedure starting with the initial condition $v_{i \to \alpha} = u_{\alpha \to i} = 0$. The minimal energy barrier to flip the variable i is then computed using:

$$b_i = f_{|\partial i|}(\{u_{\alpha \to i}\}_{\alpha \in \partial i}), \tag{55}$$

with $f_0 = 0$: an isolated spin can be flipped without modifying the energy of the system.

6.4. Probabilistic Analysis

If we now consider a random graph $\mathcal{G}$, the messages on the edges of the factor graph are random variables, with laws q_b for the messages v, and $\hat{q}_b$ for the u's. We use the same notation as in Sec. 5, there should not be confusion between the two computations. Capital letters denote again cumulative distributions $Q_b = \sum_{b' \geq b} q_{b'}$, $\widehat{Q}_b = \sum_{b' \geq b} \hat{q}_{b'}$.

Arguing as in Sec. 5.2, one can show that the recursions (54) imply the following distributional equations

$$q_b = \sum_{l=0}^{\infty} p_l \sum_{b_1,\ldots,b_l} \hat{q}_{b_1} \ldots \hat{q}_{b_l}\, \delta_{b,\, \hat{f}_l(b_1,\ldots,b_l)}\,, \qquad \widehat{Q}_b = Q_b^{p-1}, \tag{56}$$

where $p_l = e^{-p\alpha}\,(p\alpha)^l / l!$ is the Poisson distribution of parameter $p\alpha$, and we set by convention $\hat{f}_0 = 1$. The distribution for the barriers[10] b_i is then obtained using Eq. (55):

$$q_b^{\text{site}} = \sum_{l=0}^{\infty} p_l \sum_{b_1,\ldots,b_l} \hat{q}_{b_1} \ldots \hat{q}_{b_l}\, \delta_{b,\, f_l(b_1,\ldots,b_l)}\,. \tag{57}$$

Here, by convention, $f_0 = 0$.

The Eqs. (56) to (57) can be solved numerically, even if this task is a bit more involved than for the distributions of minimal size rearrangements. Some details can be found in Appendix C.2.2. The results are plotted in Fig. 8, for several values of α approaching α_{d}.

6.5. Asymptotic Behavior of the Distribution

The critical behavior of[11] Q_b, cf. Fig. 8, presents some similarities with the distribution of minimal size rearrangements. As α_{d} is approached, a plateau develops at $Q_b \approx \phi_{\text{d}}$. Eventually Q_b decreases to 0 at a scale b diverging as $\alpha \to \alpha_{\text{d}}$. The precise critical behavior can be derived analytically revealing both analogies and differences, cf. Appendix C.2.3 for technical details. Here is an overview of the results.

At the critical point $\alpha = \alpha_{\text{d}}$, the plateau is approached exponentially, $Q_b \simeq \phi_{\text{d}} + \text{cst}\; e^{-\omega_a b}$ as $b \to \infty$. The parameter ω_a is the unique positive root of the

[10] The cumulative distribution of b_i was simply denoted as Q_b in Ref. 25.

[11] For notational simplicity we refer to Q_b rather than to Q_b^{site}: the two distributions have indeed the same behavior.

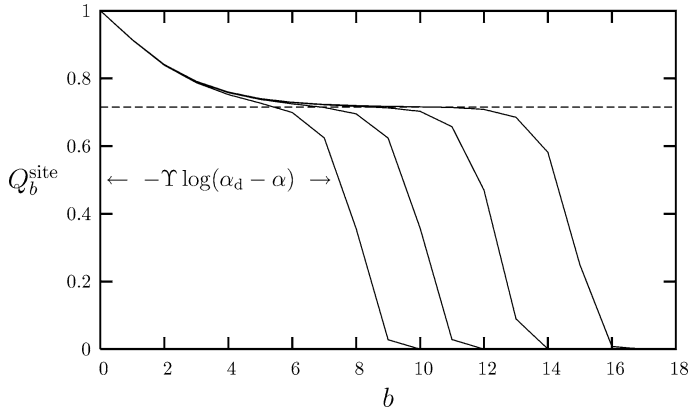

Fig. 8. Integrated law for the distribution of barriers, plotted from left to right for $\alpha = 0.816, 0.818, 0.8184, 0.81846$.

equation

$$2e^{\omega_a} - e^{2\omega_a} = \lambda \ , \tag{58}$$

where λ is defined as for minimal size rearrangements, cf. Eq. (41). A graphical representation of this equation is provided in Fig. 9, and numerical values of the solution can be found in Table II.

The scaling regime describing the plateau is defined by $\alpha \to \alpha_{\rm d}$ with $b - b_0(\alpha)$ fixed, where $b_0(\alpha) \equiv -\frac{1}{2\omega_a}\log(\alpha_{\rm d} - \alpha)$. The form of the cumulative distribution in this limit is

$$Q_b \simeq \phi_{\rm d} + (\alpha_{\rm d} - \alpha)^{1/2}\ \bar{\epsilon}_{b-b_0(\alpha)} \ . \tag{59}$$

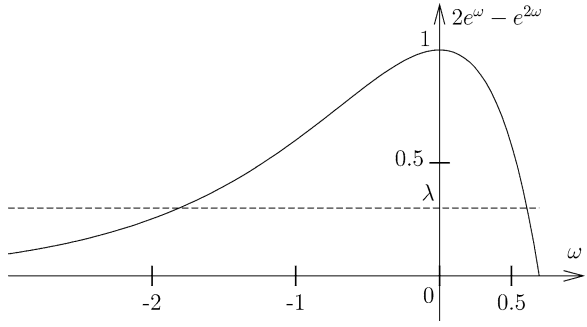

Fig. 9. The parameter ω_a (respectively $-\omega_b$) is the positive (resp. negative) root of the equation represented here, cf. Eqs. (58), (60).

Table II. Exponents for the minimal barrier rearrangements.

p	ω_a	ω_b	Υ	μ_a	μ_b	$\nu_{\rm barr}$
3	0.574317	1.495740	1.204882	0.816504	3.903496	2.015719
4	0.591180	1.640504	1.150551	0.798466	4.164498	1.944590
5	0.601050	1.737456	1.119655	0.787987	4.341305	1.904838
6	0.607719	1.809338	1.099093	0.780941	4.473350	1.878702
7	0.612614	1.865937	1.084136	0.775785	4.577858	1.859868
8	0.616408	1.912315	1.072615	0.771801	4.663830	1.845467
9	0.619461	1.951413	1.063378	0.768599	4.736535	1.833994
10	0.621990	1.985085	1.055750	0.765953	4.799310	1.824570

Here $\bar{\epsilon}_m$ is a scaling function defined on the integers. One can show that $\bar{\epsilon}_m \simeq \text{cst}\, e^{-\omega_a m}$ as $m \to -\infty$ and $\bar{\epsilon}_m \simeq -\text{cst}\, e^{\omega_b m}$ as $m \to \infty$, where

$$2e^{-\omega_b} - e^{-2\omega_b} = \lambda \,. \tag{60}$$

This implies that Q_b decreases from the plateau to 0 on a scale $b \simeq -\Upsilon \log(\alpha_{\rm d} - \alpha)$, where

$$\Upsilon = \frac{1}{2\omega_a} + \frac{1}{2\omega_b} \,. \tag{61}$$

More precisely, for any $Q_* \in (0, \phi_{\rm d})$, the smallest b such that $Q_b < Q_*$, say b_*, behaves as $b_* = -\Upsilon \log(\alpha_{\rm d} - \alpha) + O(1)$.

Finally, as $b \to \infty$, the cumulative distribution vanishes faster than exponentially: $Q_b \sim \exp\{-(2b)\log(2b)\}$. Barriers significantly larger than $-\Upsilon \log(\alpha_{\rm d} - \alpha)$ are therefore very rare and related to sites of exceptionally large degree l (leading, as in the simple example of star-like graphs, to $b \approx \lfloor l/2 \rfloor$).

6.6. Yannakakis Algorithm and Single Sample Analysis

The computation of energy barriers in the previous Sections relied on two assumptions. First, we assumed that along an optimal trajectory in phase space, each spin of the system is flipped at most once. We showed that the problem is then reduced to the computation of the minimal cut-width of a tree (once the rearrangement R_i is given). The second hypothesis was the use of the disjoint combination strategy to determine the minimal cut-width. Here we begin by revisiting this second assumption, further analytical arguments will be presented in the next Section.

In general the disjoint combination strategy is not able to find the minimal cut-width of a tree, and provides only an upper bound on it. The simplest example is provided by a binary tree (in which each vertex has two "sons") of height (number of generations) 5. As shown on the upper part of Fig. 10, the disjoint strategy

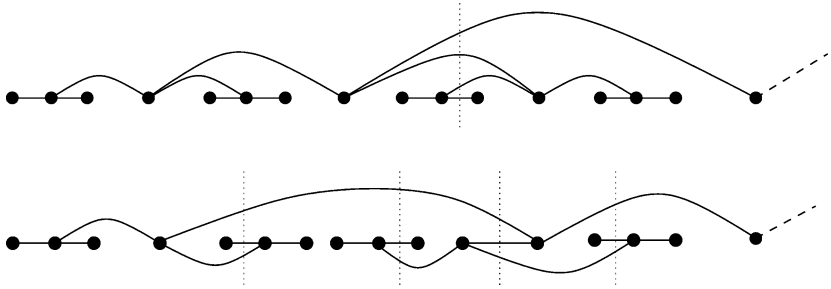

Fig. 10. Minimal cut-width problem for a binary tree of 5 generations (only one half of the tree is represented, the second follows by symmetry). *Top*: ordering produced according to the disjoint combination strategy, with a cut-width of 4 reached on the dotted line. *Bottom*: an optimal ordering of cut-width 3.

predicts in this case a minimal cut-width equal to 4. However, the ordering in the lower part of Fig. 10 achieves a cut-width equal to 3. This ordering is not disjoint: there are points in the horizontal time axis such that two height–3 subtrees are partially flipped.

Yannakakis has presented in Ref. 60 an algorithm which solves exactly the minimal cut-width problem for any tree in polynomial time. This procedure is quite involved. We shall recall here a few selected features which are relevant for the application to our case.[12] The computation relies on the definition for any rooted tree T of a cost function $c(T)$, which is a sequence of integers. The length of $c(T)$ can, in principle, be as large as the number of vertices in T. The cost function contains, along with the minimal cut-width of T, additional informations which were discarded in the disjoint strategy. Furthermore, it has two crucial properties:

- It can be computed recursively. If the root of T has l sons, which are roots of the sub-trees $T_1, \ldots, T_l$, there is a function f_l^{Y} such that $c(T) = f_l^{\mathrm{Y}}(c(T_1), \ldots, c(T_l))$.
- The cost of two trees can be compared. More precisely, there exists an order relation among costs, and the application f_l^{Y} is monotonously increasing with respects to this relation.

We want to compute the minimal barrier for a spin i in a given p-spin sample, by optimizing over the rearrangement R_i and the flipping order of the spins in R_i. Thanks to the two properties above, this task can be accomplished through an iterative message–passing procedure which uses Yannakakis strategy. Messages $u_{\alpha\to i}$ and $v_{i\to\alpha}$ are now cost functions, obeying Eqs. (54), where the minimum is taken in the sense of the order relation on cost functions, and $\hat{f}_l$ is replaced

[12] A C implementation of the algorithm is available upon request to the authors.

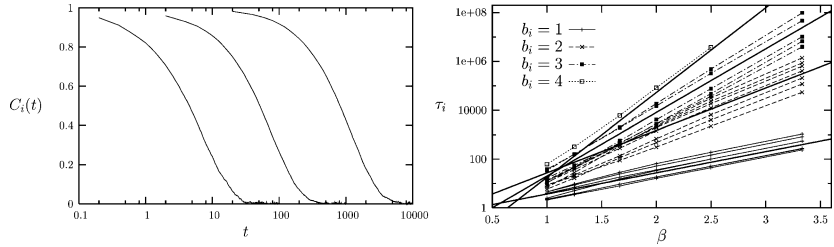

Fig. 11. Monte Carlo study of a sample of size $N = 10^4$, $\alpha = 0.6$. Local correlation functions are measured by averaging over $2 \cdot 10^3$ to 10^5 runs depending on the temperature. *Left*: local correlation function $C_i(t)$ for one spin, from left to right $T = 1$, $T = 0.5$, $T = 0.3$. *Right*: local correlation times τ_i for 20 spins of the sample, defined as $C_i(\tau_i) = 0.5$. *Bold solid lines* correspond to Arrhenius law (34) with $b_i = 1, 2, 3, 4$. The *symbols* are chosen according to the computation of b_i with the algorithm of Sec. 6.6: 7 sites have $b_i = 1$, 7 $b_i = 2$, 5 $b_i = 3$ and 1 $b_i = 4$.

by f_l^{Y}. When the fixed point of these equations has been reached, the optimal cost function for any spin is given by $c_i = f_{|\partial i|}^{\mathrm{Y}}(\{u_{\alpha\to i}\}_{\alpha\in\partial i})$. The minimal energy barrier b_i is then one piece of the information contained in c_i.

As explained before, one expects that the local correlation time τ_i of spin i is given, in the low temperature limit, by the Arrhenius law (34). We checked this fact by Monte Carlo simulations. Some results are presented in Fig. 11. On a given sample $\mathcal{G}$ of size $N = 10^4$, and constraints density $\alpha = 0.6$, we measured the correlation functions $C_i(t)$ for 20 randomly chosen spins, at various temperatures. We generated the equilibrium initial configurations efficiently using the property proved in Appendix A. In order to avoid the slowing down of usual Metropolis-type algorithms in the low-temperature limit, we implemented an n-fold Monte Carlo algorithm.[54] A few examples of correlation functions are shown in the left panel of Fig. 11. We estimated the auto-correlation time τ_i from $C_i(\tau_i) = 1/2$. The behavior of τ_i as a function of the temperature is plotted in the right panel of the same figure for 20 different sites. As expected, $\log \tau_i(\beta)$ grows linearly with β (with integer slope) at small enough temperature. The barriers b_i, computed with the algorithm of this Section, are in perfect agreement with the slopes. An interesting open problem would be the computation of the prefactor in the Arrhenius law, which might be related to the degeneracy of minimal barrier rearrangements.

The example of Fig. 10 shows that the disjoint combination algorithm does not predict the correct barrier for a general tree.[13] However balanced trees are quite special. The relevant question is whether for the random trees appearing in our model, the disjoint strategy yields in most cases the correct prediction. In particular we are interested in the critical limit $\alpha \to \alpha_{\mathrm{d}}$. Is the large rearrangements

[13] On the other hand, it has been proved[61] that the disjoint estimate is always within a factor 2 from the correct barrier.

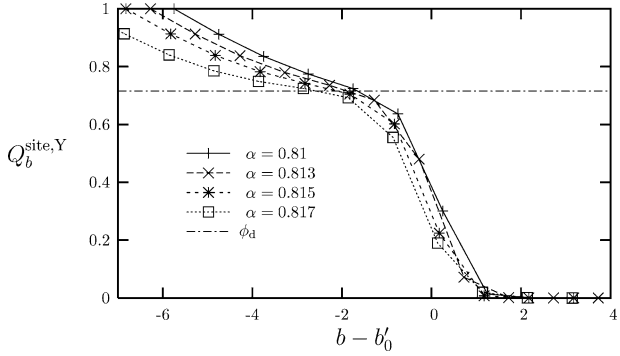

Fig. 12. The large scale part of the integrated distribution of barriers computed with Yannakakis algorithm.

divergence $b \sim -\Upsilon \log(\alpha_{\mathrm{d}} - \alpha)$ modified when barriers are computed adopting the exact Yannakakis strategy?

Unfortunately, the intricate character of the cost functions in Yannakakis algorithm forbids an analytical study of the corresponding barrier distribution along the lines of Secs. 6.4 and 6.5. We thus resorted to a numerical computation of $Q_b^{\mathrm{site,Y}}$ by running the message passing algorithm described above on large samples.

The distribution $Q_b^{\mathrm{site,Y}}$ obtained in this way has the same qualitative behavior as Q_b^{site} (cf. Fig. 8). As $\alpha \to \alpha_{\mathrm{d}}$, a plateau develops at $Q_b^{\mathrm{site,Y}} \approx \phi_{\mathrm{d}}$, whose length diverges at α_{d}. The main consequence of passing from disjoint to Yannakakis strategy is a finite (as $\alpha \to \alpha_{\mathrm{d}}$) shift of the cumulative distributions towards smaller b's. We plot in Fig. 12 $Q_b^{\mathrm{site,Y}}$ for several values of α as a function of $b - b'_0(\alpha)$, where $b'_0 = -\Upsilon \log(\alpha_{\mathrm{d}} - \alpha)$ is the typical size of large barriers within the disjoint strategy, cf Eq. (61). The good collapse of the part of the curve under the plateau supports the claim that the disjoint strategy is asymptotically optimal as $\alpha \to \alpha_{\mathrm{d}}$ and that the true barriers diverge indeed with the same law $-\Upsilon \log(\alpha_{\mathrm{d}} - \alpha)$. Further numerical evidence of this claim will be discussed in Sec. 8.

6.7. Lower Bound on the Minimal Barriers

Starting from Sec. 6.1, we assumed so far that minimum barriers can be computed restricting to trajectories such that each spin is flipped at most once along any of them ('one-spin-flip' trajectories). The numerical data presented in the previous Section give some credibility to this hypothesis. If, on the other hand, the hypothesis were not correct, the calculations of the previous pages would only provide an upper bound on the barrier size.

In this Section we will show that, removing this simplifying hypothesis, we can still construct a lower bound on the barrier size. As a consequence, we can control the error introduced by restricting to one-spin-flip trajectories. While the lower bound is not tight, it gives further support to the claim that the behavior $b \simeq -\Upsilon \log(\alpha_{\rm d} - \alpha)$ for the typical barrier of large scale rearrangements is indeed exact.

We start by recalling that, as argued in Sec. 4.2, we can restrict ourselves to the case of a tree graph $\mathcal{G}$ (eventually by considering a finite neighborhood of the site i). For simplicity of exposition, we shall first assume that the rearrangement R_i is fixed (later on we will have to optimize over R_i). As in Sec. 6, we can therefore focus on the problem of computing (a lower bound on) the energy barrier for flipping all the spins of an Ising model on a tree T rooted at i. Let σ be a configuration of such a model and $E(\sigma)$ the number of edges joining a plus and a minus spin in T (one half of the usual energy). The barrier b_i was originally defined as the minimum over all the trajectories $\{\sigma(t)\}$ joining the two ground states $\sigma^{(+)}$ and $\sigma^{(-)}$, of the maximum along the trajectory of $E(\sigma(t))$.

An equivalent (dual) definition can be obtained as follows. Let $\kappa : \{\pm 1\}^T \to \{\pm 1\}$ be a function of the configuration σ such that $\kappa(\sigma^{(+)}) = +1$ and $\kappa(\sigma^{(-)}) = -1$. Furthermore, let $\partial\kappa$ be the set of configurations σ such that $\kappa(\sigma) = +1$ and $\kappa(\sigma^{(i)}) = -1$ for some i. Here $\sigma^{(i)}$ is the configuration obtained from σ by flipping the i-th spin. It is easy to show that

$$b_i = \max_{\kappa} \min_{\sigma \in \partial\kappa} E(\sigma). \tag{62}$$

In order to construct a lower bound on b_i, we just need to exhibit a function $\kappa(\sigma)$. Computing the minimum over $\sigma \in \partial\kappa$ is of course quite difficult for a generic function $\kappa(\sigma)$. Our plan is to define $\kappa(\sigma)$ recursively, exploiting the tree structure of the graph. This will allow for a recursive evaluation of the minimum. More precisely, for each site $j \in T$, we will introduce a function $\kappa_j(\sigma)$ depending on the values of σ_j and its descendants. At any non-leaf sites i, $\kappa_i(\sigma)$ will be defined as a function of $\{\kappa_j(\sigma)\}$, with j running over the sons of i. For any leaf site j, we have $\kappa_j(\sigma) = \sigma_j$. At the end we set $\kappa(\sigma) = \kappa_i(\sigma)$.

We are left with the task of choosing the recursion which determines κ_i in terms of the functions at its sons (to be denoted generically as j). A simple (but reasonably good choice) is $\kappa_i(\sigma) = \mathsf{M}_{r_i,\Omega_i}(\{\kappa_j(\sigma)\})$, where

$$\mathsf{M}_{r,\Omega}(\kappa_1, \dots, \kappa_l) = \begin{cases} +1 & \text{if } \sum_{j\in\Omega} \kappa_j \geq l - 2r, \\ -1 & \text{otherwise.} \end{cases} \tag{63}$$

Here r is a non-negative integer and Ω a subset of $\{1, \dots, l\}$. The parameters r_j, and the sets Ω_j can be chosen in order to optimize the bound. They will depend on the tree T, but not on the configuration σ.

The lower bound on the barrier implied by this choice of the function κ can be computed recursively. Let T_j be the subtree formed by j and its descendants. Denote by $b_j(+/-)$ the lower bound on the barrier for the subsystem T_j under the condition that $\sigma_j = +/-$ (in other words, the minimum in Eq. (62) is taken only over the configurations satisfying this condition). A moment of thought shows that

$$b_i(+) = r_i + \min_{j\in\Omega_i}[\, b_j(+),\ b_j(-) + 1\,], \tag{64}$$

$$b_i(-) = (n_i - r_i - 1) + \min_{j\in\Omega_i}[\, b_j(+) + 1,\ b_j(-)\,], \tag{65}$$

where $n_i = |\Omega_i|$ is the number of descendants of i which are involved in the definition of the function $\kappa_i(\sigma)$.

First notice that, by changing $r_j \leftrightarrow n_j - r_j - 1$ for all the sites $j \in T_i$, one changes $b_i(+) \leftrightarrow b_i(-)$. We can therefore assume, without loss of generality, that $b_i(+) \le b_i(-)$. In fact it is not necessary to keep track of all the information used in Eqs. (64) and (65). We let $b_i = \min[b_i(+),\ b_i(-)]$, and define $\delta_i = 0$ if $b_i(+) = b_i(-)$ and $= 1$ otherwise.

The optimal choice of the parameters r_i's is obtained as follows. Suppose Ω_i is given and let $b_{\min,\Omega_i} = \min\{b_j;\ j \in \Omega_i\}$. If $\delta_j = 1$ for all the $j \in \Omega_i$ such that $b_j = b_{\min,\Omega_i}$ (in this case we will say that $\delta_{\min,\Omega_i} = 1$), then we set $r_i = \lfloor \frac{n_i}{2} \rfloor$. In the opposite case (which we shall denote as $\delta_{\min,\Omega_i} = 0$), the optimal choice is $r_i = \lfloor \frac{n_i - 1}{2} \rfloor$. Using these choices in Eqs. (64) and (65), we get

$$b_i = b_{\min,\Omega_i} + \left\lfloor \frac{n_i - 1 + \delta_{\min,\Omega_i}}{2} \right\rfloor, \quad \delta_i = \begin{cases} 1 - \delta_{\min,\Omega_i} & \text{for } n_i \text{ even}, \\ \delta_{\min,\Omega_i} & \text{for } n_i \text{ odd}. \end{cases} \tag{66}$$

It is useful to notice that a natural order relation can be defined on the couples (b_i, δ_i). We will say that $(b, \delta) \preceq (b', \delta')$ if $b < b'$ or $b = b'$ and $\delta \le \delta'$. It is simple to show that $(b_{\min,\Omega_i}, \delta_{\min,\Omega_i}) = \min\{(b_j, \delta_j);\ j \in \Omega_i\}$ if the minimum is taken with respect to this order relation. Furthermore, given n_i, the mapping (66) is monotonously increasing with respect to the same relation. We can therefore optimize over Ω_i, at fixed n_i as follows. First order the descendants of j by decreasing (b_j, δ_j). Then form Ω_i by retaining the first n_i items of this list. If the list of ordered couples is denoted as $\{(b_{[1]}, \delta_{[1]});\ (b_{[2]}, \delta_{[2]});\ \cdots\}$, then the optimized recursion is obtained by replacing $b_{[n_i]}$ to $b_{\min,\Omega_i}$, and $\delta_{[n_i]}$ to $\delta_{\min,\Omega_i}$ in Eq. (66). We can finally optimize over n_i to get

$$(b_i, \delta_i) = \max_{1\le n\le l_i} \left(b_{[n]} + \left\lfloor \frac{n - 1 + \delta_{[n]}}{2} \right\rfloor,\ (1 - \delta_{[n]})\, \mathbb{I}\{n \text{ even}\} + \delta_{[n]} \mathbb{I}\{n \text{ odd}\} \right), \tag{67}$$

where l_i is the number of descendants of i, and the max is taken once more with respect to the order relation $\preceq$.

As a simple application, one may consider the case of a k-generations binary tree. We saw at the beginning of Sec. 6.6 that the disjoint combination strategy overestimate the barrier in this case by a multiplicative factor which approaches 2 as $k \to \infty$. If we call (b_k, δ_k) the values of b_i and δ_i at the root of such a tree Eq. (67) implies the following recursion: $b_{k+1} = b_k + \delta_k$, $\delta_{k+1} = 1 - \delta_k$. This in turns yields $b_k = \lfloor k/2 \rfloor$ which is essentially tight.

In applying the above method to the p-spin model (1) we must consider the problem of optimizing over the rearrangement R_i. Once again, we exploit the fact that the mapping (67) is monotonously increasing with respect to the order relation $\preceq$. We can therefore construct recursively R_i also in this case. For each site j in R_i and interaction term α, at least one more site k adjacent to α must belong to R_i. In fact, it can be argued that the minimal barrier is achieved by simple rearrangements. We restrict to this case here: *exactly* one more site k (apart from j) belongs to R_i. This site can be chosen by minimizing (b_k, δ_k) with respect to this order relation.

The whole procedure can of course be implemented in a message passing style. Messages $u_{\alpha\to i}$ and $v_{i\to\alpha}$ are now couples (b, δ). They satisfy recursion relations of the form (54), with $\hat{f}_l(\,\cdot\,)$ being replaced by the mapping (67). Also the probabilistic analysis can be carried out along the lines of Sec. 6.4. The only difference is that, due to the new degree of freedom δ, one has to keep track of joint distributions $Q_{\delta,b}$, with $\delta = 0, 1$. The critical behavior of these distributions for $\alpha \to \alpha_{\rm d}$ is very close to the one obtained in Sec. 6.5 within the disjoint strategy. The main difference is that the parameters ω_a and ω_b are replaced by ω'_a and ω'_b with $\omega'_{a/b} = 2\omega_{a,b}$. As a consequence the lower bound on the typical barrier for large rearrangements is $b_{\rm lb} \simeq -\frac{1}{2}\Upsilon \log(\alpha_{\rm d} - \alpha)$. Together with the disjoint strategy analysis, this provides a rigorous proof that $b = O(-\log(\alpha_{\rm d} - \alpha))$.

As stressed above, we do not think that the lower bound described in this Section is tight, even in the critical regime. It should be possible to improve it at the price of a more intricate recursive definition of the functions $\kappa_i(\sigma)$ (in the definition used here, $\kappa_i(\sigma)$ depends only on the spins at the leaves of the rearrangement). On the other hand, it provides some support for the conjecture that the behavior $b \simeq -\Upsilon \log(\alpha_{\rm d} - \alpha)$ is asymptotically exact.

7. GEOMETRICAL PROPERTIES OF OPTIMAL REARRANGEMENTS

In the previous Sections we studied two types of *optimal* rearrangements: minimal size, and minimal barrier ones. Several refined properties can be defined and studied. First of all, what is the trade off between the two criteria of optimality? For instance, how larger are the minimal barrier rearrangements compared to the minimal size ones? Moreover, thanks to the underlying Bethe lattice, some geometrical properties of the rearrangements can be introduced. For instance, one

can study the distribution of the distances between the root of a rearrangement and the sites it contains.

Finally, the diverging rearrangement size (and barrier) as $\alpha \to \alpha_{\rm d}$ implies that dynamics becomes more and more cooperative in this regime. One possible characterization of correlations induced by the increasing cooperativity is the following. Consider a variable i and the minimal size of its rearrangements, n_i. Imagine now that a very strong external field is applied on another variable j, preventing it from being flipped, and define $n_i^{(j)}$ as the minimal size of the rearrangements for i which exclude the frozen variable j. If the two variables are sufficiently far apart, this additional constraint will be irrelevant, and one will have $n_i^{(j)} = n_i$. However if j gets closer to i, it may happen that j belonged to all optimal rearrangements for i, which will imply $n_i^{(j)} > n_i$. How close the variables have to be for this to happen allows to define a "geometric correlation length." We shall define a "geometric response function" related to the difference $n_i^{(j)} - n_i$, and a susceptibility by summing it over the positions i and j. This turns out to be a close analog of the four-point correlation function,[12,13,15,16] used in studies of the structural glass transition.

The above questions are considered in the rest of this Section. Let us briefly list the main results. The size of minimal barrier rearrangements diverges as $(\alpha_{\rm d} - \alpha)^{-\nu_{\rm barr}}$ with non-universal exponent $\nu_{\rm barr} > \nu$ (recall that ν is the analogous exponent for *minimal size* rearrangements). The typical distance between the root and a random node in a large rearrangement diverges as $(\alpha_{\rm d} - \alpha)^{-\zeta}$, with *universal* exponent $\zeta = 1/2$. Finally, the number of sites which are influential for the optimal rearrangements of site i (as measured through the above susceptibility) diverges as $(\alpha_{\rm d} - \alpha)^{-\eta}$ with universal exponent $\eta = 1$.

7.1. Average Size of Minimal Barrier Rearrangements

How large are minimal barrier rearrangements? Consider the simple example of Fig. 13. The minimal barrier rearrangements for the site 0 have barrier 1 and size 5 (one of them is obtained by flipping the variables 0, 1, 2, 3, 4 in this order). On the contrary the minimal size rearrangements (for instance, the one formed by sites 0, 5, 6, 7) have barrier 2 and size 4.

This example shows that minimal barrier rearrangements can be strictly larger that minimal size ones. It is however not clear whether the same remains true if we focus on the critical behavior as $\alpha \to \alpha_{\rm d}$. To keep the level of difficulty of the computations at an acceptable level, we compute barriers within the disjoint strategy, and assume it to be optimal in the critical regime.

For a given site i, there can be several minimal barrier rearrangements of different sizes. We can resolve this ambiguity as follows. Distinct rearrangements with equal barrier occur because the choice of which spin to include at a given function node—i.e., the minimum in Eq. (54)–can be degenerate. A random

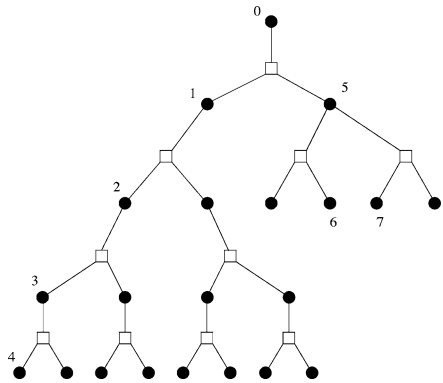

Fig. 13. An example where minimal barrier rearrangements and minimal sizes ones are distinct.

minimal barrier rearrangement[14] can be sampled by removing such degeneracies, each time they occur, uniformly at random. We call m_i (to stress the difference with the minimal size n_i) the average size of random minimal barrier rearrangements sampled in this manner.

The computation of m_i can be performed recursively, exploiting the local tree structure of the graph $\mathcal{G}$. To this aim we supplement the messages $u_{\alpha\to i}$, $v_{i\to\alpha}$ used to computed the barrier b_i, cf. Eq. (54), with messages $u'_{\alpha\to i}$, $v'_{i\to\alpha}$ defined as m_i for the corresponding cavity graphs. For instance, $v'_{i\to\alpha}$ is the average size of the rearrangements of minimal barrier rooted at site i in the graph deprived of the interaction α. The new messages obey the following recursions:

$$v'_{i\to\alpha} = 1 + \sum_{\beta\in\partial i\setminus\alpha} u'_{\beta\to i}\,, \qquad u'_{\alpha\to i} = \frac{1}{\mathcal{N}_{\alpha\to i}} \sum_{\substack{j\,\in\,\partial\alpha\,\setminus\, i \\ v_{j\to\alpha}\,=\,u_{\alpha\to i}}} v'_{j\to\alpha}, \tag{68}$$

where $\mathcal{N}_{\alpha\to i}$ is the number of sites $j \in \partial\alpha\backslash i$ such that $v_{j\to\alpha} = 4u_{\alpha\to i}$ (in other words, the degeneracy of the minimum in Eq. (54)). The sum in the second equation corresponds to an uniform average over the degeneracy at node α, as discussed above. Finally, we have

$$m_i = 1 + \sum_{\alpha\in\partial i} u'_{\alpha\to i}\,. \tag{69}$$

For random hypergraphs, the above recursions acquire a distributional meaning. Note that the messages u and u' (or v and v') on the same link are correlated.

[14] Notice that this procedure *is not* equivalent to picking a rearrangement uniformly at random among the ones of minimal size. However, it is more convenient for calculations. We expect the critical behavior not to be affected by this choice.

As messages u' and v' can take non-integer values, we will define

$$q_{b,m}\,dm = \mathbb{P}\big\{v_{i\to\alpha} = b,\, v'_{i\to\alpha} \in [m, m+dm]\big\}\,, \tag{70}$$

Analogously $\hat{q}_{b,m}$ is the joint distribution of $u_{\alpha\to i}$ and $u'_{\alpha\to i}$. Marginalizing over m, one recovers the distributions studied in Sec. 6: $\int dm\; q_{b,m} = q_b$. The explicit distributional equations read:

$$q_{b,m} = \sum_{l=0}^{\infty} p_l \sum_{b_1,\dots,b_l} \int \prod_{j=1}^{l} dm_j\; \hat{q}_{b_j,m_j}\;\; \delta_{b,\hat{f}_l(b_1,\dots,b_l)}\delta(m-1-m_1-\ldots-m_l), \tag{71}$$

$$\hat{q}_{b,m} = \sum_{k=1}^{p-1} \binom{p-1}{k} \int \prod_{j=1}^{k} dm_j\; q_{b,m_j}\; Q_{b+1}^{p-1-i}\;\; \delta\left(m - \frac{m_1+\cdots+m_i}{i}\right). \tag{72}$$

Consider the partial averages $M_b = \int dm\; q_{b,m} m$ and $\widehat{M}_b = \int dm\; \hat{q}_{b,m} m$. Notice that M_b/q_b is the average size of minimal barrier rearrangements, conditioned on their barrier[15] b. Eqs. (71), (72) imply

$$M_b = q_b + \sum_{l=1}^{\infty} p_l l \sum_{b_1,\dots,b_l} \widehat{M}_{b_1}\hat{q}_{b_2}\dots\hat{q}_{b_l}\delta_{b,\hat{f}_l(b_1,\dots,b_l)}, \tag{73}$$

$$\widehat{M}_b = M_b \frac{\hat{q}_b}{q_b}. \tag{74}$$

These equations can be solved numerically by iteration, we defer the detailed presentation of the method to Appendix C.3. In Fig. 14 we plot, for a few values of α approaching its critical value, the quantity M_b/q_b as a function of b.

Two scaling regimes can be distinguished. For barriers of intermediate size, $b \simeq -\frac{1}{2\omega_a}\log(\alpha_{\rm d}-\alpha)$, the average size M_b/q_b grows exponentially with b. In the large barrier regime $b \simeq -\Upsilon\log(\alpha_{\rm d}-\alpha)$, the size saturate at $(M_b/q_b) \sim (\alpha_{\rm d}-\alpha)^{-\nu_{\rm barr}}$. A careful asymptotic analysis reveals that

$$\nu_{\rm barr} = \frac{\mu_a}{2\omega_a} + \frac{\mu_b}{2\omega_b}, \tag{75}$$

where $\mu_{a/b}$ are positive solutions of the equations

$$\frac{(e^{\mu+\omega}-1)(e^{-\omega}+e^{-\mu}-e^{-\omega-\mu})}{(e^{\mu}-1)(e^{\omega}-1)} = \frac{\lambda}{2}, \tag{76}$$

[15] To be more precise, the conditioning is on having an anchored barrier of b. This distinction does not change the critical behavior.

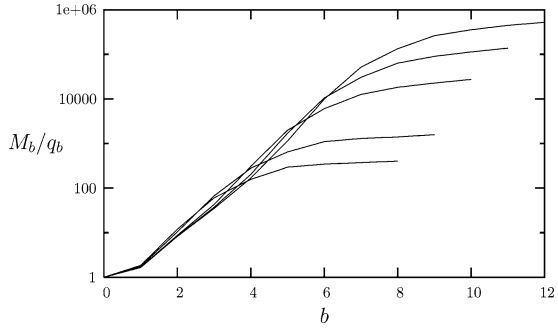

Fig. 14. The average size of minimal barrier rearrangements. From bottom to top, $\alpha = 0.7, 0.75, 0.8, 0.81, 0.814$.

with $\omega = -\omega_a$ (for μ_a) and $\omega = \omega_b$ (for μ_b). We obtain for instance $\nu_{\text{barr}} \approx 2.0157$ for $p = 3$ (cf. Table II for the other values of p), which is strictly larger than the exponent for minimal size rearrangements, $\nu \approx 1.59379$.

Let us conclude by noticing that the "inverse" computation, namely computing the energy barrier for minimal size rearrangements, is technically more challenging. However we expect the result to be analogous to the one derived here: the barrier for minimal size rearrangements should diverge as $-\Upsilon_{\text{size}} \log(\alpha_{\text{d}} - \alpha)$ with Υ_{size} strictly larger than Υ.

7.2. Average Depth of Minimal Size Rearrangements

We turn now to a study of the shape of optimal rearrangements. We define the depth of a rearrangement R_i as the sum of the distances of the sites $j \in R_i$ from i.

For a given graph $\mathcal{G}$, consider a site i with minimal rearrangement size n_i, and call t_i the average[16] depth of its optimal rearrangements. With this definition, t_i/n_i is the average distance between i and sites in the optimal rearrangements for i. We shall call this quantity the "radius" of optimal rearrangements.

Let us emphasize that in general rearrangements of same size but different depths can coexist. A simple example of this phenomenon is provided in Fig. 15. Among the eight distinct optimal rearrangements (of size $n = 4$) for the root, four are of depth 5 (they include the left branch in the first interaction) and four of depth 6 (right branch). All of them are sampled with equal probability according to our procedure, therefore $t = 11/2$, and the radius is $t/n = 11/8$.

[16] Here the average is taken with the same procedure described in Sec. 7.1. Each time the minimum in Eq. (36) is degenerate, one of the optimal branches is chosen uniformly at random.

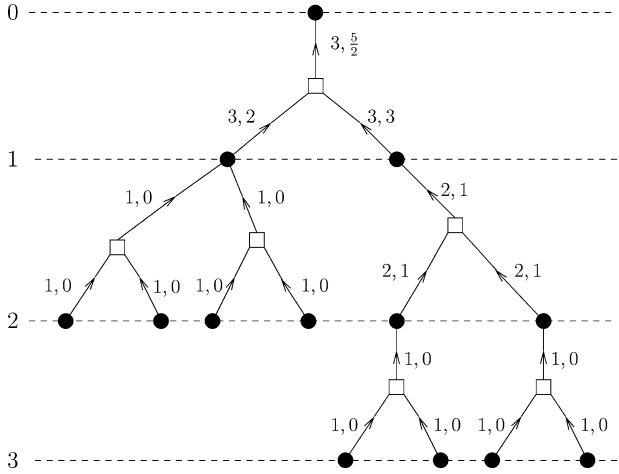

Fig. 15. An example of the computation of t_i. The numbers on the left are the distances of the sites from the root. The value of the messages u, u' (resp. v, v') are indicated next to the edges from interactions to sites (resp. from sites to interactions). They verify the recursion equations (36) and (77).

As sketched in Fig. 15, the quantity t_i can be computed in a recursive manner: along with the minimal size messages $u_{\alpha\to i}$ and $v_{i\to\alpha}$ which verify the recursion Eqs. (36), we introduce supplementary messages on every directed edge of the factor graph, $u'_{\alpha\to i}$ and $v'_{i\to\alpha}$. They are defined as t_i, but refer to cavity graphs. For instance, $v'_{i\to\alpha}$ is the average depth of the optimal rearrangements rooted in i in the graph where the interaction α has been removed. They obey the recursions:

$$v'_{i\to\alpha} = \sum_{\beta\in\partial i\setminus\alpha} [u_{\beta\to i} + u'_{\beta\to i}], \qquad u'_{\alpha\to i} = \frac{1}{\mathcal{N}_{\alpha\to i}} \sum_{\substack{j\,\in\,\partial\alpha\,\setminus\, i \\ v_{j\to\alpha} = v_{\alpha\to i}}} v'_{j\to\alpha}, \quad (77)$$

where $\mathcal{N}_{\alpha\to i}$ is the number of sites $j \in \partial\alpha\backslash i$ such that $v_{j\to\alpha} = u_{\alpha\to i}$ (the degeneracy of the minimum in Eq. (36)). In the first equation, the term $u_{\beta\to i}$ arises because the distance of a descendant of i from the parent of i is larger than its distance from i by one. Finally the site quantity can be computed in terms of the incoming messages:

$$t_i = \sum_{\alpha\in\partial i} [u_{\alpha\to i} + u'_{\alpha\to i}]\,. \quad (78)$$

The reader is invited to check the correctness of this procedure on the example of Fig. 15.

Until now the computation has been performed for a site i in a given sample $\mathcal{G}$. As in the previous Section, for a random graph $\mathcal{G}$, the distribution of t_i can be

determined from the joint law

$$q_{n,t}\, dt = \mathbb{P}\{v_{i\to\alpha} = n,\ v'_{i\to\alpha} \in [t, t+dt]\}\ . \tag{79}$$

Analogously, $\hat{q}_{n,t}$ will denote here the joint distribution of $u_{\alpha\to i}$ and $u'_{\alpha\to i}$. Because of the memoryless property of Poisson random variables, $q_{n,t}$ is also the joint distribution of n_i, t_i. The recursion relations on the messages are easily translated into equations for $q_{n,t}$ and $\hat{q}_{n,t}$:

$$q_{n,t} = \sum_{l=0}^{\infty} p_l \sum_{n_1,\dots,n_l} \int \prod_{j=1}^{l} dt_j\, \hat{q}_{n_j,t_j}\ \ \delta_{n,1+n_1+\cdots+n_l}\ \delta(t - n_1 - t_1 - \cdots - n_l - t_l), \tag{80}$$

$$\hat{q}_{n,t} = \sum_{i=1}^{p-1} \binom{p-1}{i} \int \prod_{j=1}^{l} dt_j\, q_{n_j,t_j}\ Q_{n+1}^{p-1-i}\ \ \delta\left(t - \frac{t_1 + \cdots + t_i}{i}\right). \tag{81}$$

By definition $\int dt\ q_{n,t} = q_n$, is the distribution of minimal sizes studied in Sec. 5. Hence $q_{n,t}/q_n$ is the distribution (with respect to the graph $\mathcal{G}$, and the site i) of the average depth t of optimal rearrangements, conditioned on their size n. For large scale rearrangements of diverging size in the critical limit $\alpha \to \alpha_{\rm d}$, we expect this law to have a scaling form

$$q_{n,t}/q_n \approx (\alpha_{\rm d} - \alpha)^{\zeta}\ \mathcal{S}\{(\alpha_{\rm d} - \alpha)^{\zeta} t \mid (\alpha_{\rm d} - \alpha)^{\nu} n\}. \tag{82}$$

For the sake of simplicity (and with the aim of determining the exponent ζ) we shall concentrate on the partial averages $T_n = \int dt\ t\, q_{n,t}$ and $\widehat{T}_n = \int dt\ t\, \hat{q}_{n,t}$. Hence $T_n/(nq_n)$ is the average radius of optimal rearrangements of size n. Eqs. (80) and (81) imply

$$T_n = \sum_{l=1}^{\infty} p_l\, l \sum_{n_1,\dots,n_l} (\widehat{T}_{n_1} + n_1 \hat{q}_{n_1}) \hat{q}_{n_2} \dots \hat{q}_{n_l}\ \delta_{n,1+n_1+\cdots+n_l}, \tag{83}$$

$$\widehat{T}_n = T_n \frac{\hat{q}_n}{q_n}. \tag{84}$$

To lighten the notation, let us define $\widetilde{T}_n = \widehat{T}_n + n\hat{q}_n$. We finally obtain:

$$T_n = \alpha p \sum_m q_{n-m} \widetilde{T}_m, \qquad \widetilde{T}_n = T_n \frac{\hat{q}_n}{q_n} + n\hat{q}_n. \tag{85}$$

As was the case for the distribution q_n, the sequence T_n can be efficiently determined numerically by recursion on n, the initial value being $T_1 = 0$. We present in Fig. 16 the output of such a numerical computation. For clarity we plotted the average radius $\theta_n = T_n/(nq_n)$ as a function of the size n.

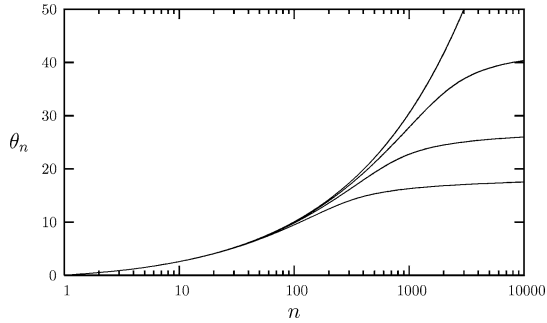

Fig. 16. The average radius θ_n in optimal rearrangements of size n, from bottom to top $\alpha = 0.8, 0.81, 0.815, \alpha_d$.

Its critical behavior can be determined analytically. The details of the computations are presented in Appendix C.4. As for the distribution of minimal sizes Q_n, two scaling regimes can be determined. For intermediate sizes, $n \sim (\alpha_d - \alpha)^{-1/2a}$, the radius grows like a power law of n. In the large size rearrangements regime, $n \sim (\alpha_d - \alpha)^{-\nu}$, the radius saturate at $\theta \sim (\alpha_d - \alpha)^{-\zeta}$, where $\zeta = 1/2$ is universal. This is consistent (as it should be) with the divergence of the point-to-set correlation length defined in Sec. 3.2.

It is not hard to realize that the same scaling $(\alpha_d - \alpha)^{-1/2}$ must hold for the radius of large minimal barrier rearrangements. This is in fact the radius below which optimal rearrangements on site i are insensitive to perturbations on other sites, see also next Section. It is also related to the number of iterations necessary for iterations of the form (56) to converge to their fixed point.

For large rearrangements, eliminating the dependency upon α yields the scaling $\theta_n \sim n^{1/2\nu}$. This can be compared with the case of uniformly random trees, which can be interpreted as a mean field model for ordinary bond percolation. In this case it is well known[55] that $\theta_n \sim n^{1/2}$. Since $\nu > 1$ always, large scale rearrangements are 'denser' than percolation cluster.

7.3. Geometrical Susceptibility

7.3.1. Minimal Size Rearrangements

We turn now to the question of dynamical correlations induced by optimal rearrangements, cf. the discussion at the beginning of this Section. Consider the portion of a graph sketched in Fig. 17, where we isolated the root site i_0 and a chain of r ($r = 3$ in the figure) sites $i_1, \ldots, i_r$ linked by interactions $\alpha_1, \ldots, \alpha_r$. We define $n_{i_0}^{(i_r)}$ as the minimal size of rearrangements for i_0 which do not include the variable i_r (one can imagine that a pinning external field has been applied on σ_{i_r} thus preventing it from flipping). This is to be compared with n_{i_0}, the

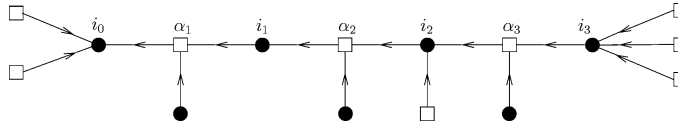

Fig. 17. A chain of $r = 3$ interactions for the computation of geometrical susceptibility.

unconstrained minimal size of rearrangements for the root i_0. The unconstrained size n_{i_0} can be computed through the message passing procedure described in Sec. 5, which makes use of messages $u_{\alpha\to i}$, $v_{i\to\alpha}$. In order to compute $n_{i_0}^{(i_r)}$, we introduce, for each edge of the chain directed towards i_0, supplementary messages $u'_{\alpha_k\to i_{k-1}}$ and $v'_{i_k\to\alpha_k}$. The edges of the graph outside the chain bears the usual single message (either $u_{\alpha\to i}$ or $v_{i\to\alpha}$).

The unconstrained (resp. constrained) size is given as follows in terms of messages:

$$n_{i_0} = 1 + u_{\alpha_1\to i_0} + \sum_{\beta\in\partial i_0\setminus\alpha_1} u_{\beta\to i_0}\,, \qquad n_{i_0}^{(i_r)} = 1 + u'_{\alpha_1\to i_0} + \sum_{\beta\in\partial i_0\setminus\alpha_1} u_{\beta\to i_0}\,. \tag{86}$$

While the messages $u_{\alpha\to i}$, $v_{i\to\alpha}$ obey the usual relation (36) for minimal size rearrangements, for the new messages we have:

$$v'_{i_k\to\alpha_k} = 1 + u'_{\alpha_{k+1}\to i_k} + \sum_{\beta\in\partial i_k\setminus\{\alpha_k,\alpha_{k+1}\}} u_{\beta\to i_k}, \tag{87}$$

$$u'_{\alpha_k\to i_{k-1}} = \min\left[v'_{i_k\to\alpha_k}, \min_{j\in\partial\alpha_k\setminus\{i_k,i_{k-1}\}} v_{j\to\alpha_k}\right]. \tag{88}$$

Notice that these equations are formally identical to Eq. (36). The constraint of excluding i_r from rearrangements whose minimal size is $n_{i_0}^{(i_r)}$, is enforced through the boundary condition $v'_{i_r\to\alpha_r} = \infty$. In this way, the variable i_r is never included in the rearrangement. Equivalently

$$u'_{\alpha_r\to i_{r-1}} = \min_{j\in\partial\alpha_r\setminus\{i_r,i_{r-1}\}} v_{j\to\alpha_r}. \tag{89}$$

The two quantities n_{i_0} and $n_{i_0}^{(i_r)}$ (as well as the messages $u_{\alpha\to i}$, $u'_{\alpha\to i}$ or $v_{i\to\alpha}$, $v'_{i\to\alpha}$) are correlated, as both of them see the same "environment." We must therefore keep track of the probability distributions

$$q_{n,n'}^{(r-t)} = \mathbb{P}\{v_{i_t\to\alpha_t} = n,\ v'_{i_t\to\alpha_t} = n'\}, \tag{90}$$

and the analogous one (denoted as $\hat{q}_{n,n'}^{(r-t)}$) for messages $u_{\alpha_{t+1}\to i_t}$, $u'_{\alpha_{t+1}\to i_t}$. Here probabilities are implicitly conditioned on the existence of a chain of interactions of length r between the root i_0 and the constrained site i_r. Since the variable node degrees are Poisson random variables, the couple n_{i_0}, $n_{i_0}^{(i_r)}$ is distributed according

to $q^{(r)}_{n,n'}$. We also define the cumulative distributions $Q^{(r-t)}_{n,n'}$ and $\widehat{Q}^{(r-t)}_{n,n'}$. The first one is, for instance, the probability that $v_{i_t\to\alpha_t} \geq n$ *and* $v'_{i_t\to\alpha_t} \geq n'$. With these definitions, the distributional equations read

$$\widehat{Q}^{(r)}_{n,n'} = Q^{(r-1)}_{n,n'} Q^{p-2}_{\max(n,n')}, \tag{91}$$

$$q^{(r)}_{n,n'} = \sum_{l=0}^{\infty} p_l \sum_{n_1,n'_1} \sum_{m_1,\ldots,m_l} \hat{q}^{(r)}_{n_1,n'_1} \hat{q}_{m_1} \ldots \hat{q}_{m_l} \delta_{n,n_1+m_1+\cdots+m_l}\, \delta_{n',n'_1+m_1+\cdots+m_l}, \tag{92}$$

where $q_n, \hat{q}_n$ are the distributions of minimal size rearrangements, i.e. the solutions of Eqs. (39) and (40).

Let $q^{(r)}_{n',\mathrm{con}} \equiv \sum_n q^{(r)}_{n,n'}$ (respectively $q^{(r)}_{n,\mathrm{unc}} \equiv \sum_{n'} q^{(r)}_{n,n'}$) be the marginal distribution of the constrained (unconstrained[17]) sizes. Define

$$s^{(r)}_n \equiv q^{(r)}_{n,\mathrm{con}} - q^{(r)}_{n,\mathrm{unc}}. \tag{93}$$

The knowledge of $s^{(r)}_n$ allows to compute the expectation of any observable of the form $f(n^{(i_r)}_{i_0}) - f(n_{i_0})$. For the sake of simplicity, we shall hereafter focus on this function, rather than solving Eqs. (91) and (92) for the joint distribution of $n^{(i_r)}_{i_0}$, n_{i_0}. Further justification for considering on this type of functions will be provided in the next Section.

Equations for $s^{(r)}_n$ are more easily written by introducing the integrated version,

$$S^{(r)}_n = \sum_{n'\geq n} s^{(r)}_{n'}. \tag{94}$$

As well as the corresponding quantities for u-messages: $\hat{s}^{(r)}_n$ and $\widehat{S}^{(r)}_n$. From Eqs. (91) and (92), and using the recursion Eqs. (39) and (40), it is easy to obtain

$$s^{(r)}_n = \sum_m \hat{s}^{(r)}_{n-m} q_m, \qquad \widehat{S}^{(r)}_n = Q^{p-2}_n S^{(r-1)}_n. \tag{95}$$

Furthermore, the first of these equations can be rewritten in terms of integrated sequences as $S^{(r)}_n = \sum_m \widehat{S}^{(r)}_{n-m} q_m$, cf. Appendix C.5.1.

For $r = 0$ one has by definition $S^{(0)}_n = 1 - Q_n$. Eqs. (95) can be used to compute $S^{(r)}_n$ efficiently by recursion (both on n and r). We show the results in Fig. 18, left panel, for $\alpha = 0.8$ and a few increasing values of r. As $n \to \infty$, $S^{(r)}_n \to 1$ if $r = 0$, (we are constraining the spin σ_{i_0} itself not to be flipped: there

[17] Note that the marginal distribution of unconstrained minimal sizes $q^{(r)}_{n,\mathrm{unc}} \equiv \sum_{n'} q^{(r)}_{n,n'}$ is distinct from q_n. In fact, in $q^{(r)}_{n,\mathrm{unc}}$, we condition on the existence of a chain of length r from the root.

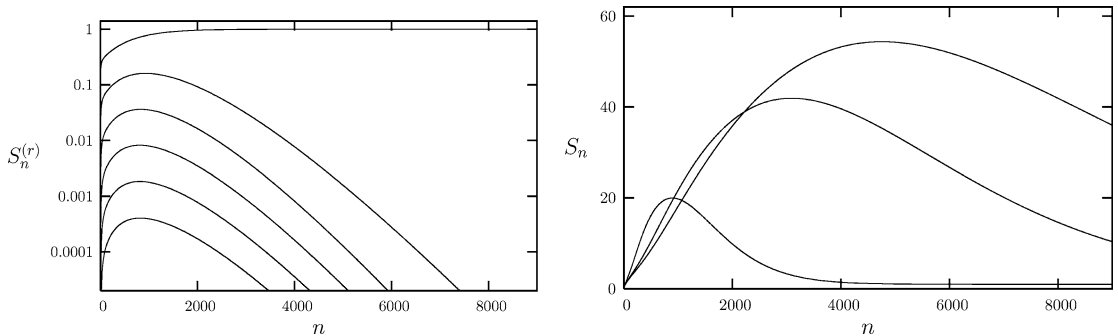

Fig. 18. *Left*: the response $S_n^{(r)}$ of the minimal rearrangement size distribution to a constraint on a site at distance r of the root. We used $\alpha = 0.8$ and, from top to bottom, $r = 0, 1, \ldots, 5$. *Right*: the corresponding susceptibility S_n. From left to right, $\alpha = 0.8, 0.81, 0.812$.

is no rearrangement of finite size satisfying such a condition), and $S_n^{(r)} \to 0$ if $r \geq 1$. Moreover one can clearly see $S_n^{(r)} \to 0$ as $r \to \infty$ at fixed n. Indeed the constraint of not flipping σ_{i_r} gets less and less relevant in this limit, and when r is much larger than the typical depth of the rearrangements $n_{i_0} \approx n_{i_0}^{(i_r)}$. From the studies of the depth of the rearrangements, one expects that the values of r where the constraint becomes irrelevant scales like $(\alpha_{\rm d} - \alpha)^{-1/2}$ in the critical limit.

Let us now define a susceptibility S_n by summing the above "response function" $S_n^{(r)}$ over the position of the constrained site. As there are on average $(\alpha p(p-1))^r$ sites at distance r of the root, we have

$$S_n = \sum_{r=0}^{\infty} (\alpha p(p-1))^r S_n^{(r)}. \tag{96}$$

We also define $\widehat{S}_n = \sum_{r \geq 1} (\alpha p(p-1))^r \widehat{S}_n^{(r)}$. Intuitively, S_n is a measure of the "spine" of optimal rearrangements of size n. By spine, we mean the subset of sites which belong to *all* of the optimal rearrangements for i.

From Eqs. (95), we get

$$S_n = 1 - Q_n + \sum_m \widehat{S}_{n-m} q_m, \qquad \widehat{S}_n = \alpha p(p-1) Q_n^{p-2} S_n \,. \tag{97}$$

The numerical solution of these equations is shown in the right panel of Fig. 18, for a few values of α approaching $\alpha_{\rm d}$. The behavior of these curves is strikingly similar to the one of the four point susceptibility close to the mode coupling transition in structural glasses.[12,13,15,16] Here n plays the role of time in MCT, and α that of the temperature. For a given value of α, the spine size has a maximum $S_*(\alpha)$ which corresponds to rearrangements of total size $n_*(\alpha)$. When $\alpha \to \alpha_{\rm d}$ both $n_*(\alpha)$ and $S_*(\alpha)$ diverge.

An analytical study of the asymptotic behavior, cf. Appendix C.5.1, confirms this remark. The main result is that $n_*(\alpha) \sim (\alpha_{\rm d} - \alpha)^{-\nu}$ scales as the typical size of large scale rearrangements, while $S_*(\alpha) \sim (\alpha_{\rm d} - \alpha)^{-\eta}$, with an universal value $\eta = 1$. The same critical behavior was recently found for the for the four point susceptibility of the fully-connected p-spin model, as well as in MCT.[14]

7.3.2. Minimal Barrier Rearrangements

A geometric susceptibility can be similarly defined in terms of minimal barrier rearrangements. In this context, $b_{i_0}^{(i_r)}$ is the minimal barrier of a rearrangement for the variable i_0 which excludes i_r, another variable at distance r from i_0. To simplify the analysis, we consider barriers obtained from the disjoint strategy. While exact barriers can only be computed through Yannakakis approach, we expect this simplification not to alter the critical behavior.

Following the same steps as in the previous Section, one is lead to define a function $S_b^{(r)}$. This is the response of the minimum barrier distribution for site i_0, to a perturbation applied on site i_r. Using Arrhenius law, it is easy to establish the relationship between $S_b^{(r)}$ and physical observables. Assume that an external field h has been applied to site i_r at distance r from i_0. Let $C^{(r)}(t;h)$ the expected (with respect to the graph $\mathcal{G}$) local correlation function for spin σ_{i_0}, under the (equilibrium) modified Glauber dynamics. The response $\chi^{(r)}(t) = C^{(r)}(t;\infty) - C^{(r)}(t;0)$ is given, in the low temperature limit, by

$$\lim_{\beta\to\infty} \chi^{(r)}(e^{2\beta b}) = S^{(r)}_{\lceil b\rceil}, \tag{98}$$

which generalizes to susceptibilities the relation (47) between barriers distributions and correlation functions. Unlike usual response functions (in which the external perturbation is infinitesimal), $\chi^{(r)}(t)$ is the response to an infinite, but localized perturbing field. Since in any case $\chi^{(r)}(t) \to 0$ as $r \to \infty$, this difference should be immaterial for the critical behavior.

Summing $S_b^{(r)}$ over the perturbation site i_r, one can define a barrier susceptibility S_b. Proceeding as in the previous Section, one can derive a set of coupled equations which determine S_b:

$$S_b = 1 - Q_b + \sum_{l=0}^{\infty} p_l \sum_{b_0,\dots,b_l} \hat{s}_{b_0}\hat{q}_{b_1}\dots\hat{q}_{b_l}\,\mathbb{I}(b \le \hat{f}_{l+1}(b_0,\dots,b_l))\,, \tag{99}$$

$$\widehat{S}_b = \alpha p(p-1)Q_b^{p-2}S_b. \tag{100}$$

These are the counterpart of Eqs. (97) for size susceptibilities.

A numerical solution of these equations, cf. Appendix C.5.2, leads to the result shown in Fig. 19. As for the size susceptibility S_n, the behavior of its barrier analog S_b is very close to the one of the four point dynamical susceptibility in MCT. The barrier height plays the role of time, and in fact they are related through Arrhenius law in the low temperature limit, cf. Eq. (98). The maximum of S_b corresponds to large scale barriers $b_*(\alpha) \simeq -\Upsilon\log(\alpha_{\rm d}-\alpha)$. Its height diverges at the dynamical transition $S_*(\alpha) \sim (\alpha_{\rm d}-\alpha)^{-\eta}$, with the same universal value $\eta = 1$. The details of this analytic study can be found in Appendix C.5.2.

8. SCALING ANALYSIS AND NUMERICAL EXPERIMENTS

In the last Sections we focused on the zero temperature limit at $\alpha < \alpha_{\rm d}$. Here we shall discuss the implications of these results on the finite temperature behavior.

In order to simplify our discussion, we take a step back and focus on the global relaxation time $\tau = \tau(\beta,\alpha)$. This is defined from the global correlation

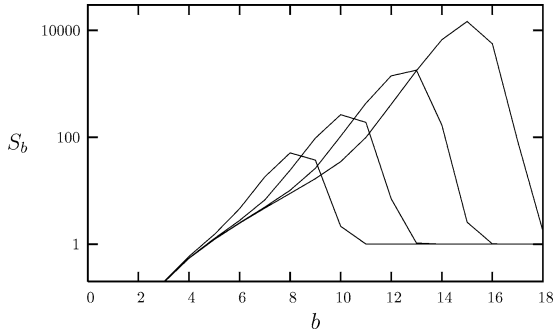

Fig. 19. Geometric susceptibility for minimal barrier rearrangements. From left to right, $\alpha = 0.816$, 0.818, 0.8184, 0.81846.

function through the condition[18] $C(\tau) = \delta$. Most of the arguments below can be easily transposed to local times.

In the low temperature, $\alpha < \alpha_{\rm d}$ regime, Arrhenius law yields $\tau \sim \exp(2\beta b_{\rm large})$, where $b_{\rm large}$ is the typical minimal barrier for large rearrangements. Substituting the critical behavior of $b_{\rm large}$, we get

$$\tau(\beta, \alpha) \sim (\alpha_{\rm d} - \alpha)^{-2\beta\Upsilon}. \tag{101}$$

This relation is valid if $\alpha \to \alpha_{\rm d}$ *after* $\beta \to \infty$. On the other hand, at any $\beta < \infty$, the relaxation time does not diverge at $\alpha = \alpha_{\rm d}$, but at a somewhat higher value of α corresponding to the dynamical line, cf. Fig. 1:

$$\tau(\beta, \alpha) \sim (\alpha_{\rm d}(\beta) - \alpha)^{-\gamma(\beta)}. \tag{102}$$

Equivalently, $\tau(\beta, \alpha) \sim (T - T_{\rm d}(\alpha))^{-\gamma(\alpha)}$. In Sec. 3.3, we derived a lower bound of this form implying $\gamma(\,\cdot\,) \geq 1/2$.

Let now $T = 1/\beta$ be some fixed small temperature, and consider the behavior of $\tau(\beta, \alpha)$ as α is increased towards $\alpha_{\rm d}$ and above. We expect that (101) remains true as long as α is not too close to $\alpha_{\rm d}$. Near $\alpha_{\rm d}$ the divergence is rounded off, and eventually a crossover to the behavior (102) takes place. In other words, the dynamics crosses over from an "activated regime," i.e. a regime for which Eq. (101) is accurate, to a "thermal" regime in which Eq. (102) holds.

At which values of α does the crossover takes place? We will produce two distinct heuristic arguments that provide the same answer. The first one is very simple. The divergence (101) is rounded off only if $(\alpha_{\rm d}(\beta) - \alpha)$ is significantly

[18] As for local relaxation times, cf. Sec. 3.3 the precise value of δ is irrelevant, as long as it is smaller than the global Edwards Anderson parameter. Note also that the relaxation time τ introduced here should not be confused with other global time scales, such as the inverse spectral gap, or the mixing time.

different from $(\alpha_{\rm d}-\alpha)$. Equivalently, $(\alpha_{\rm d}-\alpha)\sim(\alpha_{\rm d}(\beta)-\alpha_{\rm d})$. On the other hand a cavity computation, cf. Appendix D, shows that, as $\beta\to\infty$,

$$\alpha_{\rm d}(\beta)=\alpha_{\rm d}+x_{\rm d}\,e^{-2\beta}+o(e^{-2\beta}), \tag{103}$$

with $x_{\rm d}$ a finite, p-dependent constant. Therefore, the crossover regime corresponds to $(\alpha_{\rm d}-\alpha)e^{2\beta}=O(1)$.

The second heuristic argument is more involved, but more instructive. A finite temperature configuration can be characterized through the locations of energy defects, i.e. frustrated interactions. In a low temperature equilibrium configuration, these defects are very sparse, and their density is about $e^{-2\beta}$ (as long as $\alpha<\alpha_{\rm d}$). Consider now a spin σ_i, and the associated minimal barrier rearrangement R_i of size n_i and barrier b_i. Glauber dynamics will make use of energy defects in order to accelerate the relaxation of σ_i, with respect to the purely activated behavior $\exp(2\beta b_i)$. A rough intuition of this phenomenon is obtained by assuming that interactions containing an energy defect can be removed from the system. A first remark is that, as long as $n_i e^{-2\beta}\ll 1$, no energy defect is encountered along the activated path (also allowing for slightly sub-optimal rearrangements). Arrhenius behavior $\tau_i\sim\exp(2\beta b_i)$ is therefore not modified. Focusing on large rearrangements, this implies that Eq. (101) remains correct as long as $(\alpha_{\rm d}-\alpha)^{-\nu_{\rm barr}}e^{-2\beta}\ll 1$ (i.e. $\alpha_{\rm d}-\alpha\gg e^{-2\beta/\nu_{\rm barr}}$).

This simple minded argument can be refined. We expect an energy defect to be as effective in reducing the effective barrier seen by spin σ_i, as a pinning field is in augmenting it. In other words, the density of such defects must be compared to the size of the large rearrangements spine (i.e. to the peak of the geometric susceptibility), rather than to their overall size. Using the results of Sec. 7.3.2, we conclude once again that the crossover regime corresponds to $(\alpha_{\rm d}-\alpha)e^{2\beta}=O(1)$.

What is the behavior of $\tau(\beta,\alpha)$ in the crossover regime? Inspired by the anomalous dynamical scaling for diluted ferromagnets at the percolation transition [48,49] we conjecture the scaling form[19]

$$\tau(\beta,\alpha)\simeq e^{2\Upsilon\beta^2}\,\mathcal{L}((\alpha-\alpha_{\rm d})e^{2\beta}). \tag{104}$$

In order to match Eqs. (101) and (102), the scaling function $\mathcal{L}(\,\cdot\,)$ must have the following asymptotic behaviors

$$\mathcal{L}(x)\sim\exp\left\{-\frac{1}{2}\Upsilon\,(\log|x|)^2\right\}\qquad\text{as } x\to-\infty, \tag{105}$$

$$\mathcal{L}(x)\sim(x_{\rm d}-x)^{-\gamma_{\rm d}}\qquad\text{as } x\to x_{\rm d}, \tag{106}$$

where $\gamma_{\rm d}\equiv\lim_{\beta\to\infty}\gamma(\beta)$.

[19] The differences with respect to the form in Ref. 25 are due to a different normalization of the temperature.

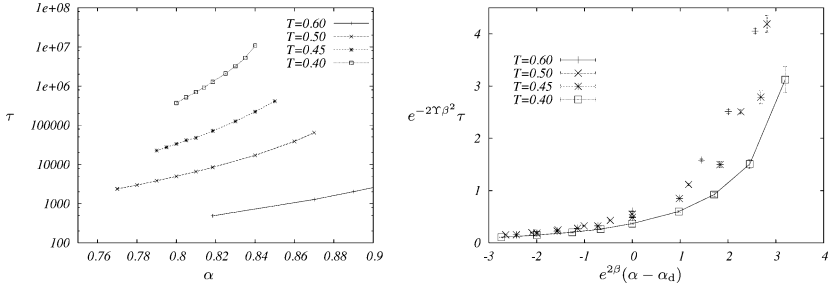

Fig. 20. *Left*: Global correlation times, as defined from the correlation function through the relation $C(\tau) = 1/2$. *Right*: Scaling plot of the same data. Notice that no fitting parameter is used here.

We carried out extensive numerical simulations in order to check this scaling hypothesis, along the lines exposed in Sec. 6.6. In Fig. 20, left frame, we reproduce the resulting global correlation time for several values of β as functions of α. In Fig. 20, right frame, we check Eq. (104) by plotting $\tau(\beta, \alpha)$, in rescaled units, for several values of β and α. Despite the variation of the relaxation time over several orders of magnitude, an acceptable agreement is found. Remarkably, Eq. (104) predicts a super-Arrhenius divergence at this value of α: $\tau(\beta, \alpha_{\rm d}) \sim 2\Upsilon\beta^2$. The prediction is well verified by numerical data, cf. Fig. 21, thus supporting the hypothesis made in computing Υ, cf. Sec. 6.

While the numerical results do not prove unambiguously Eq. (104), they support it as a valid working hypothesis. As in the case of diluted ferromagnets, Eq. (104) is consistent with temperature being a relevant perturbation (in

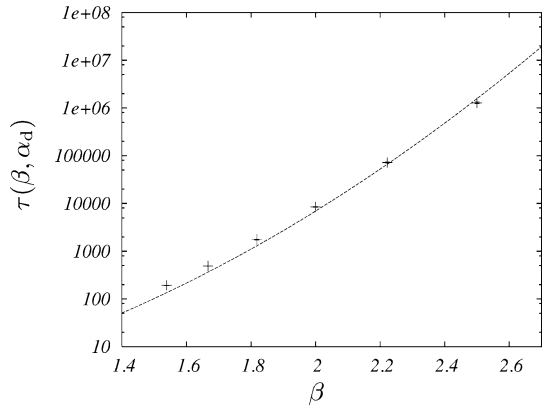

Fig. 21. Super-Arrhenius behavior of the global correlation time at the critical average degree $\alpha = \alpha_{\rm d}$, for $p = 3$. The *dashed line* represent the theoretical prediction $\tau(\beta, \alpha_{\rm d}) = A\, e^{2\Upsilon\beta^2}$, with $A = 0.45$ to fit the data.

renormalization group sense) at the critical point ($\alpha = \alpha_{\rm d}$, $T = 0$). This in turns suggests that the line $T = T_{\rm d}(\alpha)$ is ruled by a different universality class with respect to this point.

9. CONCLUSION

In Sec. 2.1 we stressed that the critical dynamics of Bethe lattice models was understood only in the fully connected $\alpha \to \infty$ limit. In the previous pages we derived several results concerning the opposite limit $T \to 0, \alpha \to \alpha_{\rm d}$. We can now leverage on the knowledge concerning these two extremal points, in order to propose a complete scenario for the whole dynamical line $(\alpha, T_{\rm d}(\alpha))$.

We found two universality classes[20] which correspond to distinct divergences of the slow time scale:

- Usual mode coupling theory (MCT) holds at the $\alpha = \infty$ point. The relaxation time divergence is as summarized in Eqs. (32), (33). The parameter $\lambda_{\rm mct}$ depends (continuously) on the model, and the critical exponent $\gamma_{\rm mct}$ is, in general, irrational.
- Activated mode coupling theory (aMCT) describes the $T \to 0$, $\alpha \to \alpha_{\rm d}$ (with $(\alpha_{\rm d} - \alpha)e^{2\beta} \gg 1$) behavior. The relaxation time diverges as in (101), with Υ determined by equations of the form (58), (60), and (61). Once again, λ depends continuously on the model, and Υ is, in general, irrational.

On the other hand, several important elements are common to the two universality classes. Among the others, the linear size of cooperative regions scales as $\delta^{-\zeta}$, and the peak of the dynamical susceptibility as $\delta^{-\eta}$, with $\zeta = 1/2$ and $\eta = 1$ (here $\delta = T - T_{\rm d}$ for the first class, and $\delta = \alpha_{\rm d} - \alpha$ for the second).[14]

In Sec. 8 we argued that temperature is a relevant perturbation at the $(\alpha = \alpha_{\rm d}, T = 0)$ point. It is therefore natural to guess that the whole $\alpha > \alpha_{\rm d}$, $T = T_{\rm d}(\alpha)$ is controlled by the ordinary MCT class. Namely, there exist a continuous function $\lambda_{\rm mct}(\alpha)$, such that the slow time scales behaves as in Eqs. (32), (33). The crossover away from the $(\alpha = \alpha_{\rm d}, T = 0)$ point is described by Eq. (104). Finally the cooperativity exponents $\zeta = 1/2$ and $\eta = 1$ remain constant on the whole line, as well as in the crossover regime.

At any finite temperature, usual MCT behavior eventually overcomes aMCT when the system is close enough to the dynamical line. On the other hand, activation can be important in a large pre-asymptotic regime, depending on the way the dynamical line is approached. Such a regime can be of experimental interest.

In the model studied in this paper, the crossover is controlled by the scaling variable $x = (\alpha_{\rm d} - \alpha)e^{2\beta}$. This can be interpreted as the ratio between two

[20] We use the term "universality" despite its content is not as clear in the present context as it is for ordinary critical phenomena.

diverging sizes at the ($\alpha = \alpha_d$, $T = 0$) point: the spine of large scale rearrangements, which scales as $(\alpha_d - \alpha)^{-1}$, and the inverse density of energy defects scaling as $e^{2\beta}$. Notice that, as usual for Ising systems in the zero temperature limit, the thermal scaling field is $e^{2\beta}$ rather than T (only the first quantity transforms multiplicatively under a scale transformation).

In terms of observable quantities, we could have written $x = T^2 C_T / \chi_4^* U^2$, where $U = \langle E(\sigma) \rangle$ is the internal energy, $C_T = \partial_T \langle E(\sigma) \rangle$ is the system specific heat, and χ_4^* is the peak value of the dynamical four point susceptibility. Notice that, in the low temperature limit $U \approx \epsilon_{\rm def} \rho_{\rm def}$, and $T^2 C_T \approx \epsilon_{\rm def}^2 \rho_{\rm def}$, with $\rho_{\rm def}$ the density of energy defects and $\epsilon_{\rm def}$ their energy. Therefore x is correctly given as a ratio of volumes.

In more general (non-mean field) systems, susceptibility-like quantities must be replaced by length scales. Therefore, the same role is likely to be played by a ratio of the form $x = \xi_{\rm th}/\xi_4$. Here $\xi_{\rm th}$ is a thermal correlation length, as can be extracted from the point to point static correlation function. It does not diverge at the dynamical transition, but it diverges in the zero temperature limit. On the other hand, ξ_4 is a dynamical correlation length extracted from four point dynamical correlations. The usual renormalization group justification for this Ansatz is that under a scale transformation, a system with correlation lengths $(\xi_{\rm th}, \xi_4)$ transforms into a different one with $(\xi'_{\rm th}, \xi'_4)$ but with the same ratio $\xi'_{\rm th}/\xi'_4 = \xi_{\rm th}/\xi_4$. Notice that a similar scaling variable describes the crossover in diluted ferromagnets at the percolation point.[62]

The methods developed in this paper can certainly be applied in a more general context. In particular, rearrangements can be defined for kinetically constrained models (Kob-Andersen, Frederickson-Andersen for instance) on Bethe lattices, and studied along the same lines.[6] Interestingly, a recent numerical study[63] has investigated the relaxation time divergence in these models and indicates a behavior of the type $\tau \sim (\rho_d - \rho)^{-\gamma}$ (ρ being the particle density).

As we mentioned in the Introduction, the problem studied here is known in computer science as XORSAT, and is a simple example in the wider family of random Constraint Satisfaction Problems.[50] The dynamical glass transition, essentially studied in this context at zero temperature as a "clustering transition" of the ground states, is a feature shared by other examples of this family, Satisfiability and Coloring in particular.[51,52] It would be of great interest to extend the refined description of the changes in the landscape properties at the clustering transition we obtained in the XORSAT problem to these other models (see also Refs. 64 and 65 for related work).

APPENDIX A: PROPERTIES OF THE EQUILIBRIUM DISTRIBUTION

We prove here the statements (i) and (ii) made in Sec. 2.1. In order to prove (i), notice that the partition function admits the usual high temperature

expansion

$$Z_{N,\beta}(J) = 2^N e^{-M\beta} (\cosh\beta)^M \left\{ 1 + \sum_{\omega \in \mathrm{hl}} \epsilon(\omega) (\tanh\beta)^{|\omega|} \right\}, \tag{A.1}$$

where the (finite) sum over ω runs over all the hyperloops in $\mathcal{G}$. $|\omega|$ denotes the size of the hyperloop ω and $\epsilon(\omega)$ the product of the signs of the interactions in it. If no hyperloop is present, only the first term survives.

Consider now (ii). Let $\mathbb{P}(J)$ be the distribution of the sign of the quenched couplings, i.e. the uniform distribution over $\{J_{i_1 \dots i_p} \in \{+1, -1\}\}$, and $\mathbb{P}(\sigma|J)$ the Boltzmann distribution for the configuration σ, given the couplings J. Sampling J from $\mathbb{P}(J)$ and then σ from the conditional distribution $\mathbb{P}(\sigma|J)$ is equivalent to sampling from the joint distribution

$$\mathbb{P}(J)\,\mathbb{P}(\sigma|J) \equiv \mathbb{P}(\sigma, J). \tag{A.2}$$

Using the form of the Boltzmann distribution, we have

$$\mathbb{P}(\sigma, J) = \frac{e^{-M\beta}}{2^M Z_{N,\beta}(J)} \prod_{(i_1 \dots i_p) \in \mathcal{G}} \exp\{\beta J_{i_1 \dots i_p} \sigma_{i_1} \dots \sigma_{i_p}\}. \tag{A.3}$$

This is in turn equivalent to sampling σ form the marginal distribution $\mathbb{P}(\sigma)$ and then J from the conditional distribution $\mathbb{P}(J|\sigma)$. We are left with the task of determining these distributions. Using the definition of marginal distribution, and the fact (i) above, we get

$$\begin{aligned} \mathbb{P}(\sigma) &\equiv \sum_J \mathbb{P}(\sigma, J) \\ &= \frac{1}{2^N (2\cosh\beta)^M} \prod_{(i_1 \dots i_p) \in \mathcal{G}} \sum_{J_{i_1 \dots i_p}} e^{\beta J_{i_1 \dots i_p} \sigma_{i_1} \dots \sigma_{i_p}} = \frac{1}{2^N}, \end{aligned} \tag{A.4}$$

i.e. the marginal distribution of σ is uniform. We can now apply the definition of Bayes theorem to get

$$\mathbb{P}(J|\sigma) \equiv \frac{\mathbb{P}(\sigma, J)}{\mathbb{P}(\sigma)} = \prod_{(i_1 \dots i_p) \in \mathcal{G}} \frac{1}{2\cosh\beta} \exp\left\{\beta J_{i_1 \dots i_p} \sigma_{i_1} \dots \sigma_{i_p}\right\}, \tag{A.5}$$

which proves our claim.

APPENDIX B: CORRELATIONS

This Appendix contains the technical details of the calculation of equilibrium correlation functions presented in Sec. 3.

B.1. *n*-Point Correlation Functions: Zero-Temperature Potential

We start by computing the annealed potential (10). By taking expectation with respect to the graph $\mathcal{G}$, and the constrained spins (but not on their number), it is elementary to obtain

$$\mathbb{E}_L \mathbb{E}_{\mathcal{G}} Z_{\mathcal{G}}(L) = \sum_{\omega} \binom{N}{N\omega} \left[\frac{1+(1-2\omega)^p}{2}\right]^{N\alpha} (1-\omega)^l. \tag{B.1}$$

Here the sum runs over $\omega = 0, 1/N, 2/N, \dots, 1$. Let us define the annealed potential at size N as $\psi_{\rm ann}(\lambda; N) \equiv N^{-1}\mathbb{E}_l \log_2 \mathbb{E}_L \mathbb{E}_{\mathcal{G}} Z_{\mathcal{G}}(L)]$. By a standard saddle point calculation, we get

$$\psi_{\rm ann}(\lambda; N) = \psi_{\rm ann}(\lambda) + \frac{1}{N}\psi^{(1)}_{\rm ann}(\lambda) + O(N^{-2}), \tag{B.2}$$

$$\psi^{(1)}_{\rm ann}(\lambda) \equiv -\frac{1}{2}\log_2[|F''_\lambda(\omega_*)|\omega_*(1-\omega_*)] + \frac{\lambda}{2(\log 2)^2(1-\omega_*)^2|F''_\lambda(\omega_*)|}. \tag{B.3}$$

Here $F_\lambda(\omega)$ is the function maximized in Eq. (10) and ω_* is the point realizing the maximum. As $\lambda \to 0$, we have $\psi^{(1)}_{\rm ann}(\lambda) = C_1\lambda + O(\lambda^2)$.

As claimed in Sec. 3, given $\varepsilon > 0$, $\psi_{\mathcal{G}}(\lambda) \le \psi_{\rm ann}(\lambda) + \varepsilon\lambda^2$ for any $\lambda \ge 0$ with high probability. Let us stress that this statement is stronger than saying that, given $\varepsilon, \lambda \ge 0$, $\psi_{\mathcal{G}}(\lambda) \le \psi_{\rm ann}(\lambda) + \varepsilon\lambda^2$ with high probability. On the other hand, it is required in order to estimate the derivatives of $\psi_{\mathcal{G}}(\lambda)$. It can be proved by distinguishing two regimes (here $1/2 < k < 1$): $\lambda \le CN^{-k}$ and $\lambda > CN^{-k}$. In the first regime, the term $(1-\omega)^l$ in Eq. (B.1) can be replaced by 2^{-l}. The relative error is of order $(\omega - 1/2)l \sim N^{-1/2}\cdot N^{1-k}$, yielding $\mathbb{E}_L\mathbb{E}_{\mathcal{G}} Z_{\mathcal{G}}(L) = 2^{N(1-\alpha)-l}\,[1 + O(N^{1/2-k})]$. Since $Z_{\mathcal{G}}(L)$ is a power of 2 by definition, the probability that $Z_{\mathcal{G}}(L) > 2^{N(1-\alpha)-l}$ is at most $O(N^{1/2-k})$ (recall that $N\alpha$ is an integer). The desired result is obtained by taking expectation with respect to l.

In the second regime, we apply Markov inequality to the random variable $Z_{\mathcal{G}}(L)$ (here we condition on a typical value of $\ell \approx N\lambda$):

$$\mathbb{P}\{\psi_{\mathcal{G}}(\lambda) \ge \psi_{\rm ann}(\lambda) + \varepsilon\lambda^2\} \le 2^{\{-N\left[\psi_{\rm ann}(\lambda)+\varepsilon\lambda^2 - N^{-1}\log_2 \mathbb{E}_L\mathbb{E}_{\mathcal{G}} Z_{\mathcal{G}}(L)\right]\}}. \tag{B.4}$$

The term $N^{-1}\mathbb{E}_L\mathbb{E}_{\mathcal{G}} Z_{\mathcal{G}}(L)$ can be safely estimated by $\psi_{\rm ann}(\lambda; N)$ (deviations of ℓ/N from λ being exponentially rare). The right hand side of the above expression is therefore (neglecting small error terms) $2^{\{-N[\varepsilon\lambda^2 - N^{-1}\psi^{(1)}_{\rm ann}(\lambda) + O(N^{-2})]\}}$. For any finite (as $N \to \infty$) λ, $N^{-1}\psi^{(1)}_{\rm ann}(\lambda) \ll \varepsilon\lambda^2$. If $\lambda \to 0$ (but $\lambda > CN^{-k}$) $N^{-1}\psi^{(1)}_{\rm ann}(\lambda) \sim N^{-1}\lambda \ll \varepsilon\lambda^2$. Therefore the probability that $\psi_{\mathcal{G}}(\lambda) \ge \psi_{\rm ann}(\lambda) + \varepsilon\lambda^2$ is exponentially small.

In Fig. 22 we plot the function $F_\lambda(\omega)$ for $p = 3$, $\lambda = 0$ and a few values of α. For $\alpha < \alpha_{\rm ann} \approx 0.889493$, $F_0(\omega)$ has a global maximum at $\omega = 1/2$ with

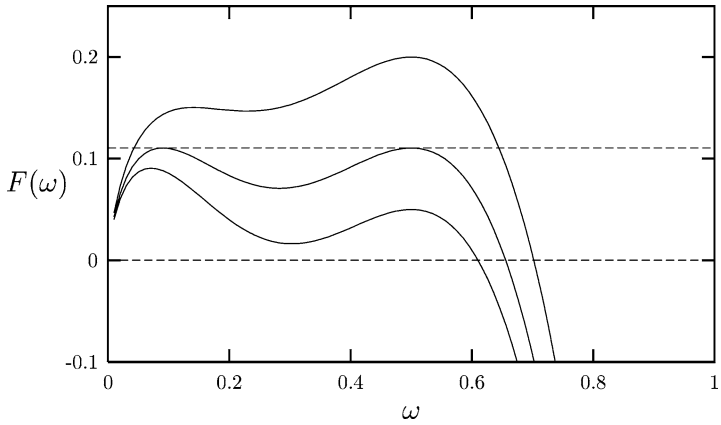

Fig. 22. The function $F_\lambda(\omega)$ (cf. Eq. (10)) for $\lambda = 0$, and from bottom to top $\alpha = 0.8$, $\alpha = \alpha_{\rm ann} \approx 0.889493$ and $\alpha = 0.95$.

$F_0(\omega) = 1 - \alpha - \frac{1}{2}(2\omega - 1)^2 + O((2\omega - 1)^3)$ in its neighborhood. This implies the expansion (11). The same is not true for $\alpha \geq \alpha_{\rm ann}$ because a second local maximum at $\omega < 1/2$ overcomes the first.

The value of $\psi_{\mathcal{G}}(\lambda)$ in the thermodynamic limit can be computed through the cavity method. Alternatively, one can use a leaf-removal argument in the spirit[21] of Refs. 30, 31 We get

$$\psi(\lambda) = \sup_{x\in[0,1]} \{-\alpha + p\alpha(1-x)x^{p-1} + \alpha x^p + \exp[-\lambda - p\alpha x^{p-1}]\}. \qquad \text{(B.5)}$$

For $\alpha < \alpha_{\rm c}$ and $\lambda = 0$, the sup is realized at $x = 0$. A straightforward calculation yields

$$\left.\frac{d\psi}{d\lambda}\right|_0 = -1\,, \qquad \left.\frac{d^2\psi}{d\lambda^2}\right|_0 = 1, \qquad \text{(B.6)}$$

in agreement with the rigorous bounds (12). Higher derivatives can be computed as well and are finite for any $\alpha < \alpha_{\rm d}$. In particular, the third derivative is easily seen to be related to the three points susceptibility $\chi^{\rm SG}_{3,N}$, in analogy with Eq. (9). Under the assumption that the limits $N \to \infty$ and $\lambda \to 0$ can be interchanged, this implies the finiteness of $\chi^{\rm SG}_{n,N}$ for $T = 0$, $\alpha < \alpha_{\rm d}$ and $n \leq 3$.

[21] We also refer to Refs. 66, 67 for an analysis of this algorithm on graph ensembles with general degree distributions. The results of Ref. 67 include Eq. (B.5).

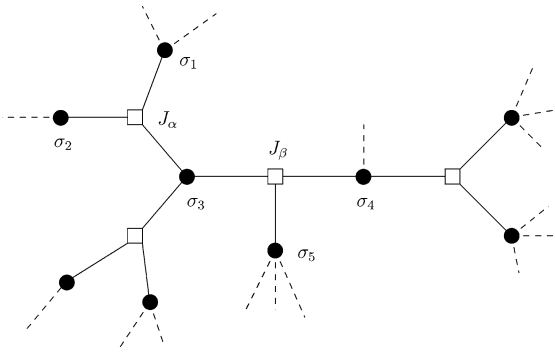

Fig. 23. Portion of the factor graph for the $p = 3$ model. *Dashed lines* indicated other parts of the graph not represented here.

B.2. *n*-Point Correlation Functions: Cavity Argument

The argument of the previous Section could be generalized to finite temperature using the Franz-Parisi quenched potential.[3] A more direct calculation consists in computing the correlation functions $\langle \sigma_{i_1} \dots \sigma_{i_n} \rangle_c$ using the cavity method.

In order to simplify the exposition, consider the three-points function $\langle \sigma_i \sigma_j \sigma_k \rangle$ for $p = 3$. Generalizing to the computation of *connected* correlation functions as well as to other values of n and p should be straightforward. As a further simplification, consider the example in Fig. 23 and $i = 1$, $j = 3$, $k = 4$. The one-step replica symmetry breaking (1RSB) cavity expression for $\langle \sigma_1 \sigma_3 \sigma_4 \rangle$ reads

$$\int \frac{1}{Z\{\rho_i\}} \left\{ \int z_{\text{cav}}\{h_i\}^m \langle \sigma_1 \sigma_3 \sigma_4 \rangle_{\text{cav}}^{\{h_i\}} d\rho_1(h_1) \dots d\rho_5(h_5) \right\} d\mathcal{Q}[\rho_1] \dots d\mathcal{Q}[\rho_5]. \tag{B.7}$$

Here m is Parisi 1RSB parameter,

$$\langle \sigma_1 \sigma_3 \sigma_4 \rangle_{\text{cav}}^{\{h_i\}} = \frac{1}{z_{\text{cav}}\{h_i\}} \sum_{\{\sigma_i\}} \sigma_1 \sigma_3 \sigma_4 \ \exp\{-\beta H_{\text{cav}}(\{\sigma_i\}; \{h_i\})\}, \tag{B.8}$$

$$z_{\text{cav}}\{h_i\} = \sum_{\{\sigma_i\}} \exp\{-\beta H_{\text{cav}}(\{\sigma_i\}; \{h_i\})\}, \tag{B.9}$$

$$H_{\text{cav}}(\{\sigma_i\}; \{h_i\}) = -J_\alpha \sigma_1 \sigma_2 \sigma_3 - J_\beta \sigma_3 \sigma_4 \sigma_5 - \sum_{i=1}^{5} h_i \sigma_i, \tag{B.10}$$

and $Z(\{\rho_i\}) = \int z_{\text{cav}}\{h_i\}^m \, d\rho_1(h_1) \dots d\rho_5(h_5)$. Finally $\mathcal{Q}[\rho]$ is the 1RSB spin glass order parameter, i.e. a distribution over the space of symmetric distributions on $\mathbb{R}$: $\rho(h) = \rho(-h)$.

If $m = 1$ (which is the case for $T > T_c(\alpha)$), these expressions simplify remarkably. One can in fact integrate explicitly over the $\{h_i\}$. Since ρ_i is symmetric, $\int d\rho_i(h_i)\, e^{\beta h_i \sigma_i}$ does not depend on σ_i. The expression in curly brackets in Eq. (B.7) is therefore given by

$$\{\cdots\} = \sum_{\{\sigma_i\}} \sigma_1\sigma_3\sigma_4\, e^{-\beta H_{\rm cav}(\{\sigma_i\};\{0\})} \prod_{i=1}^{5} \int (2\cosh\beta h_i)\, d\rho_i(h_i). \qquad \text{(B.11)}$$

An analogous expression holds for $Z(\{\rho_i\})$. Taking the ratio and integrating over $\mathcal{Q}(\rho_i)$, we get the final result

$$\langle\sigma_1\sigma_3\sigma_4\rangle = \langle\sigma_1\sigma_3\sigma_4\rangle_{\rm cav}^{\{0\}}. \qquad \text{(B.12)}$$

Notice that the cavity fields on the right hand side are set to 0. In particular, for the case at hand $\langle\sigma_1\sigma_3\sigma_4\rangle = 0$. More generally $\langle\sigma_i\sigma_j\sigma_k\rangle$ is different from 0 only if i, j, k are connected by an interaction $-J\sigma_i\sigma_j\sigma_k$. In this case we get $\langle\sigma_i\sigma_j\sigma_k\rangle = \tanh\beta J$. Proceeding analogously, one can show that $\langle\sigma_i\rangle = 0$ and therefore $\langle\sigma_i\sigma_j\sigma_k\rangle = \langle\sigma_i\sigma_j\sigma_k\rangle_c$. Summing over all the triples we find that, in the thermodynamic limit,

$$\chi_3^{\rm SG} = 6\alpha(\tanh\beta)^2. \qquad \text{(B.13)}$$

for any $\alpha < \alpha_c$. Proceeding analogously, one can compute higher order susceptibilities $\chi_n^{\rm SG}$ for any finite n.

B.3. Point-to-Set Correlation Functions at Finite T

In this Appendix we explain how to compute the point-to-set correlation length $\ell_*(\varepsilon)$ and show that it diverges at $T_d(\alpha)$. Recall that the dynamical transition is usually defined using the following equations (one-step replica symmetry breaking with Parisi parameter m)

$$\rho_i(h) = \frac{1}{\mathcal{Z}(\{\hat\rho_\alpha\};m)} \int \prod_{\alpha=1}^{l} d\hat\rho_\alpha(u_\alpha) \times \left(\frac{\cosh\beta h}{\prod_{\alpha=1}^{l}\cosh\beta u_\alpha}\right)^m \delta\left(h - u_1 - \cdots - u_l\right), \qquad \text{(B.14)}$$

$$\hat\rho_\alpha(u) = \int \prod_{i=1}^{p-1} d\rho_i(h_i)\delta\left(u - u(h_1\ldots h_{p-1})\right), \qquad \text{(B.15)}$$

where $u(h_1\ldots h_{p-1}) \equiv \frac{1}{\beta}\text{atanh}[\tanh\beta\tanh\beta h_1\ldots\tanh\beta h_{p-1}]$. The fields distributions $\rho_i(\cdot)$ and $\hat\rho_\alpha(\cdot)$ are required to be symmetric. The indices i and α refer to nodes in the factor graph. When a random factor graph is considered, $\{\rho_i(\cdot)\}$

and $\{\hat\rho_\alpha(\,\cdot\,)\}$ become i.i.d. with common distributions (respectively) $\mathcal{Q}$ and $\widehat{\mathcal{Q}}$, and l becomes a Poisson random variable with mean $p\alpha$. The above equations acquire a distributional meaning. $T_{\rm d}(\alpha)$ is defined as the largest temperature such that a non-trivial solution exists for these distributional equations with $m = 1$.

Using the symmetry of $\hat\rho_a(\,\cdot\,)$, it is easy to show that $\mathcal{Z}(m) = 1$ for $m = 1$. We can therefore average over $\{\rho_i(\,\cdot\,)\}$ and $\{\hat\rho_\alpha(\,\cdot\,)\}$. If we call, respectively $Q(\,\cdot\,)$ and $\widehat{Q}(\,\cdot\,)$ the average distributions, we get

$$Q(h) = \sum_{l=0}^{\infty} e^{-p\alpha}\frac{(p\alpha)^l}{l!}\int\prod_{\alpha=1}^{l} d\widehat{Q}(u_i)x\left(\frac{\cosh\beta h}{\prod_{\alpha=1}^{l}\cosh\beta u_a}\right)\delta(h-u_1-\cdots-u_l), \tag{B.16}$$

$$\widehat{Q}(u) = \int\prod_{i=1}^{p-1} dQ(h_i)\,\delta(u-u(h_1\dots h_{p-1})). \tag{B.17}$$

Consider now the calculation of the point-to-set correlation length $\ell_*(\varepsilon)$. First notice that, within the high temperature phase the cavity fields vanish identically. This means that an equilibrium configuration within a neighborhood of a site i can be constructed as follows. First fix $\sigma_i \in \{+1, -1\}$ uniformly at random. Then for any of the interaction terms involving σ_i, let us say $-J\sigma_i\sigma_{i_1}\dots\sigma_{i_{p-1}}$, generate the other spins from the distribution

$$p_J(\sigma_{i_1},\dots,\sigma_{i_{p-1}}|\sigma_i) = \frac{1}{2^{p-1}\cosh\beta J}\,\exp\{\beta J\sigma_i\sigma_{i_1}\dots\sigma_{i_{p-1}}\}. \tag{B.18}$$

Then repeat the same operation with those neighbors of spins $i_1,\dots,i_{p-1}$ (as well as of the other neighbors of i), which have not yet been fixed. Repeat recursively until all the spins within a distance ℓ from i are determined. This procedure is well defined, because the factor graph is a tree within any fixed distance from i.

Notice that, in order to generate the values of the spins adjacent to σ_i, we did not need to know the graph structure at any distance from i larger than 1. As a consequence, a random graph and a thermalized configuration for that graph can be generated jointly as follows (in the thermodynamic limit). First generate the degree l of site i from a Poisson distribution with parameter $p\alpha$. Then generate the values of the spins which interact with σ_i, according with the rule given above. Repeat the same operation for the $(p-1)l$ neighbors of i, and continue recursively for any fixed distance ℓ.

This gives a procedure for constructing the reference configuration $\sigma^{(0)}$ in our definition of $\ell_*(\varepsilon)$, cf. Eq. (22). The recursive nature of this procedure allows for a recursive calculation of $\ell_*(\varepsilon)$. Condition now on the event that $\sigma_i^{(0)} = \sigma \in \{+1, -1\}$ and constrain a copy of the system to have spin $\sigma_j^{(0)}$ at site j, for any j whose distance from i is at least ℓ. Let h be the effective field acting on site i

under this boundary conditions. This is of course a random quantity, because the reference configuration as well as the underlying graph are random. Denote by $P_\sigma^{(\ell)}(h)$ its distribution, and by $\widehat{P}_\sigma^{(\ell)}(h)$ its distribution under the condition that the degree of i is exactly 1. Then, it is easy to derive the recursions (here we assume, for the sake of simplicity, $J_\alpha = +1$, and use the shorthand $p(\dots|\cdot) = p_{+1}(\dots|\cdot)$)

$$P_\sigma^{(\ell)}(h) = \sum_{l=0}^{\infty} e^{-p\alpha} \frac{(p\alpha)^l}{l!} \int \prod_{a=1}^{l} d\widehat{P}_\sigma^{(\ell)}(u_i)\, \delta\left(h - u_1 - \cdots - u_l\right), \tag{B.19}$$

$$\widehat{P}_\sigma^{(\ell)}(u) = \sum_{\sigma_1 \dots \sigma_{p-1}} p(\sigma_1 \cdots \sigma_{p-1}|\sigma) \int \prod_{i=1}^{p-1} dP_{\sigma_i}^{(\ell-1)}(h_i)\, \delta(u - u(h_1 \dots h_{p-1})), \tag{B.20}$$

which hold for any $\ell > 0$, together with the boundary condition

$$P_\sigma^{(0)}(h) = \delta(h - \sigma\infty), \qquad \widehat{P}_\sigma^{(0)}(u) = \delta(u - \sigma\infty). \tag{B.21}$$

These recursions can be easily approximated numerically using the population dynamics algorithm of Ref. 1. Notice that, by construction, $P_+(h) = P_-(-h)$ and $\widehat{P}_+(u) = \widehat{P}_-(-u)$ and therefore a unique population need to be tracked. Furthermore, the recursion preserves the following property

$$P_+^{(\ell)}(-h) = e^{-2\beta h} P_+^{(\ell)}(h), \qquad \widehat{P}_+^{(\ell)}(-u) = e^{-2\beta u} \widehat{P}_+^{(\ell)}(u). \tag{B.22}$$

The point-to-set length scale $\ell_*(\varepsilon)$ can be estimated by computing the quantity (here $\mathbb{E}_\mathcal{G}$ denotes expectation with respect to the sample realization)

$$\mathbb{E}_\mathcal{G}\mathbb{E}_{\sigma^{(0)}}\left[\sigma_i^{(0)}\langle\sigma_i\rangle_\ell\right] = \int dP_+^{(\ell)}(h)\ \tanh\beta h. \tag{B.23}$$

The data shown in Fig. 4 have been obtained using this approach.

At high enough temperature, the iteration (B.19), (B.20) converges to the trivial fixed point $P_+(h) = P_-(h) = \delta(h)$. As the temperature is lowered, the convergence becomes slower and slower, and the plot of $\mathbb{E}_\mathcal{G}\mathbb{E}_{\sigma^{(0)}}[\sigma_i^{(0)}\langle\sigma_i\rangle_\ell]$ develops a plateau as a function of ℓ. Eventually, the iteration converges to a non-trivial fixed point of Eqs. (B.19), (B.20), let us denote it by $P_\sigma^*(h)$, $\widehat{P}_\sigma^*(u)$. Exploiting the property (B.22) we can rewrite the fixed point distributions as

$$P_\sigma^*(h) = \frac{e^{\beta h\sigma}}{\cosh\beta h}\, P(h), \qquad \widehat{P}_\sigma^*(u) = \frac{e^{\beta u\sigma}}{\cosh\beta u}\, \widehat{P}(u), \tag{B.24}$$

with $P(\cdot)$ and $\widehat{P}(\cdot)$ two symmetric distributions. Rewriting the fixed point condition, cf. Eq. (B.19), (B.20) in terms of $P(\cdot)$ and $\widehat{P}(\cdot)$, we recover the 1RSB equations (B.16), (B.17). We thus proved that the existence of a non trivial fixed point for the 1RSB equations is equivalent to the existence of a non trivial fixed

point for the recursion (B.19), (B.20). Under the assumption that, as soon as such a fixed point appears $P_\sigma^{(\ell)}(\,\cdot\,)$ converges to it,[22] we thus proved that $\ell_*(\varepsilon) = \infty$ for $T < T_{\rm d}(\alpha)$.

APPENDIX C: ASYMPTOTIA

In this series of Appendices we shall work out the rearrangement critical behavior, i.e. both at $\alpha = \alpha_{\rm d}$ and as $\alpha \uparrow \alpha_{\rm d}$. Throughout these Appendices $\delta \equiv \alpha_{\rm d} - \alpha$ will denote the distance to the critical point.

Before embarking in the calculations, it is interesting to draw some parallels with the analytical treatment of the schematic MCT model, and to collect technical properties we shall use in the following.

The time correlation function $C(\tau)$ of the schematic MCT (or of a fully-connected spherical spin-glass model at high temperature) obeys an equation of the form

$$\dot{C}(\tau) = -C(\tau) + \int_0^\tau d\tau'\; M(\tau - \tau')\dot{C}(\tau'), \tag{C.1}$$

where the memory kernel is a polynomial of the correlation function itself, $M(\tau) = V(C(\tau))$. These two equations share some features with the ones governing the distribution of minimal size rearrangements, cf. Eqs. (39), (40): the first one is a convolution on τ (resp. on n), the second a polynomial relation between $M(\tau)$ and $C(\tau)$ (resp. between $\widehat{Q}_n$ and Q_n). In both situations, one of the equations is simple in the "direct space" of τ or n, the other being simpler in Laplace transform (or generating function, see below).

As for MCT, the study of Q_n (and similar quantities) in the critical regime, can be carried out in three steps. First, one considers its decay exactly at the critical point, with n (or τ) fixed. In a second step, one identifies an "intermediate regime" which describes Q_n around its plateau value. Matching these two regimes yields the scale of n in the intermediate regime. The "final regime" describing the decay of Q_n from its plateau to zero can also be described by a scaling function. Again, the corresponding scale of n is derived through a matching argument.

Given a function $a(t)$ defined for $t \geq 0$, the corresponding Laplace transform will be denoted as

$$\mathsf{L}[a](y) = \int_0^\infty a(t)e^{-yt}\; dt. \tag{C.2}$$

The equivalent of Laplace transform for discrete variables is given by generating functions (g.f.). We refer to Refs. 68–70 for an extensive introduction to generating

[22] A proof of this assumption in a similar problem, due to J. Martin and E. Mossel, is reported in Ref. 14.

functions and asymptotic combinatorics methods, and recall here a few basic definitions. Given a sequence a_n defined for $n = 1, 2, \ldots$, the associated g.f. is the formal power series

$$\mathsf{gf}[a](x) = \sum_{n=1}^{\infty} a_n x^n. \tag{C.3}$$

As for Laplace transform, convolutions of discrete sequences translates into products of the corresponding generating functions. We shall sometimes introduce (right) partial sums of a sequence, denoted with the same upper-case letter:

$$A_n = \sum_{n'=n}^{\infty} a_{n'}. \tag{C.4}$$

The corresponding g.f. $f = \mathsf{gf}[a]$ and $F = \mathsf{gf}[A]$ are then related by

$$f(x) = \frac{x-1}{x} F(x) + A_1. \tag{C.5}$$

The asymptotic behavior of a function shows up in the singularities of its Laplace transform. For instance, if $a(t) \simeq A\, t^{\mu}$ when $t \to \infty$, then

$$\mathsf{L}[a](y) = A\, \Gamma(1+\mu) y^{-1-\mu} + \hat{a}_{\mathrm{reg}}(y), \tag{C.6}$$

where $\hat{a}_{\mathrm{reg}}(y)$ denotes a function having milder singularities than $y^{-1-\mu}$ at $y \to 0$. A formally identical formula holds when $a(t) \simeq A\, t^{\mu}$ when $t \to 0$ (in this case one has to look at $y \to \infty$).

Similar relations holds for generating functions. If $a_n \simeq A\, n^{\mu}$ for large n, then the associated generating function behaves as follows near $x = 1$:

$$\mathsf{gf}[a](x) = A\, \Gamma(1+\mu)(1-x)^{-1-\mu} + \hat{a}_{\mathrm{reg}}(x). \tag{C.7}$$

C.1. Minimal Size Rearrangements

Throughout this Section, we shall denote by $f(x)$ (respectively $\hat{f}(x)$) the generating function of the distribution q_n (resp. $\hat{q}_n$) of rearrangements minimal sizes. With this notation, Eq. (39) can be written as

$$f(x) = x\, \exp\{-p\alpha + p\alpha \hat{f}(x)\}\,. \tag{C.8}$$

C.1.1. Order Parameter

Let us first determine the order parameter of the transition, that is to say the fraction of variables with diverging minimal rearrangement sizes. This is defined

as $\phi = \lim_{n\to\infty} Q_n = 1 - f(1)$. Similarly, let $\hat{\phi} = \lim_{n\to\infty} \hat{Q}_n = 1 - \hat{f}(1)$. From Eq. (40) one obtains $\hat{\phi} = \phi^{p-1}$, whereas Eq. (C.8) evaluated at $x = 1$ leads to

$$\phi = 1 - \exp[-p\alpha\phi^{p-1}]. \tag{C.9}$$

This has a non vanishing solution only for $\alpha \geq \alpha_{\rm d}$, where $\alpha_{\rm d}$ is the critical point defined in Eq. (17). The critical point and the value of the order parameter at this point can be determined by the two equations

$$\phi_{\rm d} = 1 - \exp\big[-p\alpha_{\rm d}\phi_{\rm d}^{p-1}\big], \tag{C.10}$$

$$1 = \alpha_{\rm d} p(p-1)\phi_{\rm d}^{p-2} \exp\big[-p\alpha_{\rm d}\phi_{\rm d}^{p-1}\big]. \tag{C.11}$$

The last of these equations expresses the fact that the two functions of ϕ on the left and right hand sides of Eq. (C.9) become tangent at $\phi_{\rm d}$ when $\alpha = \alpha_{\rm d}$.

C.1.2. Critical Decay

We shall first place ourselves right at the transition, $\alpha = \alpha_{\rm d}$, and study the decay of Q_n towards its asymptotic value $\phi_{\rm d}$. Define $\epsilon_n = Q_n - \phi_{\rm d}$ and $\hat{\epsilon}_n = \widehat{Q}_n - \hat{\phi}_{\rm d}$. The generating functions are given by

$$f(x) = 1 - \phi_{\rm d} - \frac{1-x}{x}\,\mathsf{gf}[\epsilon_n](x), \tag{C.12}$$

and a similar expression for $\hat{f}(x)$. In terms of these quantities, Eq. (40) becomes $\hat{\epsilon}_n = (\phi_{\rm d} + \epsilon_n)^{p-1} - \hat{\phi}_{\rm d}$.

Guided by the numerical solution of Eqs. (39), (40) we look for an asymptotic behavior of the form $\epsilon_n \simeq A\, n^{-a}$ as $n \to \infty$. Here a is a positive exponent and A a constant. Equivalently $q_n \simeq A\, a\, n^{-a-1}$. Expanding the relation between ϵ_n and $\hat{\epsilon}_n$, we obtain

$$\hat{\epsilon}_n = (p-1)\phi_{\rm d}^{p-2}\epsilon_n + \binom{p-1}{2}\phi_{\rm d}^{p-3}\epsilon_n^2 + O\big(\epsilon_n^3\big). \tag{C.13}$$

Our aim is now to determine the decay exponent a, by matching the singularities around $x = 1$ in the equation on the generating functions.

Using Eq. (C.7), we obtain $\mathsf{gf}[\epsilon_n](1-s) \simeq A\,\Gamma(1-a)s^{-1+a}$ as $s \to 0$. Assuming $0 < a < 1/2$, we apply the same formula to $\hat{f}$:

$$f(1-s) = 1 - \phi_{\rm d} - \frac{s}{1-s}\,\mathsf{gf}\,[\epsilon_n](1-s)\,, \tag{C.14}$$

$$\hat{f}(1-s) \simeq 1 - \hat{\phi}_d - \frac{s}{1-s}(p-1)\phi_{\rm d}^{p-2}\,\mathsf{gf}\,[\epsilon_n](1-s) - \frac{s}{1-s}\binom{p-1}{2}\phi_{\rm d}^{p-3}\,\mathsf{gf}\,\big[\epsilon_n^2\big](1-s). \tag{C.15}$$

We can now plug these formulae in Eq. (C.8), and match the two sides order by order as $s \to 0$. The terms of order s^0 are equal thanks to the equation (C.10) on the order parameter. The terms proportional to $s\,\mathsf{gf}[\epsilon_n](1-s)$ (of order s^a) match because of Eq. (C.11). Next, on the r.h.s. of Eq. (C.8) two terms of order s^{2a} appear (while none is present on the l.h.s.): one is proportional to $s\,\mathsf{gf}[\epsilon_n^2](1-s)$, and the other to $s^2\,\mathsf{gf}[\epsilon_n]^2(1-s)$. Requiring them to cancel yields the relation (41) which fixes the exponent a.

The l.h.s. of Eq. (41) is shown in Fig. 6. As long as $\lambda \in (0, 1]$, the equation has a unique solution in $[0, 1/2)$. The exponent a is given by this solution, thus verifying the hypothesis $a < 1/2$. It order to show that $\lambda \leq 1$ for any p, we use Eq. (C.11) to simplify the expression for λ:

$$\lambda = (p-2)\frac{1-\phi_{\mathrm{d}}}{\phi_{\mathrm{d}}}. \tag{C.16}$$

Using the inequality $e^x \geq 1 + x$ in Eq. (C.10), we obtain $\alpha_{\mathrm{d}} p \phi_{\mathrm{d}}^{p-2} \geq 1$. Thanks to (C.11) we get $(p-1)(1-\phi_{\mathrm{d}}) \leq 1$, which in turns implies the thesis.

C.1.3. Intermediate Regime

We shall now study the behavior of the probability law of the minimal rearrangements sizes slightly below the critical connectivity, i.e. as $\delta \to 0$.

Inspired by the distribution of zero-temperature point-to-set correlation lengths, studied in Sec. 3.2, we guess that an intermediate scaling regime emerges when $Q_n = \phi_{\mathrm{d}} + O(\delta^{1/2})$. Using the results of the previous Section, we expect this to happen on a scale $n_0(\delta) \sim \delta^{-1/2a}$. For the time being, we only assume that $n_0(\delta)$ diverges at $\delta = 0$ more rapidly than δ^{-1}.

In order to blow up Q_n around its plateau, we define, for any $t > 0$

$$\epsilon(t) = \lim_{\delta \to 0} \delta^{-1/2}[Q_{n=tn_0} - \phi_{\mathrm{d}}], \tag{C.17}$$

and similarly $\hat{\epsilon}(t)$. Using Eq. (40), we get

$$\hat{\epsilon}(t) = (p-1)\phi_{\mathrm{d}}^{p-2}\epsilon(t) + \binom{p-1}{2}\phi_{\mathrm{d}}^{p-3}\delta^{1/2}\epsilon(t)^2 + O(\delta). \tag{C.18}$$

In order to describe the plateau regime, we must properly rescale the generating functions as $\delta \to 0$:

$$f(1-y/n_0) = 1 - \phi_{\mathrm{d}} - \delta^{1/2} y\,\mathsf{L}[\epsilon](y) + o(\delta), \tag{C.19}$$

$$\hat{f}(1-y/n_0) = 1 - \hat{\phi}_d - \delta^{1/2}(p-1)\phi_{\mathrm{d}}^{p-2} y\,\mathsf{L}[\epsilon](y) - \delta\binom{p-1}{2}\phi_{\mathrm{d}}^{p-3} y\,\mathsf{L}[\epsilon^2](y) + o(\delta). \tag{C.20}$$

In order to estimate the remainders, we assumed that $\epsilon(t)$ is smooth for $t > 0$ and has a singularity at $t = 0$ which is milder than $t^{-1/2}$.

We can plug these formulae for $f(\cdot)$ and $\hat{f}(\cdot)$, into Eq. (C.8) and compare the two sides order by order in δ. The terms of order δ^0 and $\delta^{1/2}$ match because of Eqs. (C.10) and (C.11). On the contrary the order δ determines the function $\epsilon(t)$ via

$$\lambda \, \mathsf{L}[\epsilon^2](y) = \frac{B}{y} \; + \; y\{\mathsf{L}[\epsilon](y)\}^2, \tag{C.21}$$

where $B \equiv 2/(\alpha_{\rm d}^2 p(p-1)^2 \phi_{\rm d}^{p-3})$, and λ has been defined above. Inverse Laplace transforming the equation yields to

$$\lambda \, \epsilon(t)^2 = B \; + \; \frac{d}{dt} \int_0^t \epsilon(u)\, \epsilon(t-u) \; du. \tag{C.22}$$

From this equation one can determine the asymptotics of $\epsilon(t)$, which turn out to be:

$$\epsilon(t) \underset{t\to 0}{\sim} t^{-a} \, , \qquad \epsilon(t) \underset{t\to\infty}{\sim} t^{b}, \tag{C.23}$$

where a is the exponent already found in the previous Section, and b is the positive solution of Eq. (43).

This allows us to fix the scale n_0. Consider indeed large (but independent of δ) values of n, and the limit $\delta \to 0$. From the study of the previous Section at $\alpha = \alpha_{\rm d}$, we know that $\epsilon_n \sim n^{-a}$. From the behavior of $\epsilon(t)$ we have $\epsilon_n \sim \delta^{1/2} \epsilon(n/n_0) \sim \delta^{1/2}(n/n_0)^{-a}$. Consistency in the limit $\delta \to 0$ implies thus $n_0 \sim \delta^{-1/2a}$, confirming the qualitative argument given in the beginning of this Section.

In Fig. 24 we use the numerically determined distribution Q_n in order to check the scaling form used in this Section.

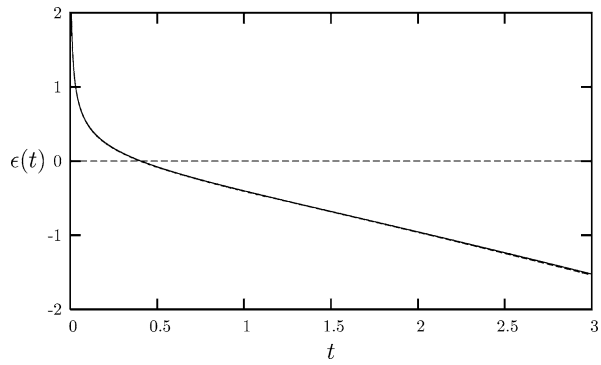

Fig. 24. The scaling function of the intermediate regime, $\epsilon(t)$, as defined in Eq. (C.17). The data used are at $\alpha = 0.816, 0.817, 0.818$, and are almost superimposed.

C.1.4. Final Regime

At what size scale $n_0'(\delta)$ does Q_n exit the plateau regime and decreases by a finite amount below $\phi_{\rm d}$? Using the intermediate regime scaling, we have $Q_{n_0'} - \phi_{\rm d} \simeq \delta^{1/2}\epsilon(n_0'/n_0) = O(1)$. From the behavior of $\epsilon(t)$ at large t, we get $n_0'(\delta) \sim \delta^{-\nu}$, where

$$\nu = \frac{1}{2a} + \frac{1}{2b}. \tag{C.24}$$

In order to describe this regime, we define the scaling limits

$$Q(t) = \lim_{\delta\to 0} Q_{n=tn_0'}, \qquad \psi(y) = \lim_{\delta\to 0} f(1 - y/n_0'), \tag{C.25}$$

and analogous ones for $\widehat{Q}_n$ and $\hat{f}(x)$ (with scaling functions $\widehat{Q}(t)$ and $\hat{\psi}(y)$). As usual, the scaling limits of generating functions are related to Laplace transforms: $\psi(y) = 1 - y\,\mathsf{L}[Q](y)$, $\hat{\psi}(y) = 1 - y\,\mathsf{L}[\widehat{Q}](y)$. Equations (40) and (C.8) imply

$$\widehat{Q}(t) = Q(t)^{p-1}, \;\; \psi(y) = \exp[-p\alpha_{\rm d} + p\alpha_{\rm d}\,\hat{\psi}(y)]. \tag{C.26}$$

This set of equations determines $Q(t)$, the scaling function of the decay of Q_n between $\phi_{\rm d}$ and 0 (this function was denoted as $Q_{\rm slow}(t)$ in Sec. 5.3). In particular they imply $Q(t) \simeq_{t\to 0} \phi_{\rm d} - {\rm cst}\; t^b$. This behavior can be matched with the intermediate regime, cf. previous Section, and can be used to confirm that $n_0'(\delta) \sim \delta^{-\nu}$.

In Fig. 25 we check the scaling form used in this Section against the numerical solution of Eqs. (39), (40).

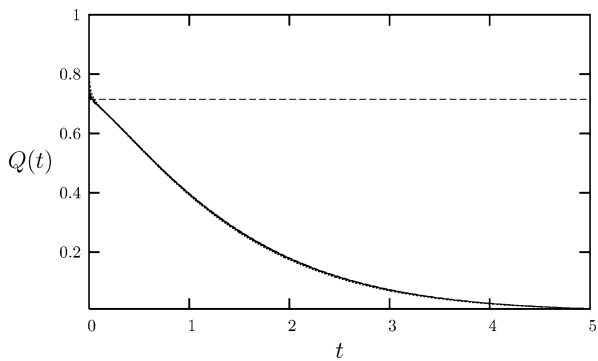

Fig. 25. The scaling function of the final regime, $Q(t)$, as defined in Eq. (C.25). The data used are at $\alpha = 0.812, 0.816, 0.817, 0.818$.

C.1.5. Extreme Decay

What is the probability of an "anomalous" minimal size rearrangement, i.e. a site i such that n_i is much larger than for most of the other sites? This question can be answered by studying the $n \to \infty$ asymptotics of the sizes distribution Q_n.

It is convenient to consider first a slightly modified model, in which the maximum allowed variable degree $l_{\max}$ is a finite number as $N \to \infty$. We refer to Ref. 28 for graph ensembles of this type. It is easy to generalize our treatment to such graphs: Eq. (40) remains unchanged, while Eq. (C.8) is modified to

$$f(x) = x \sum_{l=1}^{l_{\max}} p_l \ \hat{f}(x)^{l-1}. \tag{C.27}$$

Here p_l is the probability that an edge chosen uniformly at random in the factor graph $\mathcal{F}$ is adjacent to a variable node of degree l.

A numerical investigation of Eqs. (40) and (C.27) suggests the Ansatz

$$Q_n = \exp\{-\omega\, n^{1+z} + o(n^{1+z})\}, \tag{C.28}$$

with $z > 0$. Equation (40) implies $\widehat{Q}_n = \exp\{-(p-1)\omega\, n^{1+z} + o(n^{1+z})\}$. The corresponding generating functions can be estimated through the saddle point method. We get

$$f(x) = \exp\left\{ z\omega^{-1/z} \left(\frac{\log x}{z+1}\right)^{\frac{z+1}{z}} + o\left((\log x)^{\frac{z+1}{z}}\right)\right\}, \tag{C.29}$$

as $x \to \infty$. The analogous expression for $\hat{f}(x)$ is obtained replacing ω by $(p-1)\omega$ in the last formula. Inserting into Eq. (C.27) and matching the leading term as $x \to \infty$ determines the exponent z

$$z = \frac{\log(p-1)}{\log(l_{\max}-1)}. \tag{C.30}$$

In other words, the probability of very large rearrangements decreases faster than exponentially. In a given graph $\mathcal{G}$ of size N, the largest minimal size rearrangement $n_{\max}$ can be estimated by setting $N Q_{n_{\max}} = O(1)$, which implies

$$n_{\max} \sim (\log N)^{\frac{1}{1+z}}. \tag{C.31}$$

Let us now reconsider the original model, with unbounded degree. The expression (C.30) yields $z \to 0$. A more careful study shows that

$$Q_n = \exp\left\{-n\, e^{k\,\varphi(n)\,[1+o(1)]}\right\}, \tag{C.32}$$

where $\varphi(n)$ is a function diverging as $n \to \infty$, but more slowly than any iterated logarithm[23] (i.e., for instance, than $\log\log\log n$), and k is a positive constant.

C.2. Minimal Barrier Rearrangements

We present in this Appendix the resolution of Eqs. (56) on the distribution of minimal barriers. We shall first discuss a more general class of distributional equations. The representation developed in this context is then used to solve numerically Eqs. (56). Finally, we analyze the critical behavior of its solution.

C.2.1. Transformation of the Permutation Functionals

Equations (56) involve functionals of the probability distribution $\hat{q}$ which can be generalized to the following problem. Consider l integers (fixed) $y_1, \dots, y_l$, that without loss of generality we assume to be ordered, $y_1 \le \cdots \le y_l$, and define a function f_l of l other integers by

$$f_l(b_1, \dots, b_l) = \min_{\pi} \max_{i\in[1,l]} [b_{\pi(i)} + y_i], \tag{C.33}$$

where the minimum is over the permutations π of $[1, l]$. Assume the b_i's to be i.i.d. random variables with distribution q. What is the distribution of $f_l(b_1, \dots, b_l)$? Its cumulative distribution is

$$1 - F_b^{(l)} = \sum_{b_1,\dots,b_l} q_{b_1} \dots q_{b_l}\, \mathbb{I}(f_l(b_1, \dots, b_l) \ge b), \tag{C.34}$$

which is a functional of the law q.

A first simplification is that the minimum in the definition of f_l is achieved for a permutation π_0 which orders the b_i's by their value (and any such permutation is equivalent). In other words $x_i = b_{\pi_0(i)}$ with $x_1 \ge \cdots \ge x_l$. Now one has

$$\begin{aligned}\mathbb{I}(f_l(b_1, \dots, b_l) \ge b) &= \mathbb{I}\left(\max_{i\in[1,l]} [x_i + y_i] \ge b\right) \\ &= 1 - \mathbb{I}\left(\max_{i\in[1,l]} [x_i + y_i] < b\right) = 1 - \prod_{i=1}^{l} \mathbb{I}(x_i + y_i < b).\end{aligned} \tag{C.35}$$

It is useful to represent the y_i's in a slightly different form. Let us call $l' \in [1, l]$ the number of distinct elements in the set $\{y_1, \dots, y_l\}$, and $y'_1 < \cdots < y'_{l'}$ their values. The degeneracies of the y' are encoded in the coefficients d_j defined for $j \in [1, l']$ as the number of y_i strictly smaller than y'_j. By definition one has $0 = d_1 < \cdots < d_{l'} < l$. As an example, if for $l = 6$, $(y_1, \dots, y_6) = (3, 3, 5, 6, 6, 8)$, one

[23] More precisely, it is a solution of the Abel equation [71] $\varphi(n) = \varphi(\log n) + 1$.

obtains $l' = 4$, $(y'_1, \ldots, y'_4) = (3, 5, 6, 8)$ and $(d_1, \ldots, d_4) = (0, 2, 3, 5)$. These definitions can be used to remove the redundant constraints of Eq. (C.35): if for instance $y_i = y_{i+1}$, $x_i + y_i < b \Rightarrow x_{i+1} + y_{i+1} < b$ as the x_i's are decreasing. These eliminations lead to

$$\mathbb{I}(f_l(b_1, \ldots, b_l) \geq b) = 1 - \prod_{j=1}^{l'} \mathbb{I}(x_{d_j+1} + y'_j < b). \tag{C.36}$$

We now come back to the original variables b and define m_j, for $j \in [1, l']$, as the number of b_i's strictly smaller than $b - y'_j$. This imply that

$$x_1 \geq \cdots \geq x_{l-m_j} \geq b - y'_j > x_{l-m_j+1} \geq \ldots \geq x_l. \tag{C.37}$$

We thus have $x_{d_j+1} + y'_j < b \Leftrightarrow m_j \geq l - d_j$. We can now insert Eq. (C.36) in the definition (C.34) and trade the sum on the b_i against a sum on the m_j respecting the above derived constraints.

$$F_b^{(l)} = \sum_{\{m_j\}} \frac{l!}{\prod_{j=1}^{l'-1}(m_j - m_{j+1})! m_{l'}!} \prod_{j=1}^{l'-1} (Q_{b-y'_{j+1}} - Q_{b-y'_j})^{m_j - m_{j+1}} (1 - Q_{b-y'_{l'}})^{m_{l'}}. \tag{C.38}$$

The combinatorial factor arises from the change of variables from the b's to the m's, and the constrained sum is over

$$l = m_1 \geq \cdots \geq m_{l'}, \quad m_j \geq l - d_j \ \forall j \in [1, l']. \tag{C.39}$$

In the following, we shall repeatedly use the representation of $F_b^{(l)}$ provided by (C.38), (C.39).

Before leaving this general preliminary, let us note that if the b_i's are bounded from below by $b_{\min}$ (i.e. $q_b = 0$ for $b < b_{\min}$), $f_l(b_1, \ldots, b_l)$ is bounded from below by $b_{\min} + y_l$, hence $F_b^{(l)} = 0$ for $b \leq b_{\min} + y_l$.

C.2.2. Application to the p-Spin Model and Numerical Resolution

The equations (56), determining the barrier distribution of the p-spin model (1), can be rewritten as

$$Q_b = \sum_{l=0}^{\infty} p_l \big(1 - F_b^{(l)}[\{\hat{q}\}]\big), \qquad \widehat{Q}_b = Q_b^{p-1}, \tag{C.40}$$

where $F_b^{(l)}$ is of the general form studied in the previous pages, with the b_i's drawn with the law $\hat{q}$, and the y_i's given by $y_i = \lfloor \frac{i}{2} \rfloor$. Here we set by convention $F_b^{(0)} = \mathbb{I}(b \geq 2)$.

Following the notations of the previous Section, one has for a given value of l: $l' = \lfloor \frac{l}{2} \rfloor + 1$, $y'_i = i - 1$, $d_1 = 0$ and $d_j = 2j - 3$ for $2 \leq j \leq l'$. As the law

$\hat{q}$ is supported on the positive integers, $F_b^{(l)} = 0$ for $b \le l'$. This allows to rewrite the equation (C.40) under the form:

$$1 - Q_b = p_0\, \mathbb{I}(b \ge 2) + p_1(1 - \widehat{Q}_b) + \mathbb{I}(b \ge 3) \sum_{l=2}^{2b-3} p_l\, F_b^{(l)}[\{\hat{q}\}]\,, \qquad \text{(C.41)}$$

$$F_b^{(l)}[\{\hat{q}\}] = \sum_{\{m_j\}}{}' \frac{l!}{\prod_{j=1}^{\lfloor l/2\rfloor}(m_j - m_{j+1})!\, m_{\lfloor l/2\rfloor+1}!} \times \left(\prod_{j=1}^{\lfloor l/2\rfloor} \hat{q}_{b-j}^{\,m_j - m_{j+1}}\right) (1 - \hat{Q}_{b-\lfloor l/2\rfloor})^{m_{\lfloor l/2\rfloor+1}}, \qquad \text{(C.42)}$$

with the constraints on the sum in $F_b^{(l)}$:

$$l = m_1 \ge \cdots \ge m_{\lfloor l/2\rfloor+1}, \quad m_j \ge l + 3 - 2j \ \ \forall j \in [2, \lfloor l/2\rfloor + 1]. \qquad \text{(C.43)}$$

These equations allow to determine the distribution of messages $v_{i\to\alpha}$, $u_{\alpha\to i}$ defined in Sec. 6.3 (anchored barriers). The distribution of actual barriers to flip a spin in the system can be expressed in a similar way,

$$1 - Q_b^{\rm site} = p_0\, \mathbb{I}(b \ge 1) + p_1(1 - \hat{Q}_b) + \mathbb{I}(b \ge 2) \sum_{l=2}^{2b-2} p_l G_b^{(l)}[\{\hat{q}\}]\,, \qquad \text{(C.44)}$$

$$G_b^{(l)}[\{\hat{q}\}] = \sum_{\{m_j\}}{}' \frac{l!}{\prod_{j=1}^{\lceil l/2\rceil-1}(m_j - m_{j+1})!\, m_{\lceil l/2\rceil}!} \times \prod_{j=1}^{\lceil l/2\rceil-1} \hat{q}_{b-j}^{\,m_j - m_{j+1}} (1 - \hat{Q}_{b-\lceil l/2\rceil+1})^{m_{\lceil l/2\rceil}}, \qquad \text{(C.45)}$$

with the constraints on the sum in $G_b^{(l)}$:

$$l = m_1 \ge \cdots \ge m_{\lceil l/2\rceil}, \quad m_j \ge l + 2 - 2j \ \ \forall j \in [2, \lceil l/2\rceil]. \qquad \text{(C.46)}$$

By convention the products from $j = 1$ to $j = 0$ which appear in $G_b^{(2)}$ are equal to 1.

Unlike for the minimal size distribution, Eqs. (C.40) do not provide immediately an algorithm for computing Q by recursion over b. The reason is that the anchored barrier of a rooted tree is at least as large, but not necessarily larger, than the anchored barriers of its sub-trees. Consider now the process of merging l sub-trees (this corresponds to iterating (C.40) once). If sub-trees barrier distribution are known only up to barrier height $b - 1$, the barrier distribution of the new, larger tree is necessarily undetermined at height b.

We can propose two ways to solve this difficulty. The first one is to derive a well-behaved recursion on b. Assume that Q and $\widehat{Q}$ (resp. q and $\hat{q}$) are known upto height $b-1$ (resp. $b-2$). The only unknown of the right hand side of Eq. (C.41) is $\hat{q}_{b-1}$, which appears linearly because of the conditions $m_1 = l, m_2 \geq l-1$ in the sum (C.42). We can thus write

$$1 - Q_b = A_b\, \hat{q}_{b-1} + B_b, \tag{C.47}$$

where the coefficients A_b and B_b are computable from $\hat{q}_1, \ldots, \hat{q}_{b-2}$ using Eq. (C.42). Using $\hat{q}_{b-1} = \widehat{Q}_{b-1} - \widehat{Q}_b$, and $\widehat{Q}_b = Q_b^{p-1}$, one ends up with

$$1 - Q_b + A_b Q_b^{p-1} = A_b\, \widehat{Q}_{b-1} + B_b. \tag{C.48}$$

One can solve this equation for Q_b (recall that $\widehat{Q}_{b-1}$ is assumed to be known at this stage) and therefore determine q_{b-1}, $\widehat{Q}_b = Q_b^{p-1}$ and $\hat{q}_{b-1}$. This allows to continue the recurrence at the next barrier height.

The second method is iterative: make an initial guess for the law Q, compute the law $\widehat{Q}_b = Q_b^{p-1}$, cf. Eq. (C.40), and inject it in (C.41) to recompute Q. Any fixed point of this procedure corresponds to a solution of Eqs. (C.40). Since the solution is unique, whenever the procedure converges, it provides a good numerical approximation of this solution. It can be argued[24] that the iterative procedure indeed converges for any $\alpha < \alpha_{\rm d}$, if the initial condition $Q_b^{(0)} = \mathbb{I}\,(b \leq 1)$ is used.

C.2.3. Asymptotics

In this Appendix we work out the asymptotic behavior of minimal barrier distributions, cf. Sec. 6.5. Motivated by the results on minimal size rearrangements, cf. Sec. C.1, we look for a plateau at $Q_b \approx \phi_{\rm d}$, $\widehat{Q}_b \approx \hat{\phi}_{\rm d}$. We thus define

$$Q_b = \phi_{\rm d} + \epsilon_b, \qquad \widehat{Q}_b = \hat{\phi}_{\rm d} + \hat{\epsilon}_b\ . \tag{C.49}$$

With this definition one can set up an expansion of the functionals $F_b^{(l)}$ in powers of $\hat{\epsilon}$. We shall need in the following this expansion upto terms of order $\hat{\epsilon}^2$. Four types of terms appear at this order in Eq. (C.42) :

- $m_1 = \cdots = m_{\lfloor l/2 \rfloor + 1} = l$, which gives a term of order 1.
- $m_1 = \cdots = m_s = l, \quad m_{s+1} = \cdots = m_{\lfloor l/2 \rfloor + 1} = l-1, \quad$ with $\quad 1 \leq s < \lfloor l/2 \rfloor + 1$, of order $\hat{\epsilon}$.
- $m_1 = \cdots = m_s = l, \quad m_{s+1} = \cdots = m_{\lfloor l/2 \rfloor + 1} = l-2, \quad$ with $\quad 2 \leq s < \lfloor l/2 \rfloor + 1$, of order $\hat{\epsilon}^2$.

[24] A complete proof is beyond the scope of this Appendix. The basic idea is that the function $Q_b^{(\ell)}$ obtained after ℓ iterations, is the minimal barrier distribution for a subgraph of radius ℓ around a random node i. Convergence follows from the remark that this barriers become larger (and therefore $Q_b^{(\ell)}$ worsen, in a sense that can be made precise) as ℓ increases.

- $m_1 = \cdots = m_s = l$, $m_{s+1} = \cdots = m_t = l-1$, $m_{t+1} = \cdots = m_{\lfloor l/2 \rfloor + 1} = l-2$, with $1 \le s < t < \lfloor l/2 \rfloor + 1$, of order $\hat{\epsilon}^2$.

Summing this terms and expanding the result upto order $\hat{\epsilon}^2$, we obtain:

$$F_b^{(l)} = (1-\hat{\phi}_{\rm d})^l - l(1-\hat{\phi}_{\rm d})^{l-1}\hat{\epsilon}_b + \binom{l}{2}(1-\hat{\phi}_{\rm d})^{l-2}\big[2\hat{\epsilon}_b\hat{\epsilon}_{b-1} - \hat{\epsilon}_{b-1}^2\big] + O(\hat{\epsilon}^3). \tag{C.50}$$

Inserting this expansion in Eq. (C.41), assuming $b \ge 3$ (we are interested in the large b behavior) leads to

$$\begin{aligned} 1 - \phi_{\rm d} - \epsilon_b = &\left[\sum_{l=0}^{2b-3} p_l (1-\hat{\phi}_{\rm d})^l\right] - \left[\sum_{l=0}^{2b-3} p_l l (1-\hat{\phi}_{\rm d})^{l-1}\right]\hat{\epsilon}_b \\ &+ \left[\sum_{l=0}^{2b-3} p_l \binom{l}{2}(1-\hat{\phi}_{\rm d})^{l-2}\right]\big[2\hat{\epsilon}_b\hat{\epsilon}_{b-1} - \hat{\epsilon}_{b-1}^2\big] + O(\hat{\epsilon}^3). \end{aligned} \tag{C.51}$$

Since we are interested in the large b behavior, we can extend the sum on l upto infinity with a negligible error.[25] Moreover we can expand the first equation in (C.40) to express $\hat{\epsilon}_b$ in terms of ϵ_b. Ordering the different powers of ϵ, we get

$$\begin{aligned} &\big[1 - \phi_{\rm d} - e^{-\alpha p \hat{\phi}_{\rm d}}\big] + \epsilon_b\big[\alpha p(p-1)\phi_{\rm d}^{p-2} e^{-\alpha p\hat{\phi}_{\rm d}} - 1\big] \\ &+ \frac{\alpha p(p-1)(p-2)}{2}\phi_{\rm d}^{p-3} e^{-\alpha p\hat{\phi}_{\rm d}}\epsilon_b^2 \\ &- \frac{(\alpha p(p-1))^2}{2}\phi_{\rm d}^{2p-4} e^{-\alpha p\hat{\phi}_{\rm d}}\big(2\epsilon_b\epsilon_{b-1} - \epsilon_{b-1}^2\big) = O(\epsilon^3). \end{aligned} \tag{C.52}$$

We now consider the critical limit $\delta \to 0$ infinitesimal. The two terms in brackets vanishes at $\delta = 0$, because of Eqs. (C.10) and (C.11). Expanding also in powers of δ, we obtain

$$B\delta = \lambda\epsilon_b^2 - 2\epsilon_b\epsilon_{b-1} + \epsilon_{b-1}^2 + O(\delta^2,\ \delta\epsilon,\ \epsilon^3), \tag{C.53}$$

where B and λ are as defined in Appendix C.1, cf., for instance, Eq. (C.21).

Notice that Eq. (C.53) is simpler than the analogous equation for minimal size rearrangements, i.e. Eq. (C.21). In particular, it is not necessary to introduce generating functions or Laplace transforms: Eq. (C.53) is local in the "direct space" of barriers.

Let us consider first the large b behavior at the critical point $\alpha_{\rm d}$. The left hand side of (C.53) vanishes (as well as all corrections proportional to δ), and one

[25] More precisely, we shall eventually focus on $b = O(\log(1/\delta))$, and retain terms in this equation up to $O(\delta)$. On the other hand, extending the sums up to $l = \infty$ produces errors of order $1/b! \doteq \exp(-b\log b) \doteq (\log(1/\delta))^{\log\delta} \ll \delta$ (to the leading exponential order).

can look for a solution such that $\epsilon_b \sim e^{-\omega_a b}$ as $b \to \infty$. Injecting this Ansatz in Eq. (C.53) and requiring the terms of order $e^{-2\omega_a b}$ to cancel yields the condition $\lambda - 2e^{\omega_a} + e^{2\omega_a} = 0$, which fixes ω_a, as announced in Eq. (58).

In order for Eq. (C.53) to have a non-trivial limit within the plateau regime, we must have $Q_b = \phi_{\rm d} + O(\delta^{1/2})$ in this regime. We therefore assume the existence of a diverging scale $b_0 = b_0(\delta)$, and define $\bar{\epsilon}_m = \delta^{-1/2}\epsilon_{b=m+b_0}$. Substituting in Eq. (C.53) and taking the $\delta \to 0$ limit, we get

$$B = \lambda\bar{\epsilon}_m^2 - 2\bar{\epsilon}_m\bar{\epsilon}_{m-1} + \bar{\epsilon}_{m-1}^2. \tag{C.54}$$

It is easy to work out the asymptotic behavior of the solution of this equation. We get $\bar{\epsilon}_m \simeq C_- e^{-\omega_a m}$ as $m \to -\infty$, and $\bar{\epsilon}_m \simeq -C_+ e^{\omega_b m}$ as $m \to +\infty$, where ω_b is given by Eq. (60) and $C_\pm$ are two positive constants.

The scale b_0 is fixed by matching the behavior of ϵ_b at $\alpha_{\rm d}$ for $b \to \infty$ with the one of $\bar{\epsilon}_m$ when $m \to -\infty$. Consider a large (but independent of δ) value of b, and the limit $\alpha \to \alpha_{\rm d}$:

$$\epsilon_b \sim e^{-\omega_a b} \sim \delta^{1/2}\bar{\epsilon}_{m=b-b_0} \sim \delta^{1/2} e^{\omega_a b_0} e^{-\omega_a b}. \tag{C.55}$$

The dependence on δ cancels only if $b_0(\delta) \simeq \log(1/\delta)/(2\omega_a)$. In Fig. 26, left frame, we plot the outcome of a numerical resolution of the equations (C.40) along the lines exposed in the previous Section. The data are rescaled in such a way to exhibit the plateau scaling. More precisely, we plot

$$\delta^{-1/2}[Q_b - \phi_{\rm d}], \tag{C.56}$$

for several values of δ, as a function of $m = b - \log(1/\delta)/(2\omega_a)$. The good collapse of the curves confirm the analysis just presented.

Notice that the quantity (C.56) is not expected to converge to a unique curve as a function of m, even if $b_0(\delta)$ is chosen optimally (here we just derived its asymptotic behavior). In other words, $\bar{\epsilon}_m$ is not a scaling function in the usual sense. The reason is that Eq. (C.54) has more than one solution, and two such solutions $\bar{\epsilon}^{(1)}$ and $\bar{\epsilon}^{(2)}$ cannot be superimposed through a shift of the

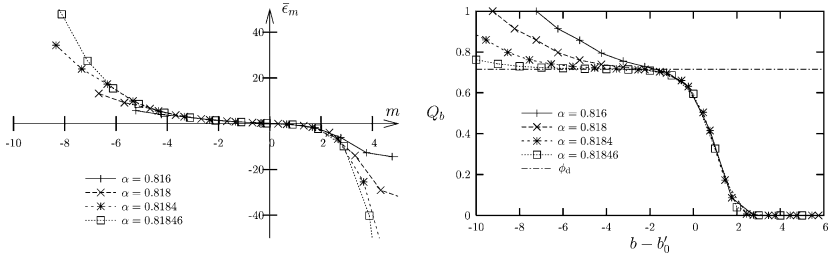

Fig. 26. *Left*: the scaling function $\bar{\epsilon}_m$ for the minimal barrier rearrangements. *Right*: collapse on the scale of exit from the plateau.

m axis (this is related to the fact that m is discrete). On the other hand, a shift can be found such that $\bar{\epsilon}_m^{(1)} < \bar{\epsilon}_m^{(2)} < \bar{\epsilon}_{m+1}^{(1)}$. Therefore the function (C.56) will converge, as a function of $m = b - b_0(\delta)$, within a $O(1)$ distance around any solution of Eq. (C.54). This is enough for the analysis presented in this pages to be valid.

Finally, the scale $b_0'(\delta)$ for the decrease of Q_b from $\phi_{\rm d}$ to 0, can be defined as the smallest b such that $Q_b < Q_*$ with Q_* any fixed number smaller than $\phi_{\rm d}$. It can be estimated by requiring ϵ_b to be of order 1, or, equivalently, $\bar{\epsilon}_b$ to be of order $\delta^{-1/2}$. This implies $\bar{\epsilon}_{b_0'-b_0} \sim \delta^{-1/2}$, i.e. $e^{\omega_b(b_0'-b_0)} \sim \delta^{-1/2}$, hence

$$b_0'(\delta) \simeq b_0(\delta) + \frac{1}{2\omega_b}\log(1/\delta) \simeq \left(\frac{1}{2\omega_a} + \frac{1}{2\omega_b}\right)\log(1/\delta), \tag{C.57}$$

as announced in Eq. (61).

Figure 26, right frame, shows Q_b (obtained from the numerical resolution of Eqs. (C.40)), as a function of $m' = b - b_0'(\delta)$. The curves for different values of δ collapse between 0 and $\phi_{\rm d}$, thus confirming our analysis.

Contrary to the minimal size case, one cannot define a scaling function for the last decay from the plateau value to 0. Indeed, this happens on an interval of b which remains of order 1 when $\delta \to 0$. This means that a finite fraction of the barriers is not just of order $b_0'(\delta)$, but within a finite additive constant from $b_0'(\delta)$.

This asymptotic study has been performed on the distributions Q and $\widehat{Q}$ of the messages on the links of the factor graph (anchored barriers). However, actual barriers to spin flips differ at most by one from anchored barriers. The discussion presented so far is thus also valid for the actual barrier distribution $Q_b^{\rm site}$.

C.3. Average Size of Minimal Barrier Rearrangement

Let us explain how to derive the results presented in Sec. 7.1 on the average size of minimal barrier rearrangements. To this aim one has to solve Eqs. (73) and (74). The first of these equations involves a constrained sum on l anchored barriers $b_1, \ldots, b_l$, whose disjoint combination $\hat{f}_l(b_1, \ldots, b_l)$ leads to a prescribed barrier b. This is similar to Eq. (56) (first equation) that was solved in Appendix C.2. Unlike in Eq. (56), one of the l barriers is not drawn from the distribution $\hat{q}$, but is the argument of the unknown sequence M. Let us define an integrated version of this sequence (as well as of the related $\widehat{M}$),

$$N_b = \sum_{b'<b} M_{b'}, \qquad \widehat{N}_b = \sum_{b'<b} \widehat{M}_{b'}. \tag{C.58}$$

Notice that, at odds with our usual conventions we integrated to the left. Equation (73) can thus be rewritten as

$$N_b = 1 - Q_b + \sum_{l=1}^{2b-3} p_l l \, N_b^{(l)},$$

$$N_b^{(l)} = \sum_{b_1,\ldots,b_l} \widehat{M}_{b_1} \hat{q}_{b_2} \ldots \hat{q}_{b_l} \mathbb{I}(\hat{f}_l(b_1,\ldots,b_l) < b). \tag{C.59}$$

The sum in $N_b^{(l)}$ can be transformed following the strategy exposed in Appendix C.2, treating the distinguished index b_1 separately from the others. A similar reasoning leads indeed to

$$N_b^{(l)} = \sum_{\{m_j, m'_j\}}{}' \frac{(l-1)!}{\prod_{j=1}^{\lfloor l/2 \rfloor}(m_j - m_{j+1})! m_{\lfloor l/2 \rfloor + 1}!} \cdot \times \left(\prod_{j=1}^{\lfloor l/2 \rfloor} \hat{q}_{b-j}^{\,m_j - m_{j+1}} \widehat{M}_{b-j}^{m'_j - m'_{j+1}} \right) (1 - \widehat{Q}_{b-\lfloor l/2 \rfloor})^{m_{\lfloor l/2 \rfloor + 1}} (\widehat{N}_{b-\lfloor l/2 \rfloor})^{m'_{\lfloor l/2 \rfloor + 1}}, \tag{C.60}$$

where the parameters of the sum obey the following constraints:

$$l - 1 = m_1 \geq \ldots \geq m_{\lfloor l/2 \rfloor + 1}, \quad 1 = m'_1 \geq \ldots \geq m'_{\lfloor l/2 \rfloor + 1}$$
$$m_j + m'_j \geq l + 3 - 2j \;\; \forall j \in [2, \lfloor l/2 \rfloor + 1]. \tag{C.61}$$

We have encoded the value of the special index b_1 in the sequence of the m'_j, with $m'_j = 1 \Leftrightarrow b_1 < b - j + 1$. The form (C.60) is suitable for numerical resolution of Eqs. (73), (74), following one of the two strategies (recursion or functional iteration) explained in Sec. 9.

Let us now study the asymptotic regime $\alpha \to \alpha_{\rm d}$. Following the notations of Appendix C.2, we can expand Eq. (C.60) in powers of $\hat{\epsilon}_b = \widehat{Q}_b - \hat{\phi}_{\rm d}$:

$$N_b^{(l)} = (1 - \hat{\phi}_{\rm d})^{l-1} \widehat{N}_b + (l-1)(1 - \hat{\phi}_{\rm d})^{l-2} [\widehat{N}_{b-1}(\hat{\epsilon}_{b-1} - \hat{\epsilon}_b) - \widehat{N}_b \hat{\epsilon}_{b-1}] + O(\hat{\epsilon}^2). \tag{C.62}$$

Inserting this expansion in Eq. (C.59), and extending the sum on l to infinity (as in Sec. C.2.3, this produces a negligible error) leads to

$$N_b = 1 - \phi_{\rm d} - \epsilon_b + \alpha p e^{-\alpha p \hat{\phi}_{\rm d}} \widehat{N}_b + (\alpha p)^2 e^{-\alpha p \hat{\phi}_{\rm d}} [\widehat{N}_{b-1}(\hat{\epsilon}_{b-1} - \hat{\epsilon}_b) - \widehat{N}_b \hat{\epsilon}_{b-1}] + O(\hat{\epsilon}^2). \tag{C.63}$$

Expanding also Eq. (74) to the same order yields

$$\widehat{M}_b = M_b (p-1) \phi_{\rm d}^{p-2} \left[1 + \frac{p-2}{2\phi_{\rm d}} (\epsilon_b + \epsilon_{b+1}) \right] + O(M\epsilon^2). \tag{C.64}$$

Next we take finite differences of Eq. (C.63) and trade $\widehat{N}$ for N, thanks to (C.64), and $\hat{\epsilon}$ for ϵ, thanks to Eq. (40). We finally get

$$\begin{aligned}\left[1-p(p-1)\alpha\phi_{\rm d}^{p-2}e^{-p\alpha\hat{\phi}_{\rm d}}\right](N_{b+1}-N_b) &= \frac{1}{2}p(p-1)(p-2)\alpha\phi_{\rm d}^{p-3}e^{-p\alpha\hat{\phi}_{\rm d}}\\ &\times(N_{b+1}-N_b)(\epsilon_b+\epsilon_{b+1}) - p^2(p-1)^2\alpha^2\phi_{\rm d}^{2p-4}e^{-p\alpha\hat{\phi}_{\rm d}}\\ &\times[N_{b+1}\epsilon_b + N_b(\epsilon_{b+1}-\epsilon_b-\epsilon_{b-1}) + N_{b-1}(\epsilon_{b-1}-\epsilon_b)] + O(1, N\epsilon^2). \quad \text{(C.65)}\end{aligned}$$

As usual, we consider three distinct asymptotic regimes. Let us begin by assuming $\alpha = \alpha_{\rm d}$ and b large. The l.h.s. of Eq. (C.65) vanishes because of Eq. (C.11). Moreover, we know from Appendix C.2.3 that $\epsilon_b \sim e^{-\omega_a b}$. Numerical computations suggest the Ansatz $N_b \sim e^{\mu_a b}$, with $\mu_a > \omega_a > 0$. Under this Ansatz terms of order 1 and $N\epsilon^2$ can be safely neglected in Eq. (C.65). Requiring the r.h.s. to vanish to the leading order $e^{(\mu_a-\omega_a)b}$, yields the condition

$$\frac{(e^{\mu_a-\omega_a}-1)\left(e^{\omega_a}+e^{-\mu_a}-e^{-(\mu_a-\omega_a)}\right)}{(e^{\mu_a}-1)(e^{-\omega_a}+1)} = \frac{\lambda}{2}. \quad \text{(C.66)}$$

It is not hard to show that the above equation admits a unique solution larger than ω_a, thus completely determining the exponent μ_a. For instance when $p = 3$ one obtains $\mu_a \approx 0.81650 > \omega_a \approx 0.57432$.

Consider now the intermediate regime, $\delta \to 0$, with $b = m + b'_0(\delta)$, where $b'_0(\delta) \simeq \log(1/\delta)/(2\omega_a)$ and m is finite. We found in this regime a scaling function $\bar{\epsilon}_m$, such that $\epsilon_b \simeq \delta^{1/2}\bar{\epsilon}_m$. Let us introduce now a similar scaling function for the N_b's, $N_b \sim \delta^{-x}\overline{N}_m$, with x a still unknown exponent that we assume to be larger than $1/2$. With this assumption, the dominant terms in Eq. (C.65) are of order $\delta^{-x+1/2}$. Imposing Eq. (C.65) to hold at this order, we obtain the following equation for the scaling function $\overline{N}_m$:

$$\begin{aligned}&\overline{N}_{m+1}\bar{\epsilon}_m + \overline{N}_m(\bar{\epsilon}_{m+1}-\bar{\epsilon}_m-\bar{\epsilon}_{m-1}) + \overline{N}_{m-1}(\bar{\epsilon}_{m-1}-\bar{\epsilon}_m)\\ &= \frac{\lambda}{2}(\overline{N}_{m+1}-\overline{N}_m)(\bar{\epsilon}_{m+1}+\bar{\epsilon}_m). \quad \text{(C.67)}\end{aligned}$$

We found in Appendix C.2.3 that $\bar{\epsilon}_m \sim e^{-\omega_a m}$ (resp. $\bar{\epsilon}_m \sim e^{\omega_b m}$) in the $m \to -\infty$ (resp. $+\infty$) limit. Using these results, one can derive the asymptotic behavior of $\overline{N}_m$ in these two limits. When $m \to -\infty$, we have $\overline{N}_m \sim e^{\mu_a m}$, where μ_a is the exponent previously determined. When $m \to +\infty$, $\overline{N}_m \sim e^{\mu_b m}$, where μ_b is the unique positive solution of

$$\frac{(e^{\mu_b+\omega_b}-1)(e^{-\omega_b}+e^{-\mu_b}-e^{-\mu_b-\omega_b})}{(e^{\mu_b}-1)(e^{\omega_b}+1)} = \frac{\lambda}{2}. \quad \text{(C.68)}$$

For instance, we obtain $\mu_b \approx 3.90350$ for $p = 3$.

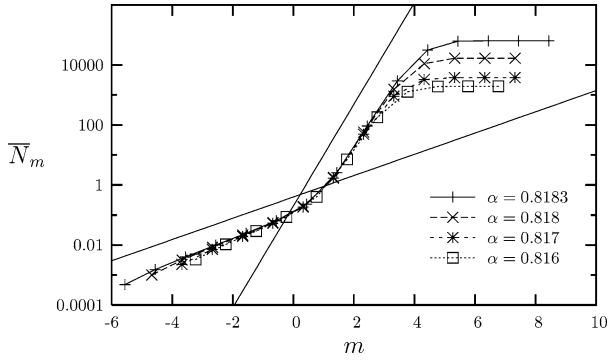

Fig. 27. The intermediate regime scaling function for the study of the size of minimal barrier rearrangements. The two *solid straight lines* have the slope of the asymptotic behaviors, $\overline{N}_m \sim e^{\mu_{a/b} m}$ when $m \to \pm\infty$.

The exponent x is obtained by matching the limit $b \to \infty$ of the $\alpha = \alpha_{\rm d}$ solution, and the limit $m \to -\infty$ of the intermediate regime:

$$N_b \sim e^{\mu_a b} \sim \delta^{-x} e^{\mu_a (b-b_0)} = e^{\mu_a b} \delta^{-x+\frac{\mu_a}{2\omega_a}}. \tag{C.69}$$

For the dependence on δ to cancel, we have to take $x = \mu_a/(2\omega_a)$. Note that the assumption $x > 1/2$ is a posteriori confirmed, as $\mu_a > \omega_a$.

This analysis of the intermediate regime is confirmed by Fig. 27. Here we plot $\delta^x N_b$, versus $m = b - \log(1/\delta)/(2\omega_a)$, with N_b computed numerically for several values of δ, and x determined analytically as explained above.

Finally, we look for the asymptotic behavior of N_b when $b \sim b_0'(\delta)$ the typical height of large minimal barriers (recall that $b_0'(\delta) \simeq \Upsilon \log(1/\delta)$). From the behavior of $\overline{N}_m$ when $m \to +\infty$, we get

$$N_b \sim \delta^{-x} e^{\mu_b (b_0' - b_0)} \sim \delta^{-\nu_{\rm barr}}, \quad \nu_{\rm barr} = \frac{\mu_a}{2\omega_a} + \frac{\mu_b}{2\omega_b}. \tag{C.70}$$

As q_b is of order 1 in this regime, the exponent $\nu_{\rm barr}$ is indeed the one which controls the divergence of M_b/q_b, the average size of large scale minimal barrier rearrangements.

C.4. Average Distance in Minimal Sizes Rearrangements

We study in this Appendix the asymptotic behavior of the solution T_n of Eqs. (85). This allows to compute the average radius of minimal size rearrangements. Let us denote $g(x)$ and $\tilde{g}(x)$ the g.f.'s associated respectively to T_n and $\widetilde{T}_n$. The first of Eqs. (85) can be rewritten as

$$g(x) = p\alpha\, f(x)\tilde{g}(x), \tag{C.71}$$

where f is the g.f. of the q_n's.

Consider first the solution at $\alpha = \alpha_{\rm d}$. From the results of Sec. C.1 we have the following asymptotic behaviors as $n \to \infty$ ($s \to 0$):

$$f(1-s) = 1 - \phi_{\rm d} - A\Gamma(1-a)s^a + o(s^a), \tag{C.72}$$

$$\frac{\hat{q}_n}{q_n} = (p-1)\phi_{\rm d}^{p-2} + A(p-1)(p-2)\phi_{\rm d}^{p-3}n^{-a} + o(n^{-a}), \tag{C.73}$$

$$n\hat{q}_n = Aa(p-1)\phi_{\rm d}^{p-2}n^{-a} + o(n^{-a}). \tag{C.74}$$

Motivated by the numerical solution of Eqs. (85), we assume that, when $\alpha = \alpha_{\rm d}$, T_n admits a finite limit T_∞ as $n \to \infty$. This implies $g(1-s) = T_\infty s^{-1} + o(s^{-1})$ as $s \to 0$. Using the second of equations (85), together with the formulae (C.73), (C.74), we get

$$\begin{aligned}\tilde{g}(1-s) = (p-1)\phi_{\rm d}^{p-2}\, g(1-s) + A\Gamma(1-a)(p-1)\phi_{\rm d}^{p-3} \\ \times ((p-2)T_\infty + a\phi_{\rm d})s^{a-1} + o(s^{-1+a}).\end{aligned} \tag{C.75}$$

Plugging this Ansatz in Eq. (C.71) along with the expansion (C.72), one realizes that terms of the type $\mathrm{cst}\cdot g(1-s)$ (with cst an s-independent constant) cancel because of Eq. (C.11). The leading surviving terms are of order s^{-1+a}. Imposing them to vanish, we get

$$T_\infty = \frac{a(1-\phi_{\rm d})}{1-\lambda}. \tag{C.76}$$

Let us now turn to the intermediate regime, on the scale $n_0(\delta) = \delta^{-1/2a}$, and define the scaling variable $t = n/n_0(\delta)$. We found in Sec. C.1.3 that

$$f(x = 1 - y/n_0) = 1 - \phi_{\rm d} - \delta^{1/2}\, \text{L}[\epsilon](y) + o(\delta^{1/2}), \tag{C.77}$$

$$\frac{\hat{q}_n}{q_n} = (p-1)\phi_{\rm d}^{p-2} + (p-1)(p-2)\phi_{\rm d}^{p-3}\delta^{1/2}\epsilon(t) + o(\delta^{1/2})\,, \tag{C.78}$$

$$n\hat{q}_n = -(p-1)\phi_{\rm d}^{p-2}\delta^{1/2}\, t\epsilon'(t) + o(\delta^{1/2}), \tag{C.79}$$

where $\epsilon(t)$ is the scaling function of Q_n around the plateau, introduced in Eq. (C.17).

Let us make the following Ansatz on this scale:

$$T_n \simeq F(t = n/n_0), \qquad \widetilde{T}_n \simeq \widetilde{F}(t = n/n_0)\,. \tag{C.80}$$

In this regime, the second of equations (85) reads

$$\widetilde{T}_n = (p-1)\phi_{\rm d}^{p-2}T_n + \delta^{1/2}(p-1)\phi_{\rm d}^{p-3}((p-2)F(t)\epsilon(t) - \phi_{\rm d}t\epsilon'(t)) + o(\delta^{1/2}). \tag{C.81}$$

Next we insert this formula in Eq. (C.71) and expand in δ. Leading order terms are of the form $\mathrm{cst}\cdot T_n$ (of order δ^0), and cancel as usual. The scaling function

$F(t)$ is is determined by the vanishing of $O(\delta^{1/2})$ terms, which leads to

$$y\,\mathsf{L}[\epsilon](y)\;\mathsf{L}[F](y) - \lambda\,\mathsf{L}[\epsilon F](y) = -(1-\phi_{\mathrm{d}})\,\mathsf{L}[t\epsilon'](y). \tag{C.82}$$

Studying the limit $y \to \infty$ of this equation, one can check that $F(t)$ reaches for small t the value T_∞ determined above, fulfilling the consistency condition between the end of the finite n regime and the beginning of the "intermediate" one. Consider now the limit $t \to \infty$, and assume $F(t) \sim t^x$, with x a yet unknown positive exponent. Recalling that $\epsilon(t) \sim t^b$ as $t \to \infty$, the above equation yields:

$$\frac{\Gamma(1+x)\Gamma(1+b)}{\Gamma(1+x+b)} = \lambda. \tag{C.83}$$

It follows from the convexity of $\log\Gamma(1+x)$ for $x \geq 0$ that this equation has a unique positive solution, which, because of Eq. (43), is $x = b$.

Finally, let us turn to the large rearrangements regime, $n = tn_0'(\delta)$, with $n_0'(\delta) \sim \delta^{-\nu}$. We define scaling functions on this last scale by

$$T_n \simeq \delta^{-\zeta} G(t = n/n_0'), \qquad \widetilde{T}_n \simeq \delta^{-\zeta}\widetilde{G}(t = n/n_0'). \tag{C.84}$$

We defined in Appendix C.1.4 the scaling function $Q(t)$ for the minimal size distribution Q_n in this regime. From this definition, we have

$$f(x = 1 - y/n_0') \simeq \psi(y) = 1 - y\int_0^\infty Q(t)e^{-yt}\,dt, \tag{C.85}$$

$$\frac{\hat{q}_n}{q_n} \simeq (p-1)Q(t)^{p-2}, \tag{C.86}$$

$$n\hat{q}_n \simeq -(p-1)t\,Q'(t)Q(t)^{p-2}. \tag{C.87}$$

These last two formulae allow to relate $G(t)$ and $\widetilde{G}(t)$, using the second of equations (85). Assuming $\zeta > 0$ (which is consistent with the outcome of numerical computations), we get

$$\widetilde{G}(t) = (p-1)Q(t)^{p-2}G(t). \tag{C.88}$$

Injecting this expression in Eq. (C.71), we finally obtain an equation determining the scaling function $G(t)$,

$$\mathsf{L}[G](y) = p(p-1)\alpha_{\mathrm{d}}\psi(y)\,\mathsf{L}[Q^{p-2}G](y). \tag{C.89}$$

Using Eq. (C.26), it is not hard to show that $G(t) = -\theta_*\,t\,Q'(t)$ is, for any $\theta_* > 0$, a solution of this equation. This solution yields $G(t) \sim t^b$ for $t \to 0$, consistently with the above study of the intermediate regime.

A matching argument allows to fix the exponent ζ. Consider indeed $n = tn_0(\delta)$, with $t \gg 1$ but independent of δ. From the limit $t \to \infty$ of the intermediate regime we have $T_n \sim t^b$. Consider instead the limit $t \to 0$ of the final regime, we

get

$$T_n \sim \delta^{-\zeta} \left(t n_0(\delta)/n_0'(\delta)\right)^b \sim t^b \, \delta^{-\zeta+\frac{1}{2}}. \tag{C.90}$$

Matching the two asymptotics, we obtain the universal exponent $\zeta = 1/2$.

Let us finally compute the quantity $\theta_n = T_n/(nq_n)$, i.e. the average radius of a rearrangement of size n. Using the above solution we find, on the scale of large minimal size rearrangements $n \sim n_0'(\delta)$:

$$\theta_n \simeq \delta^{-\zeta} \frac{G(t)}{-t\,Q'(t)} = \theta_* \, \delta^{-\zeta}. \tag{C.91}$$

C.5. Geometrical Susceptibility

In this Appendix we work out the critical behavior of the geometrical susceptibility defined in Sec. 7.3.

C.5.1. Minimal Size Rearrangements

The susceptibility for minimal size rearrangements is determined by solving Eqs. (97). It is helpful to rewrite the first of these equations as

$$S_n = 1 - Q_n + (1 - Q_n)\widehat{S}_n + \sum_{m=1}^{n-1} q_m(\widehat{S}_{n-m} - \widehat{S}_n). \tag{C.92}$$

As usual, we start by considering the large n behavior at $\alpha = \alpha_{\rm d}$. Numerical computations suggest the Ansatz $S_n \simeq S_* n^w$, with $w > 0$ an exponent to be determined. From the second of Eqs. (97), and recalling that $Q_n = \phi_{\rm d} + An^{-a} + o(n^{-a})$, we get

$$\widehat{S}_n = p(p-1)\alpha_{\rm d}\phi_{\rm d}^{p-2} S_n + p(p-1)(p-2)\alpha_{\rm d}\phi_{\rm d}^{p-3} A S_* n^{w-a} + o(n^{w-a}). \tag{C.93}$$

This implies in particular $\widehat{S}_n \simeq p(p-1)\alpha_{\rm d}\phi_{\rm d}^{p-2} S_* n^w$. This expression can be substituted in Eq. (C.92). The leading terms are of the type cst S_n (and of order n^w) and cancel because of Eq. (C.11). We get an equation of the form

$$0 = 1 - \phi_{\rm d} + A S_* C \, n^{w-a} + o(1, n^{w-a}), \tag{C.94}$$

where C is n-independent and given by

$$C = p(p-1)\alpha_{\rm d}\phi_{\rm d}^{p-2} \left\{ \lambda - \frac{\Gamma(1-a)\Gamma(1+w)}{\Gamma(1-a+w)} \right\}, \tag{C.95}$$

and λ is the constant already introduced in Sec. C.2.4. Notice that Eq. (C.94) cannot be satisfied for $w < a$ (in this case, it would imply $0 = 1 - \phi_{\rm d}$), nor for

$w > a$ (it can be shown[26] that $C < 0$ for $w > 0$). Therefore we have necessarily $w = a$, and Eq. (C.94) determines the prefactor S_*.

Next we consider the intermediate scale $n_0(\delta) = \delta^{-1/2a}$. Since $S_n \sim n^a$ at $\alpha = \alpha_{\rm d}$, we expect $S_n \sim \delta^{-1/2}$ for $\alpha < \alpha_{\rm d}$ and $n \sim n_0(\delta)$. We assume the scaling behavior

$$S_n \simeq n^{-x}\, R(t = n/n_0(\delta)), \tag{C.96}$$

with an analogous Ansatz for $\widehat{S}_n$ (with scaling function $\widehat{R}(t)$), and $x > 0$ an exponent yet to be determined. Equations (97) yield (cf. also the form (C.92))

$$\begin{aligned}\widehat{R}(t) &= p(p-1)\alpha_{\rm d}\phi_{\rm d}^{p-2} R(t) + p(p-1)(p-2) \\ &\quad \times \alpha_{\rm d}\phi_{\rm d}^{p-3}\epsilon(t)R(t)\,\delta^{1/2} + o(\delta^{1/2}), \qquad \text{(C.97)} \\ R(t) &= (1-\phi_{\rm d})\delta^x + (1-\phi_{\rm d})\widehat{R}(t) - \epsilon(t)\widehat{R}(t)\,\delta^{1/2} - \delta^{1/2} \\ &\quad \times \int_0^t \epsilon'(s)[\widehat{R}(t-s) - \widehat{R}(t)]\, ds + o(\delta^{1/2}). \qquad \text{(C.98)}\end{aligned}$$

Eliminating $\widehat{R}(t)$, we obtain an equation determining the scaling function $R(t)$. For $x = 1/2$ we get:

$$(1-\phi_{\rm d})^2 + (\lambda - 1)\epsilon(t)R(t) - \int_0^t \epsilon'(s)[R(t-s) - R(t)]\, ds = 0. \tag{C.99}$$

Other values of x can be excluded via an analysis of the resulting equations: we shall stick to $x = 1/2$ hereafter. The asymptotic behavior of the solution of Eq. (C.99) can be determined by recalling that $\epsilon(t) \sim t^{-a}$ as $t \to 0$, and $\epsilon(t) \sim -t^b$ as $t \to \infty$. We get $R(t) \sim t^a$ for $t \to 0$ and $R(t) \sim t^b$ for $t \to \infty$. The choice $x = 1/2$ is confirmed by matching the $t \to 0$ behavior with the analysis of the finite n regime, explained above.

In Fig. 28, left frame, we plot $\delta^{1/2} S_n$ versus $\delta^{1/2a} n$, with S_n determined via a numerical solution of Eqs. (97). The good collapse confirms the validity of the above analysis.

Let us finally consider the scale of large rearrangements $n_0'(\delta) = \delta^{-\nu}$, and assume in this regime

$$S_n \simeq \delta^{-\eta}\, S(t = n/n_0(\delta)), \tag{C.100}$$

with an analogous Ansatz for $\widehat{S}_n$, and $\eta > 0$ a new critical exponent. Injecting this form in Eqs. (97), and recalling that $Q_n \simeq Q(t = n/n_0(\delta))$ on the same scale, we

[26] Consider the expression in curly brackets in Eq. (C.95) (the prefactor is positive). Proving that it is negative is equivalent to proving that $F_a(1 + w - a) > F_a(1 - 2a)$, where $F_a(x) = \log\Gamma(x + a) - \log\Gamma(x)$. This in turns follows from the fact that $\log\Gamma(x)$ is strictly convex for $x > 0$.

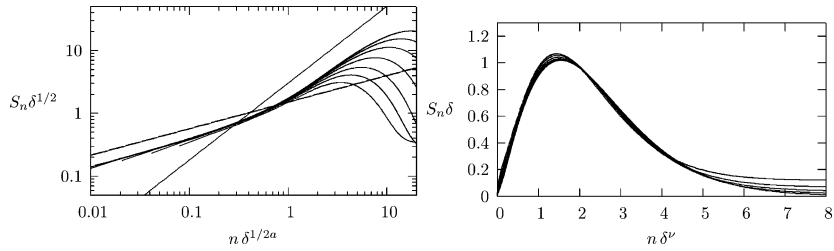

Fig. 28. Critical scaling of the geometrical susceptibility for minimal size rearrangements. Different curves refer to $p = 3$ and $\alpha = 0.7, 0.75, 0.78, 0.8, 0.81, 0.814, 0.816$. *Left*: intermediate regime. The *straight lines* correspond to the asymptotic behaviors t^a (as $t \to 0$) and t^b (as $t \to \infty$). *Right*: large scale rearrangements regime.

get:

$$S(t) = (1 - \phi_{\rm d})\widehat{S}(t) - \int_0^t Q'(s)\widehat{S}(t-s)\,ds\,, \tag{C.101}$$

$$\widehat{S}(t) = p(p-1)\alpha_{\rm d}\,Q(t)^{p-2}S(t). \tag{C.102}$$

Studying these equations in the $t \to 0$ limit allows to determine the asymptotic behavior $S(t) \sim t^b$ as $t \to 0$. This allows to determine the exponent η through a matching procedure. If we let $n = t\,n_0(\delta)$, with t large but δ–independent, from our study, respectively, of the intermediate and final regimes, we get

$$S_n \sim \delta^{-1/2}\,t^b \sim \delta^{-\eta}(t\,n_0(\delta)/n_0'(\delta))^b. \tag{C.103}$$

This in turn implies $\eta = 1$.

In Fig. 29, right frame, we check the scaling hypothesis in the final regime (as well as the exponent $\eta = 1$) against a numerical solution of Eqs. (97).

C.5.2. Minimal Barrier Rearrangements

This part of the Appendix is devoted to the resolution of Eqs. (99,100) for the geometric susceptibility of minimal barrier rearrangements. Using the fact that $\sum_b \hat{s}_b = 0$, Eq. (99) can be rewritten as

$$S_b = 1 - Q_b - \sum_{l=0}^{2b-4} p_l S_b^{(l+1)}, \quad S_b^{(l)} = \sum_{b_1,\ldots,b_l} \hat{s}_{b_1}\hat{q}_{b_2}\ldots\hat{q}_{b_l}\mathbb{I}(\hat{f}_l(b_1,\ldots,b_l) < b). \tag{C.104}$$

The quantity $S_b^{(l)}$ is very similar to $N_b^{(l)}$ defined in Eq. (C.59), with the sequence $\hat{s}_b$ replacing $\widehat{M}_b$. In particular $S_b^{(l)}$ admits a representation of the form (C.60), where $\widehat{N}_b$ is replaced by $-\widehat{S}_b$. The numerical computation of S_b proceeds along the lines exposed in Sec. C.3.

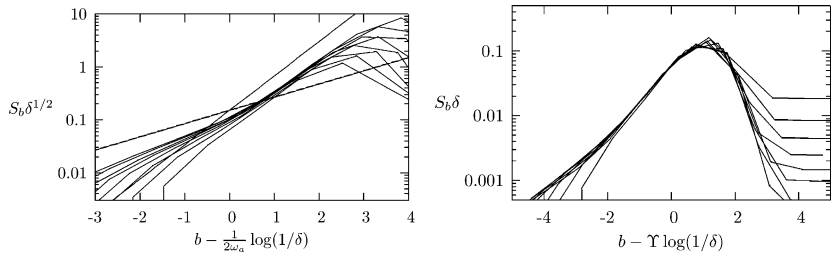

Fig. 29. Scaling of the geometrical susceptibility for minimal barrier rearrangements. Different curves refer to $p = 3$ and $\alpha = 0.8, 0.81, 0.814, 0.816, 0.817, 0.8175, 0.818, 0.8182$. *Left*: intermediate regime. The straight lines correspond to the asymptotic behaviors $e^{\omega_a m}$ (as $m \to -\infty$) and $e^{\omega_b m}$ (as $m \to \infty$). *Right*: large scale rearrangements regime.

The expansion of Eqs. (99), (100) in powers of $\epsilon_b = Q_b - \phi_{\rm d}$ is also analogous to the one of Sec. C.3. We get

$$S_b = 1 - \phi_{\rm d} - \epsilon_b + e^{-\alpha p \phi_d^{p-1}} \widehat{S}_b + \alpha p(p-1)\phi_{\rm d}^{p-2} e^{-\alpha p \phi_d^{p-1}} \times [\widehat{S}_{b-1}(\epsilon_{b-1} - \epsilon_b) - \widehat{S}_b \epsilon_{b-1}] + O(\epsilon^2 S), \tag{C.105}$$

$$\widehat{S}_b = \alpha p(p-1)\phi_{\rm d}^{p-2} S_b + \alpha p(p-1)(p-2)\phi_{\rm d}^{p-3} \epsilon_b S_b + O(\epsilon^2 S). \tag{C.106}$$

Next we eliminate $\widehat{S}_b$ from the above equations and assume the asymptotic behavior $S_b \simeq S_* e^{wb}$, with $w > 0$ to be determined. Recalling that $\epsilon_b \simeq A\, e^{-\omega_a b}$, we get

$$0 = (1 - \phi_{\rm d}) + C S_*\, e^{(w-\omega_a)b} + o\big(1, e^{(w-\omega_a)b}\big), \tag{C.107}$$

where

$$C = p(p-1)\alpha_{\rm d}\phi_{\rm d}^{p-2} \left\{\lambda - [e^{\omega_a} - (e^{\omega_a} - 1)e^{-w}]\right\}, \tag{C.108}$$

and λ is defined in Sec. C.3. Using an argument similar to the one in the previous Section, one can show that Eq. (C.107) implies $w = \omega_a$.

Let us consider now the intermediate regime $b = m + b_0(\delta)$, where $b_0(\delta) = \log(1/\delta)/(2\omega_a)$ and $\epsilon_b \sim \delta^{1/2}\overline{\epsilon}_m$. Inserting the Ansatz $S_b = \delta^{-x}\overline{S}_m$ in Eqs. (C.105), (C.106), dominant terms (of order δ^{-x}) cancel. For next-to-leading terms to cancel, one has to choose $x = 1/2$. The scaling function $\overline{S}_m$ is then found to obey

$$\lambda \overline{S}_m \overline{\epsilon}_m + \overline{S}_{m-1}(\overline{\epsilon}_{m-1} - \overline{\epsilon}_m) - \overline{S}_m \overline{\epsilon}_{m-1} + (1 - \phi_{\rm d})^2 = 0. \tag{C.109}$$

The asymptotic behavior of $\overline{S}_m$ can be deduced from this equation, using the results on $\bar{\epsilon}_m$, cf. Sec. C.2.3. One finds $\overline{S}_m \sim e^{\omega_a m}$ as $m \to -\infty$ (thus matching the behavior in the first regime) and $\overline{S}_m \sim e^{\omega_b m}$ as $m \to \infty$.

In Fig. 29, left frame, we compare the postulated scaling in the intermediate regime with a numerical solution of Eqs. (99), (100).

Finally, on the large rearrangement scale $b_0'(\delta) \sim \Upsilon \log(1/\delta)$, we expect $S_b \sim \delta^{-\eta}$. The exponent η can be determined by matching this behavior with the large

m asymptotics in the intermediate scale:

$$S_{b_0'} \sim \delta^{-1/2}\overline{S}_{m=b_0'-b_0} \sim \delta^{-1/2}\exp\left\{\omega_b \frac{1}{2\omega_b}\log(1/\delta)\right\}. \tag{C.110}$$

We thus have $\eta = 1$ as claimed in Sec. 7.3.2.

APPENDIX D: LOW TEMPERATURE BEHAVIOR OF THE DYNAMICAL LINE

In Sec. 8, we claimed that the dynamical transition line behaves as described in Eq. (103) in the low temperature limit. A proof of this statement requires a particularly involved asymptotic calculation, and goes beyond the scope of this paper. On the other hand, a simple argument can be constructed as follows.

Consider $\alpha > \alpha_{\rm d}$ and expand the solution of the 1RSB equations (B.14), (B.15) as $T \to 0$, with α and $m < 1$ fixed. At $T = 0$, the order parameters $\mathcal{Q}(\rho)$, $\widehat{\mathcal{Q}}(\hat\rho)$ concentrate over local field distributions $\rho(h)$, $\hat\rho(u)$ supported on integer fields $h, u \in \mathbb{Z}$. More precisely, $\hat\rho(u) = \frac{1}{2}\delta(u-1) + \frac{1}{2}\delta(u+1)$ with probability $\hat\phi$ (corresponding to hyperedges in the backbone), and $\hat\rho(u) = \delta(u)$ with probability $1-\hat\phi$ (hyperedges outside the backbone). Analogous expressions hold for $\mathcal{Q}(\rho)$.

A small non-zero temperature has two effects on $\widehat{\mathcal{Q}}(\hat\rho)$. First of all, any local field distribution $\hat\rho(u)$ in the support of $\widehat{\mathcal{Q}}$ aquires a peak for $u \approx 0$. Second, the peaks on integer fields acquire a small width. In general, this width is of order T and the last effect dominates. For XORSAT, the width is of order $e^{-2\beta}$ and can be neglected to first order (this can be checked through usual population dynamics algorithms and yields indeed a consistent low T expansion). Therefore, the leading correction is captured by the form $\hat\rho(u) \approx \frac{1}{2}(1-\hat\rho_0)\delta(u-1) + \hat\rho_0\delta(u) + \frac{1}{2}(1-\hat\rho_0)\delta(u+1)$. The distribution $\widehat{\mathcal{Q}}(\hat\rho)$ is concentrated over $\hat\rho(u)$ of this form and is completely determined as

$$\hat\rho_0 = \begin{cases} n2^m e^{-2\beta m} & \text{with probability } \widehat{Q}_n, \\ 1 & \text{with probability } 1-\hat\phi. \end{cases} \tag{D.1}$$

The distribution $\widehat{Q}_n$ has normalization $\sum_n \widehat{Q}_n = \hat\phi$, and satisfies the equations

$$\widehat{Q}_n = \sum_{n_1 \dots n_{p-1}} Q_{n_1} \dots Q_{n_{p-1}}\, \delta_{n-n_1-\dots-n_{p-1}}, \tag{D.2}$$

$$Q_n = [1-\bar p_0 - \bar p_1 - \bar p_2]\,\delta_{n,0} + \bar p_2\,\delta_{n,1} + \bar p_1 \frac{\widehat{Q}_n}{\hat\phi}. \tag{D.3}$$

where $\bar p_l = (p\alpha\hat\phi)^l e^{-p\alpha\hat\phi}/l!$, and Q_n parameterizes the functional distribution $\mathcal{Q}(\rho)$. At any fixed $\alpha > \alpha_{\rm d}$, the leading correction to $\rho(h)$, $\hat\rho(u)$ is of order $e^{-2\beta m}$.

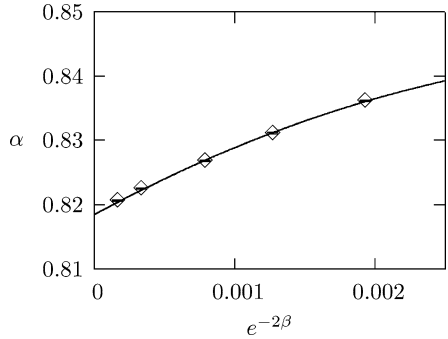

Fig. 30. Low temperature behavior of the dynamical transition line. Symbols (*with error bars*) correspond to a numerical determination of $\alpha_{\rm d}(\beta)$ along the lines of Appendix B.3. The line is a fit to the form $\alpha_{\rm d}(\beta) = \alpha_{\rm d} + x_{\rm d} e^{-2\beta} + y_{\rm d} e^{-4\beta}$.

Since $m < 1$, it is consistent to neglect the $O(e^{-2\beta})$ width of the peaks on integer u's.

By studying Eqs. (D.2), (D.3) as $\alpha \downarrow \alpha_{\rm d}$, one can show that the typical scale of n diverges as $(\alpha - \alpha_{\rm d})^{-1}$. The above low-$T$ expansion breaks down when $\hat{\rho}_0 \sim (\alpha - \alpha_{\rm d})^{-1} e^{-2\beta m} = O(1)$, i.e. for $\alpha = \alpha_{\rm d} + O(e^{-2\beta m})$. The DPT corresponds to a singularity in the solution of Eqs. (B.14), (B.15) at $m = 1-$. If we identify this singularity with the low-T expansion breakdown, we get the scaling (103).

The above argument does not fix the coefficient $x_{\rm d}$. In order to determine it numerically (for $p = 3$), we computed $\alpha_{\rm d}(\beta)$ numerically for several values of β, and fitted the results to the form (103). At each value of β, $\alpha_{\rm d}$ was determined by computing the length $\ell_*(\varepsilon)$ defined in Sec. 3.2 using the method of Appendix B.3 and fitting the result using the form $\ell_*(\varepsilon) \approx A(\alpha_{\rm d}(\beta) - \alpha)^{-1/2}$. The resulting critical points are reported in Fig. 30.

Next, the values for $T \leq 0.32$ were fitted using the form $\alpha_{\rm d}(\beta) = \alpha_{\rm d} + x_{\rm d} e^{-2\beta} + y_{\rm d} e^{-4\beta}$. This gives a very good description of the data if $x_{\rm d} = 11.76$, and $y_{\rm d} = 1378$. The final result (with a somehow subjective estimate of the error) is

$$x_{\rm d} = 11.7(5). \tag{D.4}$$

We conclude by stressing that, in general mean-field models on sparse graphs, the low-temperature behavior of the dynamical transition line can be different from Eq. (103), because of $O(T)$ cavity fields.

ACKNOWLEDGMENTS

This work has been partially supported by the integrated project EVERGROW (n. 1935 in the complex systems initiative of the Future and Emerging Technologies

directorate of the IST Priority, EU Sixth Framework), and the Research Training Network STIPCO (HPRN-CT-2002-00319).

REFERENCES

1. M. Mézard and G. Parisi, *Eur. Phys. J. B* **20**:217 (2001).
2. S. Franz, M. Mézard, F. Ricci-Tersenghi, M. Weigt, and R. Zecchina, *Europhys. Lett.* **55**:465 (2001).
3. S. Franz and G. Parisi, *J. Phys. I (France)* **5**:1401 (1995).
4. G. Semerjian, L. F. Cugliandolo, and A. Montanari, *J. Stat. Phys.* **115**:493 (2004).
5. F. Ritort and P. Sollich, *Adv. Phys.* **52**:219 (2003).
6. A. Montanari and G. Semerjian, Large Scale Rearrangements in Kinetically Constrained Models, in preparation.
7. T. R. Kirkpatrick and D. Thirumalai, *Phys. Rev. B* **36**:5388 (1987).
8. T. R. Kirkpatrick and P. G. Wolynes, *Phys. Rev. A* **35**:3072 (1987).
9. W. Götze and L. Sjögren, *Rep. Prog. Phys.* **55**:241 (1992).
10. J.-P. Bouchaud, L. F. Cugliandolo, J. Kurchan, and M. Mézard, *Physica A* **226**:243 (1996).
11. J.-P. Bouchaud, L. F. Cugliandolo, J. Kurchan, and M. Mézard, Out of equilibrium dynamics in spin-glasses and other glassy system, in *Spin Glasses and Random Fields*, A. P. Young ed., (World Scientific, Singapore, 1997).
12. C. Donati, S. C. Glotzer, and P. H. Poole, *Phys. Rev. Lett.* **82**:5064 (1999).
13. C. Bennemann, C. Donati, J. Baschnagel, and S. C. Glotzer, *Nature* **399**:246 (1999).
14. G. Biroli and J.-P. Bouchaud, *Europhys. Lett.* **67**:21 (2004).
15. S. Franz and G. Parisi, *J. Phys: Condens. Matter* **12**:6335 (2000).
16. C. Donati, S. Franz, S. C. Glotzer and G. Parisi, *J. Non-Cryst. Sol.* **307–310**:215 (2002).
17. J.-P. Bouchaud, `cond-mat`/0408617.
18. B. I. Halperin, *Phys. Rev. B* **8**:4437 (1973).
19. A. Crisanti and H.-J. Sommers, *Z. Phys. B* **87**:341 (1992).
20. A. Crisanti, H. Horner, and H.-J. Sommers, *Z. Phys. B* **92**:257 (1993).
21. L. F. Cugliandolo, Dynamics of glassy systems, in *Slow Relaxations and Non-equilibrium Dynamics in Condensed Matter*, J.-L. Barrat *et al.* eds. (Springer, Berlin, 2003).
22. J. Kurchan, G. Parisi, and M. A. Virasoro, *J. Phys. I (France)* **3**:1819 (1993).
23. A. Cavagna, I. Giardina, and G. Parisi, *Phys. Rev. B* **57**:11251 (1998).
24. W. Kob, Supercooled liquids, the glass transition, and computer simulations, in *Slow Relaxations and Non-equilibrium Dynamics in Condensed Matter*, J.-L. Barrat *et al.* eds. (Springer, Berlin, 2003).
25. A. Montanari and G. Semerjian, *Phys. Rev. Lett.* **94**:247201 (2005).
26. N. Creignou and H. Daudé, *Discrete Appl. Math.* **96–97**:41 (1999).
27. F. Ricci-Tersenghi, M. Weigt, and R. Zecchina, *Phys. Rev. E* **63**:026702 (2001).
28. B. Bollobas, *Random Graphs*, 2nd Ed., (Cambridge University Press, Cambridge, 2001).
29. E. Gardner, *Nucl. Phys.* **B257 [FS14]**:747 (1985).
30. M. Mézard, F. Ricci-Tersenghi, and R. Zecchina, *J. Stat. Phys.* **111**:505 (2003).
31. S. Cocco, O. Dubois, J. Mandler, and R. Monasson, *Phys. Rev. Lett.* **90**:047205 (2003).
32. B. Pittel, J. Spencer, and N. Wormald, *J. Comb. Theory B* **67**:111 (1996).
33. G. Semerjian and M. Weigt, *J. Phys. A* **37**:5525 (2004).
34. J. P. L. Hatchett, I. Pérez Castillo, A. C. C. Coolen, and N.S. Skantzos, `cond-mat/0504313`.
35. J. Zinn-Justin, *Quantum Field Theory and Critical Phenomena* (Oxford University Press, Oxford, 1989).
36. F. R. Kschischang, B. J. Frey, and H.-A. Loeliger, *IEEE Trans. Inform. Theory* **47**:498 (2001).

37. J.-P. Bouchaud and G. Biroli, *J. Chem. Phys.* **121**:7347 (2004).
38. A. Montanari and F. Ricci-Tersenghi, *Phys. Rev. Lett.* **90**:017203 (2003).
39. A. Montanari and F. Ricci-Tersenghi, *Phys. Rev. B* **68**:224429 (2003).
40. G. Parisi, `cond-mat/0211608`, `cond-mat/0208070`.
41. M. Mézard and A. Montanari, Reconstruction on trees and spin glass transition, `cond-mat/0512295`.
42. D. Aldous and J. A. Fill, *Reversible Markov Chains and Random Walks on Graphs*, book in preparation. Draft available at `http://www.stat.berkeley.edu/users/aldous/RWG/book.html`
43. T. P. Hayes and A. Sinclair, "A general lower bound for mixing of single site dynamics on graphs," to appear in FOCS 2005.
44. M. Dyer, A. Sinclair, E. Vigoda, and D. Weitz, *Rand. Struct. Alg.* **24**:461 (2004).
45. N. Berger, C. Kenyon, E. Mossel, and Y. Peres, *Prob. Theory Rel. Fields* **131**(3):311–340 (2005).
46. C. L. Henley, *Phys. Rev. B* **33**:7675 (1986).
47. J. C. Anglès d'Auriac, M. Preissmannd, and A. Sebö, *Math. Comput. Model.* **26**:1 (1997).
48. C. L. Henley, *Phys. Rev. Lett.* **54**:2030 (1985).
49. R. Rammal and A. Benoit, *Phys. Rev. Lett.* **55**:649–652 (1985).
50. T. Schaefer, in Proceedings of the 10th Annual ACM Symposium on the Theory of Computing, San Diego, 216 (1978).
51. M. Mézard, G. Parisi, and R. Zecchina, *Science* **297**:812 (2002).
52. R. Mulet, A. Pagnani, M. Weigt, and R. Zecchina, *Phys. Rev. Lett.* **89**:268701 (2002).
53. M. Mézard, G. Parisi, and M. A. Virasoro, *Spin Glass Theory and Beyond* (World Scientific, Singapore, 1987).
54. A. B. Bortz, M. H. Kalos, and J. L. Lebowitz, *J. Comput. Phys.* **17**:10 (1975).
55. K. Athreya and P. Ney, *Branching Processes* (Springer-Verlag, New York, 1972).
56. S. Cocco, R. Monasson, A. Montanari, and G. Semerjian, Approximate analysis of search algorithms with 'physical' methods, in *Computational Complexity and Statistical Physics*, A. Percus, G. Istrate and C. Moore eds. (Oxford University Press, Oxford, 2006).
57. M. Vogel, B. Doliwa, A. Heuer, and S. C. Glotzer, *J. Chem. Phys.* **120**:4404 (2004).
58. S. C. Glotzer, *J. Non-Cryst. Solids* **274**:342 (2000).
59. J. Diaz, J. Petit, and M. Serna, *ACM Comput. Surv.* **34**:313 (2002).
60. M. Yannakakis, *J. ACM* **32**:950 (1985).
61. T. Lengauer, *SIAM J. Alg. Disc. Meth.* **3**:99 (1982).
62. R. B. Stinchcombe, Dilute magnetism, in *Phase Transitions and Critical Phenomena*, C. Domb and J. L. Lebowitz eds. (Academic, New York, 1983), Vol. 7.
63. G. Biroli, M. Sellito, and C. Toninelli, *Europhys. Lett.* **69**:496 (2005).
64. H. Zhou, *Phys. Rev. Lett.* **94**:217203 (2005).
65. H. Zhou, *New J. Phys.* **7**:123 (2005).
66. M. G. Luby, M. Mitzenmacher, M. A. Shokrollahi, and D. A. Spielman, *IEEE Trans. Inform. Theory* **47**:569–584 (2001).
67. C. Méasson, A. Montanari, and R. Urbanke, `cs.IT/0506083`.
68. H. S. Wilf, *Generatingfunctionology* (Academic Press, San Diego, 1990).
69. A. M. Odlyzko, Asymptotic enumeration methods, in *Handbook of Combinatorics*, R. L. Graham, M. Groetschel, and L. Lovasz, eds. (The MIT Press, Cambridge, 1995), vol 2.
70. P. Flajolet and R. Sedgewick, *Analytic Combinatorics*, book in preparation. Draft available at `http://algo.inria.fr/flajolet/Publications/books.html`
71. M. Kuczma, B. Choczewski, and R. Ger, *Iterative Functional Equations* (Cambridge University Press, Cambridge, 1990).